Towards Single Molecule Electronics

Michael Krüger

aus Lörrach, Deutschland

Basel, 2000

Genehmigt von der Philosophisch-Naturwissenschaftlichen Fakultät
auf Antrag von:

      Prof. Dr. C. Schönenberger
      Prof. Dr. L. Schlapbach
      Prof. Dr. H. Siegenthaler

Basel, den 4. Juli 2000

                  Prof. Dr. Andreas D. Zuberbühler

Contents

Chapter 1

Introduction

The size of electronic devices has decreased tremendously during the last decades. Since 1948, when the first transistor was fabricated [1], until now the dimensions of the devices were reduced by a factor of million. However, semiconductor based microelectronics might reach its limit in the device size within next ten years. Fig. 1.1.shows the development of device sizes in the last decades, and the predicted development leading possibly to nanoelectronic devices and nanometer scaled molecular electronics in the near future.

New technologies and materials must be discovered and established in order to reach the nanoelectronic approach. Considerable interdisciplinary work has been done in the field of nanoscience within the last two decades, involving various scientific fields like physics, chemistry, biology, material science, biotechnology etc.. Mesoscopic physics, a rapidly growing branch of solid state physics is an example of this trend. Mesoscopic physics explores physical properties of materials in the nanometer size regime, which is in between the macroscopic world of classical physics and the microscopic world of quantum mechanics. At these dimensions non-classical size-dependent effects become important, and the understanding of their details is crucial for a successful approach to the fabrication of nanoelectronic devices. Mesoscopic devices, in the simplest case contacted metal wires, are usually fabricated by electron-beam lithography (EBL) and have sizes down to 20-50 nm in width. In order to reach smaller dimensions, either new technologies for structuring materials must be developed or molecules with a diameter from 0.1-1 nm (atoms, atomic clusters) to a few nm (clusters, organic molecules, proteins, polymers, carbon nanotubes, DNA) must be used. This leads to an interesting and challenging research field of molecular electronics.
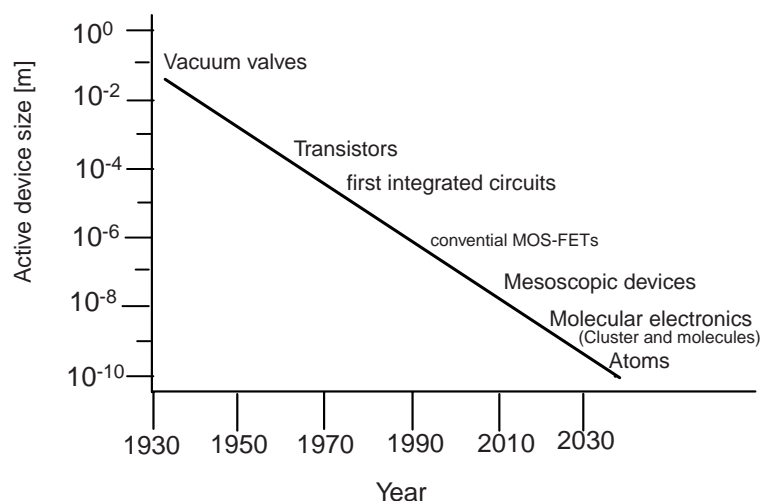
3

Figure 1.1: Development of the device sizes in the last 50 years and the expected development following Moores law [2]

1.1 Molecular Electronics

As outlined above there are two strategies in reaching molecular electronics. One is to establish techniques for reducing the dimensions of known conducting materials like metals. In this case the ultimate limit in size is a chain of atoms. The other is to search for conducting molecules which already have dimensions in the nanometer regime and to develope new methods and technologies to make electrical contacts to these molecules. The latter approach is central to this thesis. There are several possible future applications of molecular nanodevices. One can think about the possibilities to store information in the form of quantized electronic or magnetic states of molecules and atoms, which leads us to the field of digital devices. In combination with the fast-growing on-chip technologies, new detectors, rectifiers, sensors or even controlled local chemical reactions are possible applications as well. The research community developing controlable neural networks and more complex tunable molecular systems is growing faster and and faster. Biological systems for example, like neuron cells are integrated into silicon based microelectronic devices, controlling the biological activity electrostatically by a field effect transistor (FET) [3]. Furthermore, recent results show that DNA, the molecule of life, can conduct electrical current [4, 5]. This could even open the door for biomolecular electronics, as DNA has an enormous potential to store and copy information. Indeed, the possibilities of employing molecular systems in advanced electronics are astonishingly rich quantitatively and qualitatively.
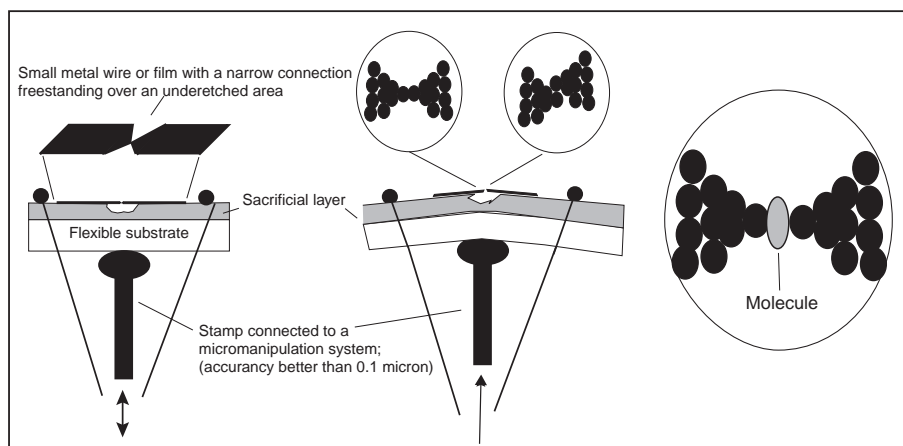
Figure 1.2: Break junction technique for achieving the contacts to atoms and molecules.

1.1.1 Electrical Contacts to Single Molecules

For investigating the electrical properties of molecules one must connect them to conducting electrodes. The crucial parameter is the contact resistance between the molecule and the electrode. This resistance can often be much larger than the resistance of the molecule itself. In order to reduce the contact resistance different methods can be used. An early method for measuring the electronic properties of molecules made use of Scanning Tunneling Microscopy (STM) by positioning a metallic tip above molecules deposited on a conducting substrate [1] [7, 8]. In order to achieve a better mechanical stability of the contacts further methods such as the mechanically controllable break junction (MCB) technique have been developed [11, 12]. In this method, schematically shown in Fig. 1.2. a small metallic wire laying on top of a flexible substrate is broken in a controlled way by applying an adjustable pressure at the backside of the substrate. By reducing the pressure the broken contact can be restored. In this way a contact of one or a few atoms is available, as proven by the observation of quantized conductance [13] and direct transmission-electron microscopy (TEM) images [14].

A method similar to MCB can also be used to contact molecules. Broken ends of the wire can be chemically modified in order to attach molecules by specific chemical interactions. The gap between the two facing electrodes can be adjusted to a distance comparable to the length of the molecule that is to be contacted. Electrical transport measurements through very few or, possibly

---

[1] By using STM or AFM one can also manipulate molecules and move them on the substrate surface [9, 10].
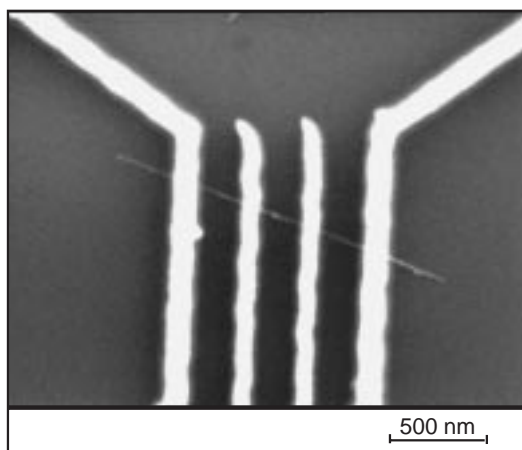
Figure 1.3: SEM image (topview) of a single multiwalled carbon nanotube contacted by four Au electrodes for transport measurements.

a single molecule, chemically bound to the two electrodes, have been carried out using this methode [15, 16]. If the molecules are longer than approximately 5 nm they can be contacted to the electrodes by EBL. The contacts can be made in the first step, in the form of a serie of metallic electrodes on the substrate, which is then followed by putting the molecules onto thus prepared structures. In most of the cases some molecules will be connected between two neighbouring electrodes [17, 18]. The other possibility is to put the molecules onto the surface and carry out EBL afterwards, knowing the exact position of the molecules on the substrate. In this case the electrodes are created on top of the molecules [19] (an example is shown in Fig. 1.3.). Both methods have been used successfully, in particular to investigate carbon nanotubes (CNs) .

There are some additional new methods for contacting molecules electrically. These are: template synthesis of metallic and conducting polymer wires in mesoporous membranes and a method of electrostatic trapping conducting molecules between two closely faced electrodes. The electrodes are fabricated by EBL and shown in Fig. 1.4.a). They are separated by a 50-200 nm gap. There are different ways to reduce the gap size to molecular dimensions. An elegant method is to use electrochemical deposition to reduce the gap size [20]. Since electrochemical deposition is reversible closing and re-opening of the gap is easily achievable. In measuring the resistance between the two faced electrodes a sharp decrease of the resistance indicates the contact during deposition, whereas a sharp increase of the resistance during dissolution indicates the opening of the gap. By stopping just after the resistance increase one can obtain gap sizes below 5-10 nm (this can not be resolved by SEM). One example of a closed and re-opened gap is shown
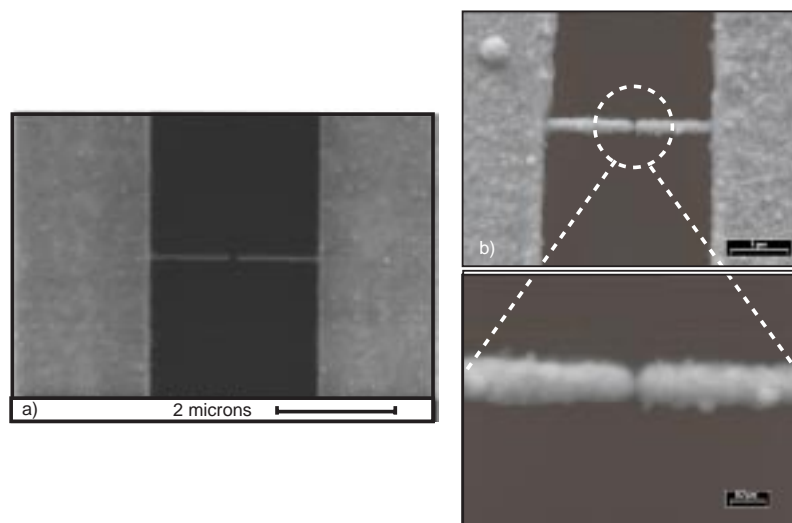
Figure 1.4: a) SEM image of two closely faced Au electrodes fabricated by EBL. The gap between the electrodes is about 130 nm in length. b) SEM imges after closing and re-opening the gap by electrochemical Au (or Ni) deposition. The gap smaller than 10 nm cannot be resolved by SEM.

in Fig. 1.4.b). Conducting molecules dissolved in a non-conducting solvent can be trapped[2] between this separated electrodes, as has been successfully demonstrated [21]. Even measurements on molecules like DNA were possible [5]. The template synthesis method will be described in chapter 3 in more detail.

1.2 This Thesis

The aim of this thesis is to contribute to the modern research on molecular electronics. New methods for nanostructuring of materials (metals, conducting polymers, carbon nanotubes, DNA, metal clusters) with an emphasis on the methods for making reliable electrical contacts were developed.

---

[2]A high voltage (e.g. AC voltage with a high frequency) is applied between the two facing electrodes. Conducting molecules near at the electrode surface are attracted by electrostatic forces between the electrodes and establish an electrical contact. By using a high-ohmic resistance in series most of the voltage drops over the resistance after one or more molecules connect both electrodes. The electric field decreases, and the electric force is no more strong enough to attract conducting molecules.

- In the early stage of the work presented, the electrochemical synthesis of macroscopic films of conducting polymers (polypyrrole, polythiophene poly-3-methylthiophene) was investigated, in order to determine the bulk resistivity of these materials. By using commercially available polycarbonate membranes with a pore size down to 30 nm, nanowires of conducting polymers (CPs) and metals (Ni, Co) were electrochemically synthesized. A method to contact these wires was developed, too.

- Alumina membranes with a pore size down to 9 nm were fabricated by ourselves using electrochemical oxidation of aluminum films in sulfuric acid. Ni nanowires can be grown successfully within these pores.

- Lateral nanopores within a polyimide resist were created on top of four contact electrodes, in order to achieve a four-terminal contact to the wire. This method was used for materials which usually have a high contact resistance, e.g. CPs, and which can be deposited by an electrochemical synthesis.

- Multiwalled carbon nanotubes (MWNTs) spread on top of a silicon-oxide surface were contacted by Au electrodes as mentioned above and shown in Fig.1.3.. Electrical transport measurements were carried out on thus prepared MWNTs. A significant change in the resistivity was observed, due to the doping state of the MWNTs. The electronic state of a MWNT can be changed by electrochemical doping, as well as by convential doping using a backgate electrode. The effect of the electrochemical doping is actually much stronger, as one can change easily the state of the tube from p-doping to n-doping.

- A nearby Al/Al_2O_3 gate electrode on top of the tube produces the same effect as in the case of electrochemical doping. Low-temperature measurements on one sample were carried out, and a fine structure representing the density of electronic states (DOS) was observed by measuring the resistance as a function of the applied gate voltage.

- The electronic state of MWNTs is sensitive to environmental conditions like the take-up of oxygen, probably doping the MWNTs. Oxidizing und reducing agents can change the electronic state very easily. A preliminary annealing experiment of a MWNT in vacuum indicates that oxygen can influence the electronic properties of the tube.

Chapter 2

Conducting Polymers

2.1 Introduction

In 1968 Berets and Smith found that the conductivity of pressed pellets of poly-acetylene (PA) can be varied over the range 10^{-9} to 10^{-2} S/cm exposing them to various Lewis acids and bases[1][22]. PA is, like other conducting polymers (CPs), a π-conjugated polymer with alternating double and single carbon-carbon covalent bonds. In Fig. 2.1. the chemical structures of some CPs are shown. PA was viewed as a wide-bandgap semiconductor with low intrinsic conductivity [23]. This encouraged many scientists to synthesize other CPs with a lower band gap in order to improve the electric conductivity, in hope for a future replacement of widely-used metals with this cheaper and non-corrosive materials. In addition, the specific weight of CPs is much lower than the weight of any technologically used metal or metal alloy, which is of an importance for some specific applications as well.

A breakthrough in this field came in 1974 when Ito and Shirakawa synthesized free standing films of PA [24]. This opened a possibility to investigate the physical properties of PA by different methods and in a more accurate way. PA was found to be intrinsically semiconducting with an energy bandgap of 1.4 eV [25]. Oxidation and reduction of these films by different agents, so-called doping, led to much higher conductivities i.e. of the order of 10^2 to 10^3 S/cm. In the late 1980's conductivities greater than 10^5 S/cm were reported which is comparable to the room-temperature conductivity of copper, namely 6.5 x 10^5 S/cm [26, 27, 28, 29, 30]. Stimulated by these exciting results, within the following years much of academic and industrial research has been done. However, until now CPs are still far away from substituting normal metals as conductors, because of their susceptibility to environmental conditions (like oxygen) and the difficulties in

---

[1]From a chemical point of view Lewis acids are electron-pair accepting and Lewis bases are electron-pair donating compounds.
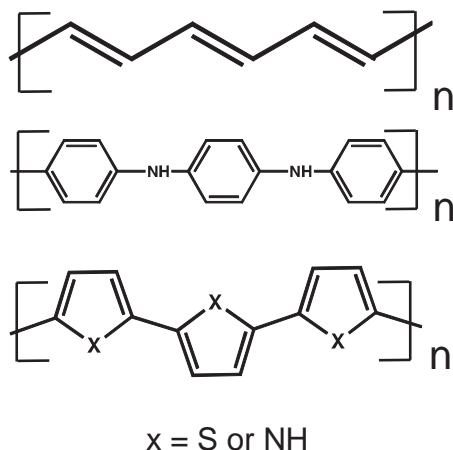
x = S or NH

Figure 2.1: Examples of conducting polymers: a) trans-polyacetylene (PA), b) polyaniline c) polypyrrole (for X = NH) and polythiophene (for X = S).

handling them. Considerable work has been done to solve these problems. New CPs with higher environmental stability were found and improved conditions of synthesis led to an enhanced stability and structural uniformity. New applications were proposed, giving hope for more promising applications of CPs and their use in a wider range of device applications and technologies[2]. Fig. 2.2. gives a rough overview of possible applications. To date commercial products based on CPs are in the form of protecting layers against metal corrosion or light emitting diodes (LEDs). First prototypes of LED displays made from CPs already exist and are probably on the way to become a commercially available product.

2.2   Structure and Electronic Properties of Conducting Polymers

As mentioned above, CPs are π-conjugated polymers with alternating double and single carbon-carbon bonds[3]. They are built from n basic molecular units to form a polymer by chemical or electrochemical polymerization reactions. In CPs the carbon atoms are sp^2 hybridized. Beside the normal carbon-carbon σ-bond an additional overlap of the p_z-orbitals are possible, which are perpendicular to the C-C-backbone. This overlap forms a weaker carbon-carbon π-bond, as shown in Fig. 2.3. In the polymerized system, where in the case of PA n acetylene molecules

---

[2]For an overview of possible applications of CPs see Refs. [31] and references therein.
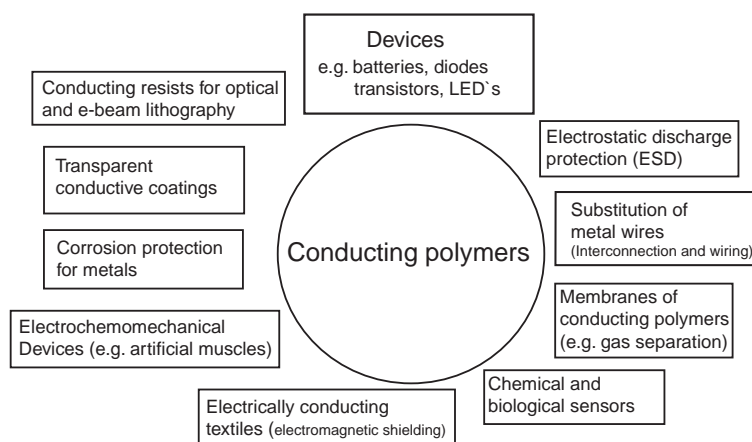[3]For an overview see [32, 33, 34]

Figure 2.2: Applications for conducting polymers.

are connected, the individual π-wavefunctions can overlap with the neigbouring once and form the broader energy bands. By increasing the number of repeating units n one would expect to obtain a complete delocalization of the π-electron cloud over the complete molecule. This would result in a metallic behaviour (Fig. 2.3.b)).

A theoretical description of the electron structure of CPs is given by the method of the linear-combination of atomic orbitals to form molecular orbitals (LCAO - MO). The expected situation is shown in Fig. 2.3.c). By increasing the number of monomeric units n to infinite the gap E_g between the highest occupied molecular orbitals (HOMO), which form the valence band (VB), and the lowest unoccupied molecular orbitals (LUMO), which form the conduction band (CB), vanishes. The electrons should be completely delocalized over the polymer molecule which should therefore be metallic. But this simple picture is *wrong* because of the Peirls instability. PA as well as other CPs are intrinsic semiconductors. Instead of equal bonds, double bonds alternate with single bonds. Because the bonds have different length, the unit cell is doubled. Instead of having a half filled band (metal), the new valence band is completely filled (insulator) and a gap is formed at the Fermi level. The gap formation allows the system to lower its energy.

Beside the electronic part of the Hamiltonian which describes the behaviour of the π electrons, a vibrational part must be taken into account in the quantum mechanical calculations within the LCAO-MO theory, which has been done by Su, Schrieffer and Heeger, so-called SSH-Theory [35]. The system reduces its energy by a slight distortion leading to different bond lengths. The completely filled valence band is in a lower energy state in comparison to the undistortet
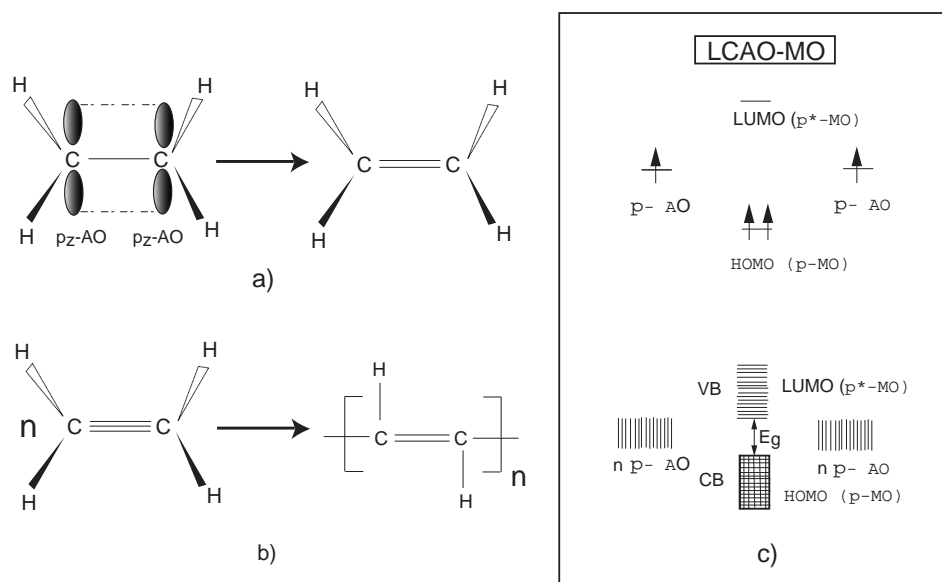
Figure 2.3: a) π-bond formation by overlap of two p_z-orbitals of ethylene, b) PA as a conjugated π-system with alternating single and double bonds b) Band formation of a conjugated system according the LCAO-MO-theory.

situation (Fig. 2.4.a)) with equal bond lengths which is shown in Fig. 2.4.b). This sort of transition was described by Peierls, known as Peierls transition [36].

The double bonds cannot be considered as individual entities, they are a part of a collective, so-called conjugated system, a well known phenomena in organic chemistry. Many natural products, such as β-carotene, the orange pigment in carrots, maintain such conjugated π-systems of alternating single and double bonds. From the viewpoint of solid state physics such collective systems represent a charge density wave in a π-electron system. The double bond contains more electrons than a single bond. Therefore the electron density oscillates periodically along the chain. If the system is disturbed at one side the whole system will be affected. The pertubation can propagate along the chain.

2.3   Conjugational Defects by Doping

Conjugational defects within a π-electron system can be realized by changing the number of electrons within the polymer chain. This can be done by exposing CPs to oxidizing or reducing agents (dopants), by exposure to light (photogeneration), or by charge injection either induced by a gate electrode or bound functional chemical groups which act as electron donors or acceptors. Electron

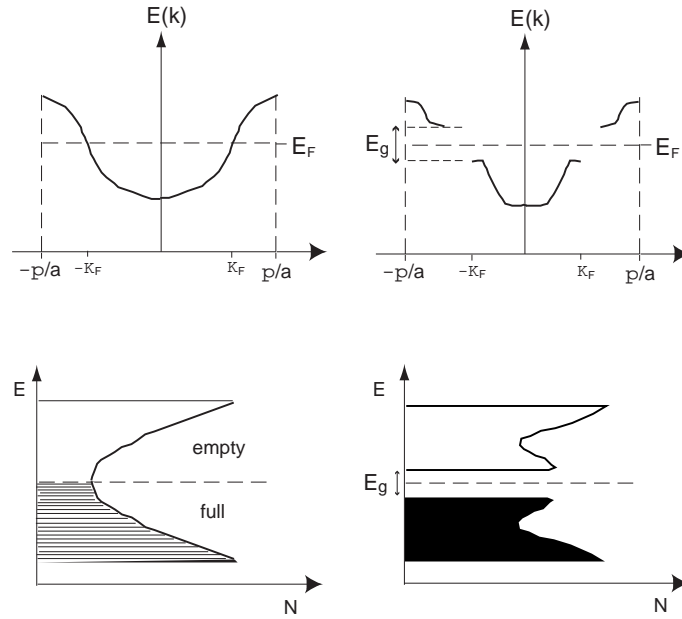Figure 2.4: a) Electron dispersion relation for the metallic state of PA without any Peierls distortion. b) Electron dispersion relation after the Peierls transition in PA. A gap is formed. The Fermi Energy E_F is in the middle of the gap.

transfer steps occur between the two partners, one is donating electrons (reducing agent), the other is accepting electrons. The polymer chain acts as electron donating agent in the case of p-type doping. Conjugational defects like radicals or radical cations (positively charged radicals) occur in the chain. In the case of electrochemical doping, a positiveley charged electrode (anode) acts as electron acceptor (oxidizing agent). Conjugational defects are induced in CPs just after polymerisation and covering the elctrode. The negatively charged ions of the electrolyte act as dopants stabilizing and localizing the electrochemically induced positively charged defects.

Only p-type doping is important for CPs, because n-type doping is difficult to obtain due to the specific structural instabilities of the CPs. Various defects can be created this way, either neutral or charged ones. They can also have a spin. Two neighbouring defects can combine and build up a self-standing structural and conjugational defect. Fig. 2.5.b) shows some examples of various possible defects in trans-PA. Every defect can be treated like a quasi-particle and be formally described as a soliton, polaron, bipolaron and so on. In Fig. 2.5.c) the polaron and bipolaron defects of polypyrrole or polythiophene are shown. Every local defect could be regarded as a local suppressor of the Peierls transition, each

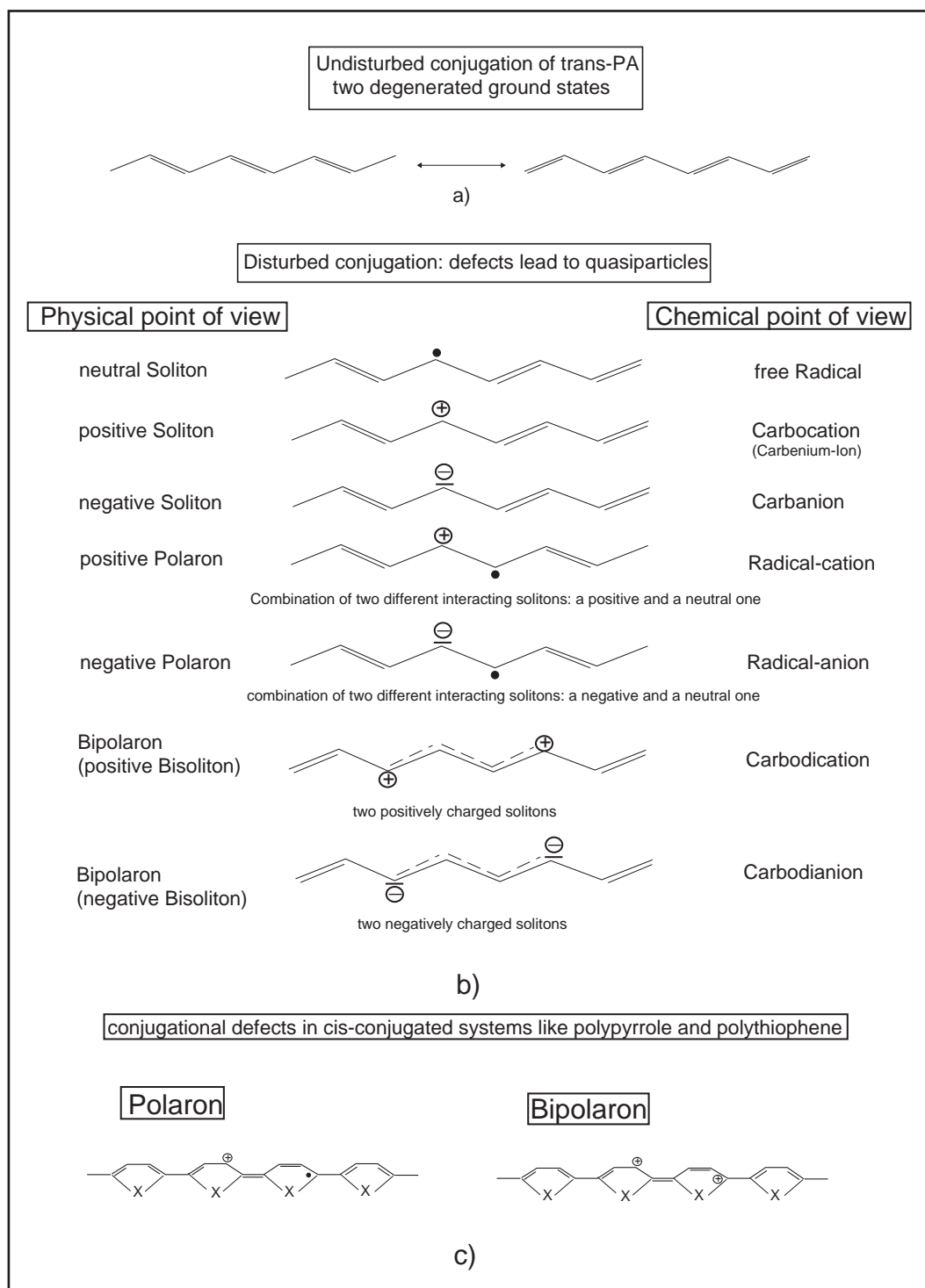Figure 2.5: a) Two possible degenerated ground states for trans-PA (undisturbed conjugation); b) Different kind of defects due to disturbed conjugation of the π-electronic system. At the left site the physical expressions and at the right site the chemical expressions for these defects are mentioned; c) Conjugational defects in cis-conjugated systems like polypyrrole and polythiophene are shown.

forming an electronic state in the middle of the gap. The midgap state can be unoccupied or it can carry one or more electrons, depending on the charge of the defect. Every defect is created as a pair, e.g. as soliton/antisoliton pair, because of the conservation of the particle number. An uncharged soliton can diffuse freely along the polymer chain and recombine with an antisoliton of a different soliton defect. It is also possible that an interaction of the defects located at different chains occurs, leading to an increased localization.

In the case of the used CPs polypyrrole, polythiophene an poly-3-methyl-thiophene only polarons and bipolarons as conjugational defects are important. A polaron can be considered as a bound state of two interacting solitons, a charged one and a neutral one, otherwise annihilation would take place. A bipolaron can be considered as a bound state of two equally charged solitons, stabilized by the Coulomb repulsion: the interchain interaction pushes them together, the electrostatic repulsive force keeps them apart. It is built when two polarons approach each other and the neutral solitons annihilate. Two charged solitons remain and build a bipolaron. For a polaron and a bipolaron there exist two states in the gap because it consists out of two solitons. Because of their interaction their levels are pushed out of the midgap and approach the edges of the valence and the conduction band which is indicated in Fig. 2.6..

With increasing doping levels more and more states within the gap should occur forming a band structure. One would expected that the gap will be closed and metallic behaviour could be investigated, which actually could be seen for highly doped trans-PA [37]

2.4   Electrochemical Synthesis of Conducting Polymers

CPs can be synthesized either chemically or electrochemically [38] mostly, by an polymerisation reaction with radicals as reactive agents[4]. With the exception of PA all important CPs can be produced electrochemically by anodic oxidation. In this method the polymer film is formed directly on the electrode surface, being in its doped (conducting) state. In comparison to standard chemical procedures this method is advantageous, in the sense of control of the growth process and the possibility of performing further investigations by electrochemical and/or spectroscopical techniques.

The electrochemical synthesis of polypyrrole, polythiophene and poly-3-methyl-thiophene can be realized under different experimental conditions which lead to different film morphologies and different values of the electric conductivity. The schematics of the electrochemical cell used in this method is given in Fig. 2.7..

---

[4]An example of the polymersation mechanism (for polypyrrole) is given in Appendix A [39, 40]
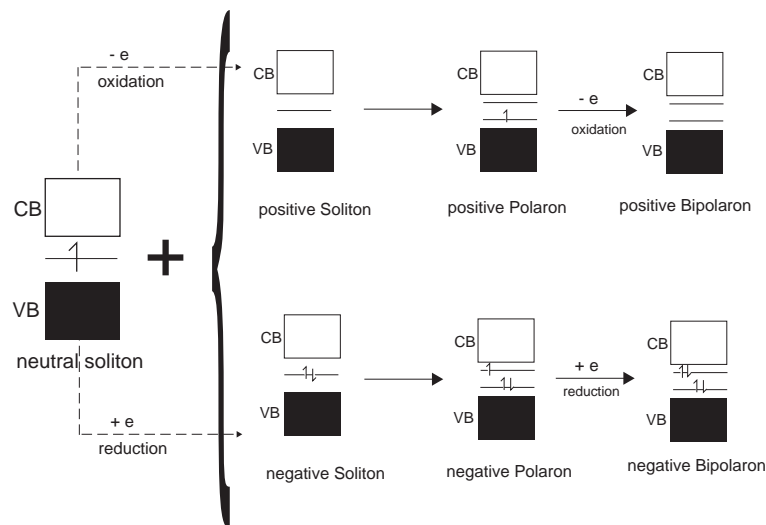
Figure 2.6: Polaronic and bipolaronic states within the gap between the valence band and the conduction band.

Between the working electrode and the counter electrode, separated by an ionic solution, a voltage is applied and the current is measured simultaneously. The third so-called reference electrode is kept at a fixed and stable reference potential. The potential between the working electrode and the reference electrode is controlled automatically by a potentiostat. The current flows between the working electrode and the counter electrode, therefore the potential drop of the working electrode/solution interface can be measured with respect to the fixed reference potential of the reference electrode[5].

The primary role of the ions in the solution as a background electrolyte is to carry the current in the bulk solution between the working and the counter electrode. Most of the potential drops at the electrode/solution interface, so-called Helmholtz layer[6]. Consequently, there is a very high electric field at the surface of the electrodes depending on the applied voltage. This high field leads to electron transfer processes between the electrode and the molecules in the solution near the electrode surface. Electrons can be put on the molecules (reduction

---

[5]No current is flowing between the working and the reference electrode.

[6]This layer which corresponds to the simplified picture of a one-ion thick layer on the electrode surface.
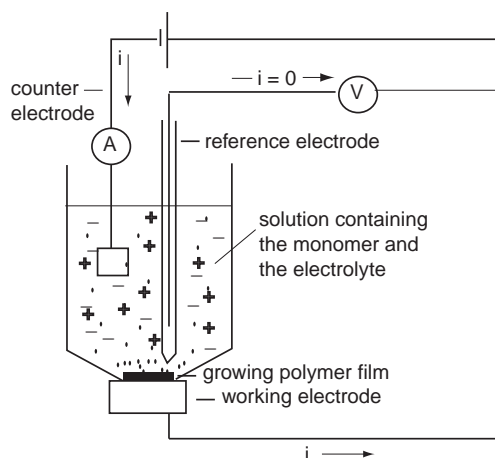
Figure 2.7: Electrochemical cell with a three-electrode alignment for the electrochemical synthesis of CPs.
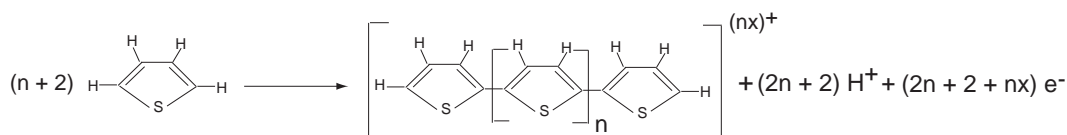
Figure 2.8: Formula for the synthesis reaction of polypyrrole or polythiophene.

process) or removed from them (oxidation process) due to the applied voltage. Hence, the electrochemical current can act as an oxidizing or a reducing agent.

The electrochemical polymerisation takes place at the interface of the anode (positively charged working electrode) and the solution, where monomeric units of pyrrole or thiophene are oxidized at a certain applied potential forming reactive radicals. These radicals can undergo further polymerisation reactions with additional monomers to oligomers and polymers. Increasing chain length of the thus-synthesized oligomers or polymers leads to their insolubility in the solvent, and they are deposited on top of the electrode forming a uniform film. Additional growth and crosslinking to other polymer chains or oligomer chains occurs. Further oxidation of the deposited polymer creates conjugational defects like polarons and bipolarons, which are responsible for the conducting state of the polymer. The positively charged film attracts some negatively charged counter ions (dopants) because of the charge balance. The dopant localizes the polaronic or bipolaronic defect, and can also build bridges between two defects localized at different polymer chains [41].

Figure 2.9: a) Typical *I-t* graph for the potentiostatic growth of polythiophene at +1.9 V vs. standard calomel electrode (SCE) in propylene carbonate (0.4 M thiophene, 0.1 M LiClO$_4$) b) Typical *I-V* graph of a cyclic-voltammetric grown thin film of polythiophene (film thickness below 1 μm), scans between -0.2 V and +1.8 V in propylene carbonate (0.1M LiClO$_4$ and 0.4 M thiophene with a scan velocity of 25 mV/s).

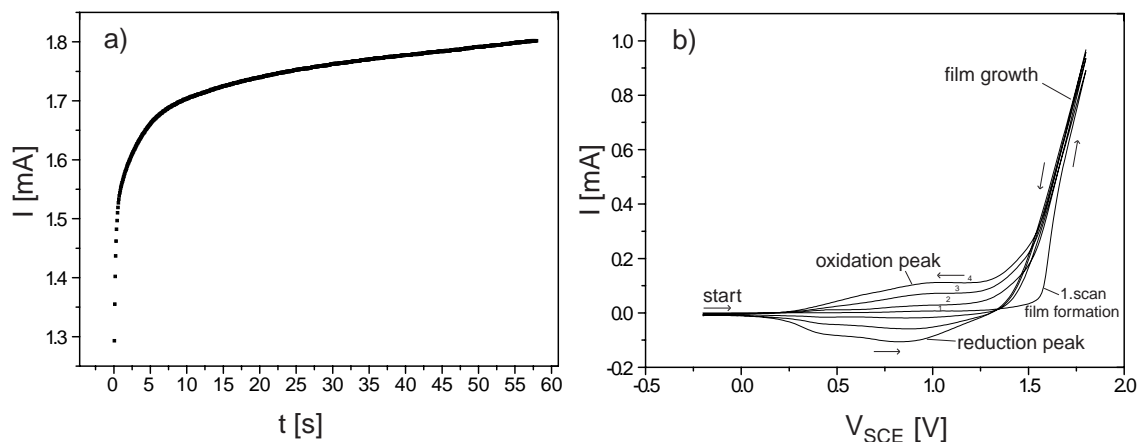In the polymerisation process two electrons per molecule are required for the film formation, and the additional charge of 0.25 to 0.4 electrons per molecule for the partial reversible oxidation (doping) of the film (depending on the doping level). This means that every 3rd to 4th monomeric subunit of the polymer film is charged[7]. The electrochemical stoichiometry of the polymerisation and oxidation processes is shown in Fig. 2.8.. By polymerisation of $[n+2]$ monomeric units $[2n+2]$ electrons are used for the polymerisation itself, while the additional charging of the polymer film requires nx electrons $[x = 0.25 - 0.4]$. It can be seen that $[2n+2]$ free protons are produced during the reaction, reducing the pH-value of the solution (Figure 2.8.). The thickness of the deposited film can therefore be controlled by the charge passed during the deposition process. The electrochemically induced film growth can be realized by holding the applied positive potential constant (potentiostatical growth), by sweeping the potential in a cyclic manner (cyclic voltammetric growth) or by holding the current density constant (galvanostatic growth). Characteristic *I-t* graphs for the potentiostatic growth of polypyrrole and *I-V* graphs for the cyclic-voltammetric growth of polythiophene are shown in Fig. 2.9..

In our case, the films were synthesized mainly under potentiostatic conditions,

---

[7]Since the concentration of dopants is relatively high, the optical, mechanical and overall physical properties of the doped film are often quite different from those in the undoped state.

and in some cases also under cyclic-voltammetric conditions. Cyclic-voltammetry in a pure monomer-free solution was used to reduce and reoxidize the film in a reversible way in order to investigate the film behaviour with respect to the doping state. The parameters of synthesis (applied voltage, solvent, monomer concentration, dopant, temperature, electrode material, current density, water and oxygen residues in the solvent, etc..) influence the morphology and conductivity of the polymer film drastically. The solvent used must have a high dielectric constant, in order to ensure the ionic conductivity by dissolving and dissociating the supporting electrolyte. It also must be stable in the voltage range where the polymerisation and oxidation of the monomer takes place.

2.4.1 Electrochemical Synthesis of Polypyrrole Films

Polypyrrole films were synthesized under different experimental conditions[8], in order to obtain information about the bulk conductivity and stability of the synthesized film. Polypyrrole ist the only CP which can also be synthesized in an aqueous solution, in contrast to other CPs like thiophene and 3-alkyl-substituted thiophenes where the use of organic solvents is necessary.

Our first synthesis of polypyrrole films in concentrated phosphoric acid and under cyclic-voltammetric growth conditions led to poorly conducting films being $\sigma = 0.008 - 0.06$ S/cm [42]. Potentiostatic growth in phosphoric acid yielded films of a bad stability. By using $LiClO_4$ as the dopant in water an improvement in film conductivity has been achieved. Conductivities of about 0.2 S/cm (cyclic-voltammetric growth) and 0.3 - 7 S/cm, depending on the monomer concentration (potentiostatic growth at +0.8 V), were obtained. Relatively brittle films with a characteristic flower-like rough surface structure were obtained as well (Fig. 2.10.a)). On the same figure two SEM images of surface structures of poly-3-methyl-thiophene, grown under different conditions of synthesis are shown for comparison.

---

[8]The chemicals and solvents used were distributed by " Fluka" (Switzerland) if not specified otherwise. The deionized water used had a resistivity value of $18\,G\Omega cm$. The electrochemical synthesis and cyclic-voltammetric observations of the polymer films were carried out using a EG&G (USA) 263 A potentiosatat/galvanostat. Pyrrole always was distilled immediately before use. Oxygen was removed from the solvents (water, phosphoric acid, propylene carbonate, acetonitrile), by treatment in an ultrasonic bath and by subsequent blowing of nitrogen through the solvent for 30 minutes before use. A self-made electrochemical cell of the type shown in Fig. 2.7. was used having $0.25\,cm^2$ area for the film deposition on the working electrode. The working electrode (gold) was fabricated by using a glass substrate $d = 18\,mm$, on to a Ti or Cr adhesion layer (10 - 20 nm in thickness) and a gold layer (30 - 50 nm in thickness) was deposited. As the reference electrode a saturated standard calomel electrode (SCE) in saturated KCl solution was used (the reference potential is +0.2415 V with respect to the standard hydrogen electrode), supplied by "Radiometer" (France). As the counter electrode a platinum foil ("Goodfellow", UK) with an area of about $4\,cm^2$ was used.
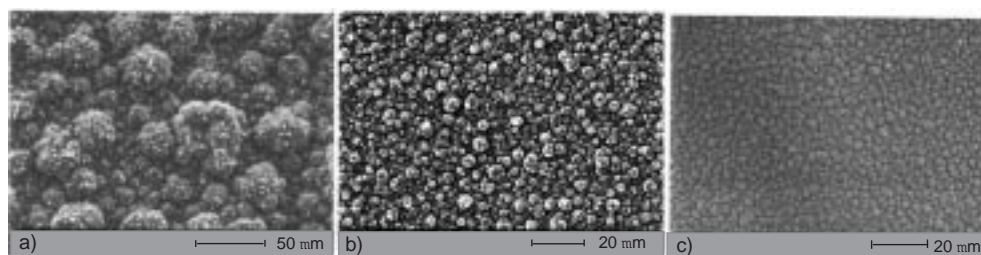
Figure 2.10: SEM pictures of the surface of different CPs synthesized under potentiostatic conditions: a) Polypyrrole, grown at +0.8 V in an aqueous solution with LiClO$_4$ as the dopant (0.33 M Pyrrole, 0.1 M LiClO$_4$). The film thickness is 7-8 μm; b) Poly-3-methyl-thiophene grown at +1.9 V in propylene carbonate with LiClO$_4$ as the dopant (0.2 M 3-methyl-thiophene, 0.3 M LiClO$_4$). The film thickness is 6 μm; c) Poly-3-methyl-thiophene grown at +1.9 V in propylene carbonate with tetraethylammonium-hexafluorophosphate as dopant. The film thickness is 18.5 μm.

The conductivity values decreased in time, especially fast for the perchlorate doped films. The cyclic-voltammetry shows irreversibility, especially for thicker films, of some microns and more in thickness (not shown). The reduction and oxidation peaks are quite broad. The oxidation peak cannot be resolved because the current response of the growing film is just starting within the same potential window, leading to an overlap of the oxidation peak (Fig. 2.11.a)).

By using para-toluenesulfonic-acid as electrolyte in water a further improvement in the film conductivity was achieved, yielding 11 - 80 S/cm for films, grown at +0.8 V under potentiostatic conditions. The films were stable, easy to handle and flexible. The cyclic-voltammetric investigation showed a better reversibility (Fig. 2.11.b)).

The best film quality was obtained with tetraethylammonium-hexafluorophosphate as electrolyte in water, resulting in conductivity values between 10 and 32 S/cm. These films were much smoother and more flexible. The polypyrrole films with higher conductivity values show a good reversibilty in the cyclic-voltammetry. In Fig. 2.11.b) a cyclic-voltammetric investigation of a potentiostatically grown thin polypyrrole film of a higher conductivity is shown. This curve was measured after the film was washed and treated by monomer-free electrolyte solution. By increasing the potential to higher values a loss of redox activity of the film occurs. The experimental conditions (monomer concentrations, electrolyte concentrations, applied oxidation potentials) are given in Table 2.1. in more detail. The conductivity mesurements were done using the method of van der Pauw [50, 51], described in subsection 2.4.4., especially for the brittle polymer

solvent system and methode	concentration of monomer [M/l]	electrolyte [M/l]	conductivity range [S/cm]	resistivity range [Ohm cm^{-1}]	film characteristic
phosphoric acid (H_3PO_4, 85%),cyclic-voltammetric conditions (CV), scans between -0. 2V to +1.3 V	0.5	is highly concentrated	0.01 - 0.06 v. d. Pauw method	16 - 100 DC measurement	black brittle films, quick decrease of conductivity, low reversibility of charging and discharging the films;
water (deion.) with $LiClO_4$ as electrolyte, CV between -0.8 and 1.15 V	0.5	0.1	0.1 - 1.0 v.d.Pauw method	1 - 10 DC measurement	black films with a rough surface, brittle, low reversibility of charging and discharging the film, inhomogenity of the thickness;
water (deion.) potentiosatatic growth at +0.8 V with $LiClO_4$ as electrolyte	0.3 - 0.5	0.1- 0.4	1 - 6 films were pressed over structured Au electrodes, DC and AC measurements	0.17 - 1	black films, better stability and handling of the film was possible, film thickness is still quite inhomogenious, within one week, more than 50 % loss in conductivity was recognized;
propylene carbonate potentiosatatic growth at +0.8 V $LiClO_4$ as electrolyte	0.3 - 0.5	0.2 - 0.4	1 - 5 films were pressed over structured Au electrodes, AC measurements	0.2 - 1	black films, good mechanical stability and handling of the film was possible,film surface becomes smoother cyclic-voltammetry shows more reversible behaviour;
water (deion.) potentiosatatic growth at +0.8 V with p-toluenesulfonic acid as electrolyte,	0.1- 0.3	0.1 - 0.3	11 - 80 films were pressed over structured Au-electrodes, AC measurements	0.0125 - 0.091	black stable films with a high elasticity and density, the films are more smooth and can be strechtched; cyclic-voltammetry shows more reversible behaviour;
propylene carbonate potentiosatatic growth at +1.0 V (Et)$_4$NPF) as electrolyte,in some cases 1% of water was added to the organic solvent but without substantial influence of the conductivity;	0.05 -0.1	0.06 - 0.1	7 - 42 films were pressed over structured Au electrodes, AC measurements	0.024 - 0.143	the conductivity decrease within one week is less than 50 %, the black films show a good mechanical stability with a more open structure of less density; these films have the lowest loss of conductivity as a function of time;

Table 2.1: Synthesis conditions for polypyrrole films and the related values of the conductivity and the resistivity. The values given are the lowest and the highest one which were found and have no statistic significance.
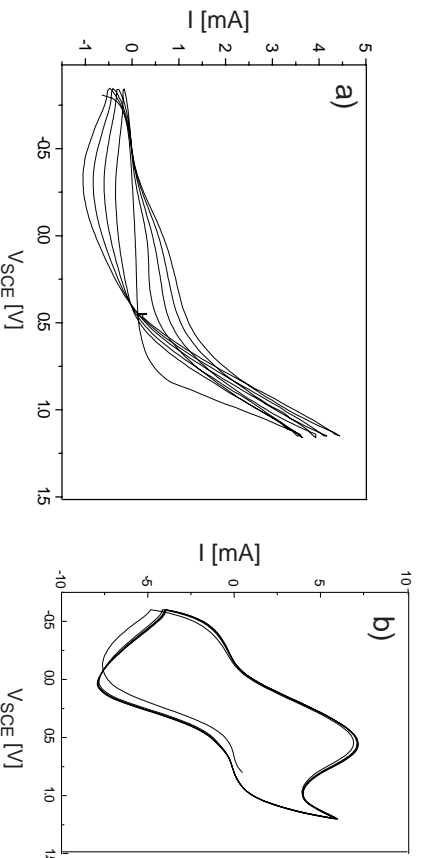
Figure 2.11: a) *I–V*-curve of the cyclic-voltammetric (CV) synthesis of polypyrrole in aqueous solution (0.5 M) with LiClO$_4$ as the dopant (0.1 M) between -0.85 V and +1.15 V; 5 scans were made at a scan velocity of 25 mV/s. The oxidation and reduction signals are more flat. The current increase for film formation is overlaying the oxidation peak. b) CV of a potentiostatically grown polypyrrole film (0.1 M in aqueous solution with p-toluenesulfonic acid (0.1 M) as the dopant at V = +0.8 V) in a monomer-free aqueous solution of p-toluenesulfonic acid (0.1 M); scan range: +0.8 to -0.6 V$_{SCE}$ and scan velocity: 2000 mV/s;

films. More flexible films can be cut into a square or rectangle shaped film, and pressed over four gold contacts in order to measure the resistivity. The film thickness of the measured films were 5-10 μm[9]. Both measurement methods employed are four-terminal methods, allowing to measure the intrinsic film resistivity. Because the thickness varied within the films the conductivity values are not very accurate. Table 2.1. summarizes our results. The highest and lowest measured resistivity values are reported.

Discharging of the so called p-doped polypyrrole films by applying a negative voltage lead to a decrease of the conductivity. Recharging the films in order to reach the original value of the conductivity was not possible for any of the polypyrrole films investigated. This indicates an irreversibility in the film behaviour, probably related to a loss of the redox activity. Such conclusion is supported by the cyclic-voltammetry, were the peak heights of the oxidation and the reduction processes decreased in time. Irreversible reactions with oxygen or water, especially at higher positive potentials, are well-known phenomena in polypyrrole [43, 44, 45]. These overoxidation processes lead to irreversible structural changes,

---

[9]If the thickness was lower it was almost impossible to scratch off the film from the electrode without destroying it, especially for the more brittle films with lower conductivies.

defects in the polymer chains, and consequently to lower conductivity values.

In the case of poly-3-methyl-thiophene with the hexafluorophosphate anion as dopant such overoxidation processes seems to play a minor role, as seen by a better reversibility of the oxidation and reduction. It is possible to discharge and recharge the poly-3-methy-thiophene films, restoring the original values of conductivity (subsection 2.4.4.). For this purpose the synthesized black conducting film was pressed onto a structured gold electrode (schematically shown in Figure 2.16) and reduced within a monomer-free solution of the electrolyte. At different points of the discharging process, the film conductivity was measured ex situ. Because of the thickness of the film, only the upper surface part of the film which is in contact with the solution is affected to the reduction process. Therefore no infinite value for the resistivity was observed.

2.4.2 Electrochemical Synthesis of Polythiophene and Poly-3-Methyl-Thiophene Films

The electrochemical synthesis of polythiophene and poly-3-methyl-thiophene films were usually done in propylene carbonate as the solvent[10]. Our first experiments by using highly-concentrated phosphoric acid or acetonitrile as the solvent systems led to films of lower quality. In case of acetonitrile, the gold electrode was usually attacked and partially dissolved, probably because of the reaction of gold with cyanid ions in the solution. Potentiostatically grown films of polythiophene and poly-3-methyl-thiophene were synthesized at high positive potentials ($1.9 - 1.95\ \mathrm{V}_{SCE}$). The black films were rather flexible, having high elasticity and mechanical stability. An example of a cyclic-voltammetric synthesized film of polythiophene has been shown in Fig.2.9.b). In Fig. 2.12. a cyclic-voltammetric investigation of a p-doped polythiophene film with perchlorate as the dopant anion is shown. After the cyclic-voltammetric synthesis, the film has been washed in a monomer-free solution before the further cyclic-voltammetric investigation was carried out in propylene carbonate containing the same concentration of the background electrolyte as during the synthesis. The poly-3-methyl-thiophene films show even better visible oxidation and reduction peaks, in comparison to the polythiophene films grown under the same experimental conditions and investigated under identical cyclic-voltammetric conditions (not shown).

The conductivity values of the polythiophene films grown under potentiostatic conditions at $+1.9 - 1.95\ \mathrm{V}_{SCE}$ in propylene carbonate with $LiClO_4$ as the supporting electrolyte is of the same magnitude as in the case of comparable polypyrrole films, and is in the range between 0.5 and a few S/cm,(measured with the van der Pauw method). The typical concentrations of the monomer

---

[10]Polythiophene and poly-3-methyl-thiophene was stored in the fridge and used without further purification.
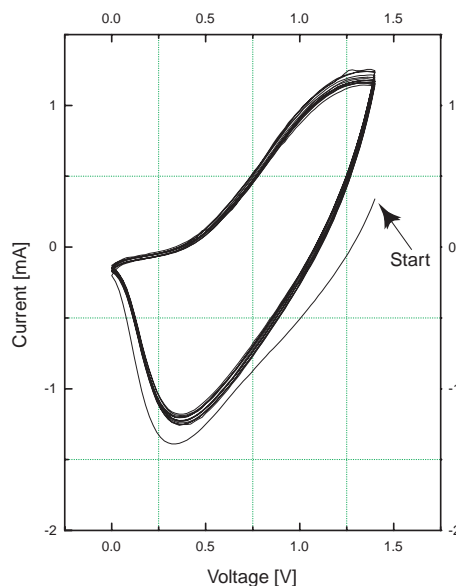
Figure 2.12: Cyclic-voltammetric investigation of an polythiophene film within +1.4 V and +1.9 V in monomer free propylene carbonate containing 0.1 M LiClO$_4$ (scan rate 100 mV/s).

and the electrolyte varied between 0.1 M and 0.4 M. In the case of poly-3-methyl-thiophene the conductivities are significantly higher, 30 - 50 S/cm, for the same solvent and electrolyte system.

By using ((Et)$_4$NPF$_6$) as the dopant salt the conductivity increased again to values between 64 and 154 S/cm. If the synthesis would be carried out at lower temperatures (5° C), one would expect even higher values for the conductivity [46]. The typical concentration of the monomer in this case was between 0.1 M and 0.4 M and for the electrolyte 0.1 M or 0.2 M. The thickness of the measured films varied between 8 and 20 μm, otherwise it was difficult to scratch off the film from the Au electrode without destroying it. The decrease of conductivity in time was much lower than for the polypyrrole films. For poly-3-methyl-thiophene films with hexafluorophosphate as the doping anion reversibility of the conductivity due to the doping state was found. By discharging of the oxidized film the conductivity was measured ex situ and decreased a few orders of magnitude. Subsequent recharging of the film led to the same initial value of the conductivity. This shows that films of poly-3-methyl-thiophene have a good reversibility in their redox behaviour and that effects like overoxidation processes play a minor role, when compared to the polypyrrole films. Fig. 2.13. shows the change of the sheet resistance during discharging the poly-3-methyl-thiophene film at +0.2 V$_{SCE}$ and
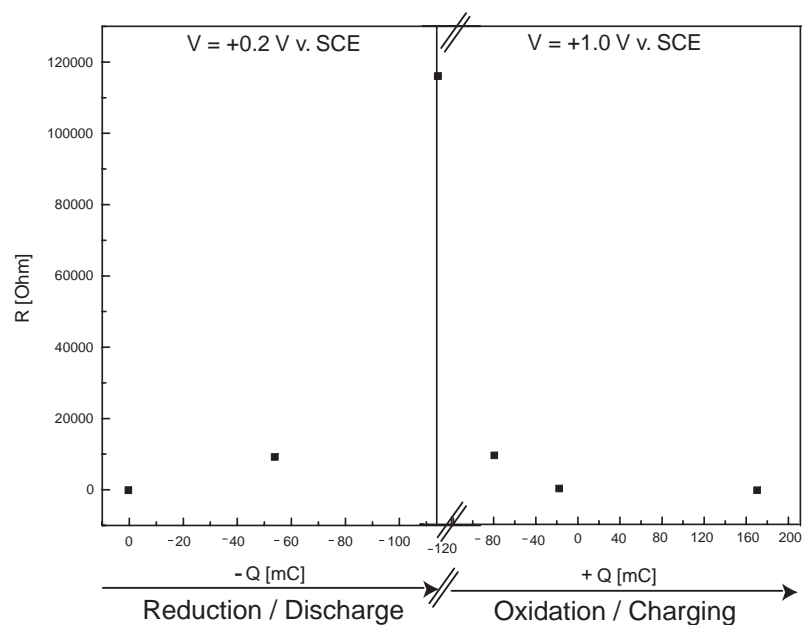
Figure 2.13: Sheet resistance of a potentiostatically grown poly-3-methyl-thiophene film versus discharging and recharging. The original value for the resistance was restored after recharging, indicating the reversibility of the oxidation and reduction processes.
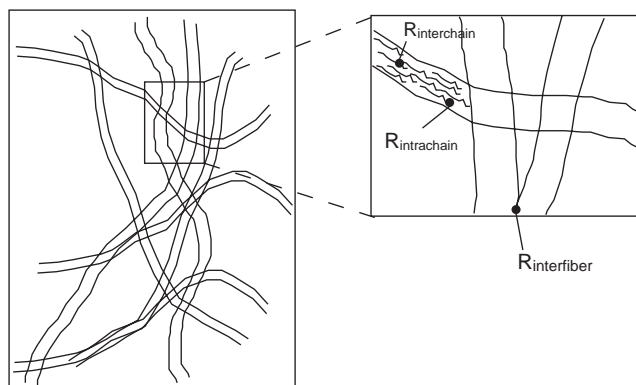
Figure 2.14: Schematic of a random fiber polymer structure as in the case for trans-PA. The total resistance is a sum of at least three different parts.

recharging the film at $+1.0\,\mathrm{V}_{SCE}$. The charged state of the film after its synthesis is set to zero charge (reference point for the following discharging and recharging). The initial conductivity value was 69.17 S/cm, and after the discharge this value decreased approximately by five orders of magnitude. Recharging of the film leads to the conductivity value of 68.68 S/cm, which is very close to the initial value[11].

2.4.3   Conductivity of Conducting Polymers

Films of CPs have no specific structure. A polymer film of PA contains many randomly distributed fibers, similar like spaghetties laying on a plate. Each fiber is a bundle of 100 - 1000 polymer chains. Different fibers are connected by inter-fiber contacts building up larger areas which can be detected by surface-imaging techniques like AFM or SEM. The measured conductivity is influenced by the intra-chain resistance, inter-chain resistance and an inter-fiber resistance (Fig. 2.14.)[12].

In the case of polypyrrole or polythiophene, a more grain-like structure instead of the fiber-like structure is present. Different sorts of chain, fiber or grain contacts act as barriers, and the main determining mechanism for electric conductivity is a temperature dependent hopping mechanism. In the case of amorphous semiconducting CPs the temperature dependence obeys the variable-range

---

[11]Between every charging or discharging step, the film was washed in pure propylene carbonate, in order to get rid of the free ions, and rinsed with ethanol. After pressing the film on top of the structured gold electrode and an annealing and drying step at 50°C for 20-30 minutes, the resistance was measured by a lock-in technique.
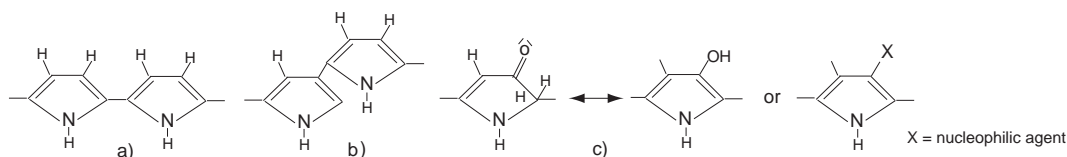
[12]For an overview see Ref.[33].

Figure 2.15: a) α-α connected monomers, leading to an undisturbed conjugated system; b) α-β connected monomers leading to pertubations within the conjugated sytem; c) Defects caused by side reactions; the radical cationic species can react with water or other nucleophilic agents, forming products with disturbed π-conjugation.

hopping model (VRH) of Mott [47]. Therefore the measured bulk conductivity is mainly determined by the three-dimensional structural inter-connecting effects and does not resemble the intrinsic conductivity of a single polymer chain. Dopant ions can act as bridges between two structural defects and can lower the hopping barrier between chains or fibers, leading to a higher bulk conductivity with increasing doping level. Even within a single polymer chain structural defects can occur, limiting the conductivity. Besides the normal α-α connection of the monomeric units in poypyrrole, the α-β connection can occur as a side reaction affecting 5-10% of all molecule connections, leading to an irreversible structural defect. Reactions of the CPs with oxygen or nucleophilic agents in the β-position of the radical cation structure, lead to such disturbations of the conjugated π-electron system, with the consequence that the conductivity is lowered (Fig. 2.16.)).

Principle of the Conductivity Measurements

Because of the inhomogenious structure of CPs, the conductivity values can vary either from sample to sample or even within a sample, especially if the temperature, pressure or the doping level are changed. Inhomogenity can also lead to an anisotropy of the conductivity within a sample. For example stretching a film increases the conductivity because of the increased order in the direction of the stretching [48, 49]. Since the contact resistances can sometimes be quite high the four-terminal method is usually used for measuring the resistivity of a sample. The current I is applied through the side leads and the voltage V between two central contacts is measured. The setup is shown schematically in Fig. 2.16.. The resistance is calculated using Ohm's law. The resistivity and conductivity values are obtained from the relation

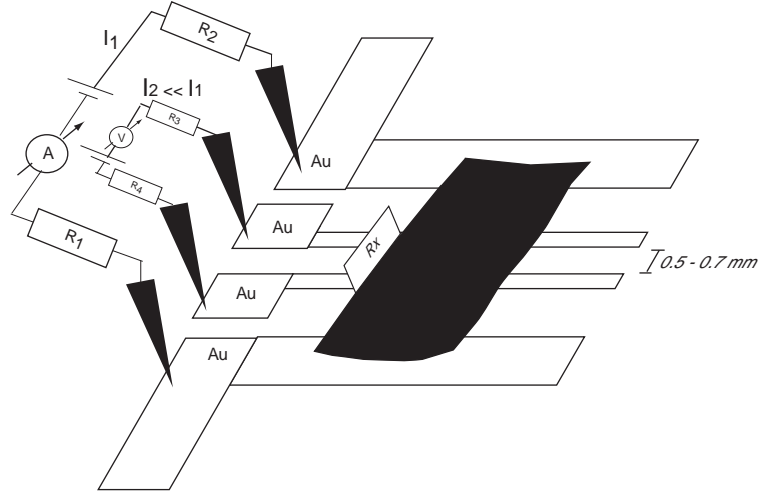$$R = \frac{\rho l}{A}, \qquad (2.1)$$

Figure 2.16: Schematics of the four-terminal method for measuring the conductivity of polymer films.

where ρ is the resistivity, l the distance between the two voltage contacts and A the cross section of a single contact. Its inverse is the conductivity

$$\sigma = \frac{1}{\rho}. \tag{2.2}$$

R_1 and R_2 in Fig. 2.16. represent the resistances of the leads and the contacts from the leads to the sample with the voltage drops $R_1 I_1$ and $R_2 I_2$. By measuring the voltage drop at the inner leads one can avoid these voltage drops. The voltage drop of the inner leads, measured by the voltmeter is the sum of three parts shown in equation 2.3,

$$U = R_3 I_2 + R_x(I_1 + I_2) + R_4 I_2, \tag{2.3}$$

where I_2 is the current flowing in the voltmeter circuit. With $I_2 \ll I_1$ the measured voltage drop U is determined by R_x even if R_3 and R_4 are much higher than R_x.

For the ex situ measurements during charging and discharging the films (Subsection 2.4.2), the films were pressed on top of the gold electrodes which where prepared by optical lithography (Appendix B). For the measurements of conductivity as a function of temperature the films were contacted by indium wires pressed on top of the films. Sometimes a silver paint was applied for additional support of the contacts. For brittle films or films with an inhomogeneous thickness d, it is difficult to determine the geometrical factor l/A. To overcome this
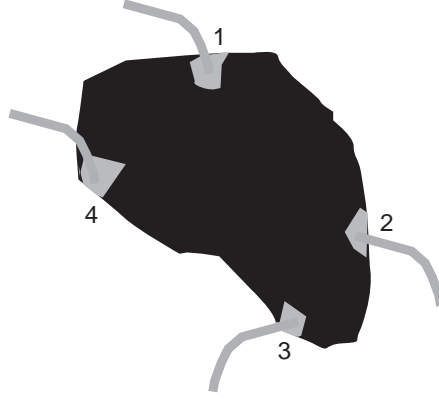
Figure 2.17: Schematic of a contacted polymer film prepared for conductivity measurements using the van der Pauw method. Indium wires are fixed with silver paint at the edges of the samples. The resistivity can be calculated using equation 2.4..

problem the method of van der Pauw [50] was used to obtain conductivity values. The van der Pauw method allows to measure the conductivity of a thin film of arbitrary shape, provided that the material is homogeneous in the measuring volume.

$$\rho = \frac{\pi d}{ln2} \frac{R_{12,34} + R_{23,41}}{2} f(\frac{R_{12,34}}{R_{23,41}}), \qquad (2.4)$$

where d is the sample thickness, $R_{12,34}$ the voltage between contacts 1 and 2 divided by the current through the contacts 3 and 4. $R_{23,41}$ is the voltage between the contacts 2 and 3 divided by the current through the contacts 1 and 4 and is obtained by a cyclic interchange of the contacts. f is a function of the ratio of the measured resistances $R_{12,34}/R_{23,41}$ and is between 1 and 0.2 for the ratio of the resistances between 1 and 1000. Tabulated data for f are found in the literature [50, 51, 52].

Hopping Transport in Conducting Polymers

The temperature dependence of electric conductivity provides important information on the transport mechanism within a sample. In the case of moderately-doped conducting polymers a hopping conductivity analogous to the one specific of amorphous semiconductors is found for a considerable number of CPs. The temperature dependence of the conductivity agrees with the VRH-model of Mott [47] with

$$\sigma = \sigma_0 exp[-(T_0/T)^{\gamma}], \qquad (2.5)$$

where γ depends on the dimensionality D of the hopping process:

$$\gamma = \frac{1}{1+D}. \tag{2.6}$$

For a three-dimensional ($D = 3$) hopping process found in bulk samples of CPs $\ln\sigma \propto T^{-1/4}$. The two parameters σ_0 (conductivity at infinite temperature) and T_0 (characteristic temperature) depend on microscopic parameters α and $N(E_F)$, where α is the inverse of the localization length and $N(E_F)$ is the electron density of states at the Fermi level.

$$\sigma_0 = e^2 N(E_F) R^2 v_{hop} \tag{2.7}$$

R is the average hopping distance, and v_{hop} is the hopping attempt frequency.

$$R = [8/9\pi\alpha N(E_F)kT]^{-\gamma} \tag{2.8}$$

and

$$T_0 = \frac{(8\alpha)^3}{9\pi k N(E_F)} \tag{2.9}$$

The VRH-model explains also the doping dependence of the conductivity quite well. The doping creates defects leading to localized in-gap states. The density of states is therefore roughly proportional to the doping concentration c :

$$ln\sigma \propto c^{-\gamma} \tag{2.10}$$

The term "hopping" is in fact a word used to describe phonon-assisted quantum-mechanical tunneling processes. The origin of these processes is in the high degree of disorder within the polymer films due to their amorphous structures, impurities and counter-ion effects. Many intrinsic and extrinsic parameters affect the charge transport in CPs (e.g. inter-chain and intra-chain interactions, the dopant ions, anisotropic diffusion of the charge carriers, etc.). To date the strongly intrinsic and extrinsic contributions to the charge transport could not be quantified and separated experimentally. The created localized states within the energy gap are randomly distributed in space as well as in energy. Electrons can hop (tunnel) from occupied to empty states, because there are sufficient excited phonons at room temperature. By cooling a sample the hopping probability decreases. The average hopping distance R decreases with decreasing temperature. Actually, it is the "variability of hopping as function of temperature", which leads to the expression "variable range hopping".

Compared to inorganic semiconductor materials, which have a well defined energy gap, CPs have a more continuous distribution of localized states in the gap, which leads to a "softer" exponential dependence of the conductivity on

temperature. For the case of a single polymer chain one would expect that the disorder has a much stronger influence on the temperature dependence of the conductivity. The lower the temperature, the less disorder is needed to localize the electronic states. In strictly one-dimensional systems as a single polymer chain, any sort of disorder will localize the states, so consequently all one-dimensional conductors should become insulators at absolute zero. This implies that the conductance cannot be scaled down to small dimensions in an easy way and that very thin wires can behave differently than their bulk components. A monomolecular chain behaves therefore differently from a molecular wire. Molecular wires as DNA, for example, have a three-dimensional structure and are not really one-dimensional systems.

The electronic behaviour of semiconducting polymers is dominated by the substantial amount of disorder, so that no finite DC conductivity for T $\rightarrow$ 0 was observed. Within the last decade the extent of disorder in doped CPs has been reduced by optimizing the conditions of their synthesis, using the improved polymer systems and stretched films. Metallic behaviour has been found for advanced polymer systems, and a disorder-induced metal-insulator transition was identified within this new generation of CPs [53, 54, 55, 56, 57, 58, 59][13].

VRH Behaviour of the Synthesized Polypyrrole Films in Aqueous Solution

Temperature dependence of the conductivity of polypyrrole films, synthesized in aqueous solution under potentiostatic conditions, with para-toluenesulfonic acid as dopant, obey the VRH-model of Mott as shown in Fig. 2.18.. The measurements were carried out in a He-4-cryostat in the range 4.2 - 300 K. A strong increase of the resistivity was observed below approximately 50 K. By plotting the logarithmic values of the conductivity σ versus $T^{-1/4}$ a linear graph is obtained, indicating that the three-dimensional VRH-model can be applied to this system to describe the temperature dependence of the conductivity. This is in good agreement with Ref.[60] where the same behaviour was found for para-toluenesulfonate anions, as well as for perchlorate- and tetrafluoroborat anions as dopant ions for polypyrrole films prepared under various conditions of synthesis. For other systems of CPs the temperature dependence of the conductance was not investigated. During the development of a method to contact single metal and CP nanowires (described in Chapter 3), it was clear that only polypyrrole wires, synthesized in aqueous solution were useful because of the incompatibility of the used protecting organic resists to organic solvents like propylene carbonate. The temperature dependence of the polypyrrole/p-toluenesulfonic acid system shows that there exist an amount of disorder, like it is expected for moderately doped
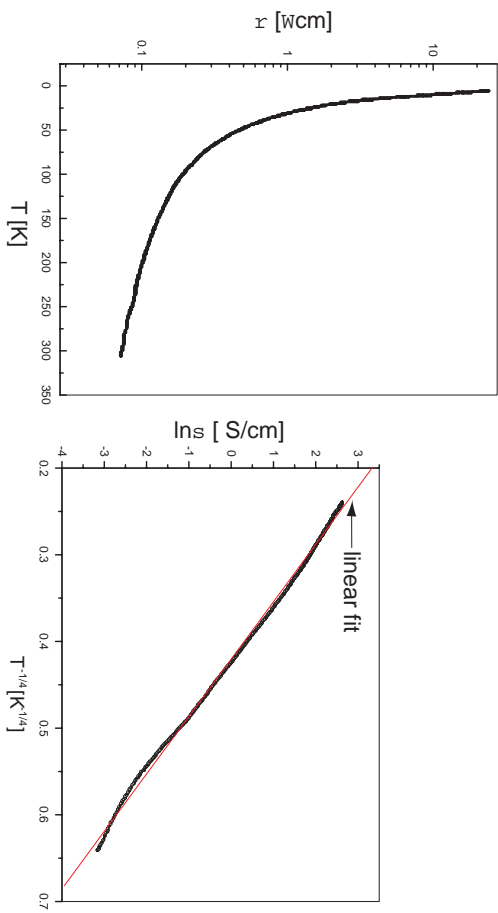
---

[13]And references therein.

Figure 2.18: a) *R-T* curve of a potentiostatically grown polypyrrole film in an aqueous solution with p-toluenesulfonic acid as the dopant (V = +0.8V, the dopant concentration 0.1 M, 0.1 M pyrrole), b) $\ln T$ is plotted versus $T^{-0.25}$. A nearly linear behaviour indicates an agreement with the VRH-model.

semiconducting CPs.

2.4.4 Film Growth of Conducting Polymers Between Two Microelectrodes

Because the experiments mentioned in subsection 2.4.2, where the sheet resistance of a poly-3-methyl-thiophene film could be restored after discharging and recharging (Figure 2.13) were very time consuming we wanted to establish a method for measuring the sheet resistance in situ as a function of the applied voltage. On top of an oxidized Si wafer we fabricated a microelectrode array with five Au microelectrodes in parallel by optical lithography (see Appendix B)[14].

Two small Au contacts separated by a gap of about $2\,\mu m$ were fabricated by EBL and Au evaporation. The inner part of such microelectrode structure is shown in Fig. 2.19.. The two e-beam fabricated Au electrodes are the voltage contacts. The left and right electrodes are the current contacts. So, a four-terminal measurement is possible. The polymer film is synthesized on top of the current contacts under the same experimental conditions described in section

[14]The same lithographical mask is used as for the four Au contact pads shown in chapter 3.6. for contacting a lateral nanowire.
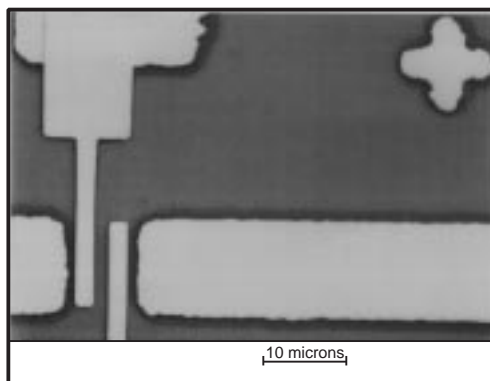
Figure 2.19: SEM image of the Au microelectrode arrangement; the bigger pads are the current contacts and the smaller pads are the voltage contacts.

2.4.. Lateral growing of the polymer film on the SiO$_2$ substrate occurs in time, reaching the voltage contacts. After the voltage contacts have been contacted by the growing polymer film, film formation between the small gap proceeds until the gap is closed. In Fig. 2.20.a-b) top-view SEM images are shown for polythiophene film formation between two microelectrodes. The polymer film is grown on top of the Au electrodes (black deposit). Fig. 2.20.c) shows a side-view image of such device.

It can be clearly seen that the lateral growth occurs beside the microelectrode arrangement as well, producing an additional contact of the electrodes. Hence the real cross-section cannot be determined to calculate the conductivity it is hardly to determine even the cross-section of the CP film between the two microelectrodes. The film growth on the SiO$_2$ surface also behaves quite differently. The structure is more cluster-like in comparison to the film parts grown on the Au electrode, as shown in Fig. 2.21.. This structural change affects the physical properties like conductivity. The measured values were by estimating the contact area were at least one order of magnitude lower than for the bulk film samples. The growth of thicker films of CPs in order to reduce the uncertainty of the cross section was not possible because shortcuts occured also at the outer parts between the different contact pads. The lateral film growth at this outer part was enhanced compared to the lateral film growth near the microelectrode arrangement (Fig. 2.21.). By depositing films of thicknesses more than 1-1.5 μm these sort of shortcuts occured.

Because of the difficulties to determine the cross-section, and low conductivity of the films grown on SiO$_2$, this microelectrode arrangement was not used to investigate the film conductivity as a function of the applied voltage.
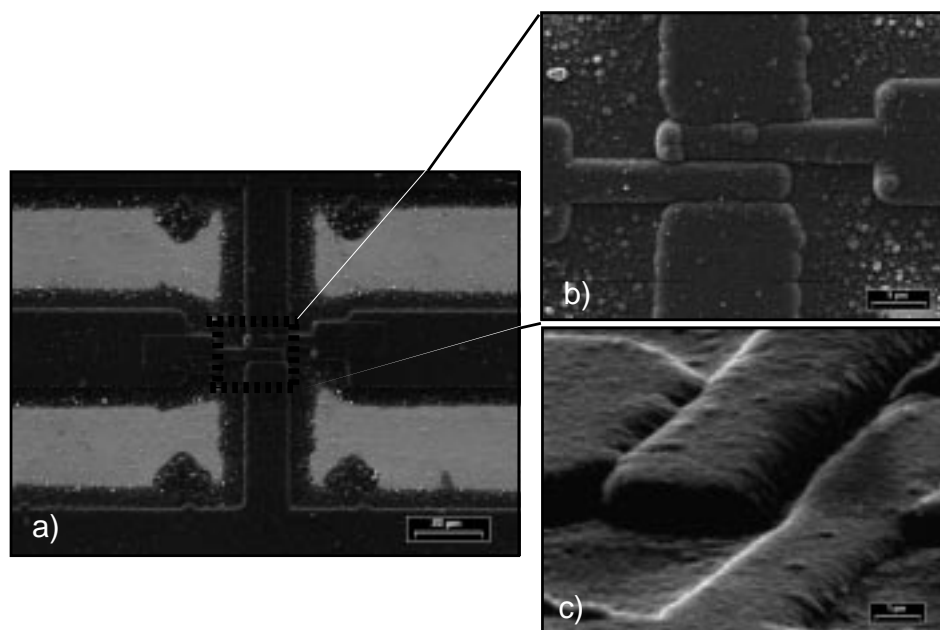
Figure 2.20: Polythiophene film deposited electrochemically on a Au microelec-
trode arrangement a) SEM top-view image: beside the microlectrodes lateral
growth of the polymer film (black deposit) occured; the film on top of SiO$_2$ has
a more roughly grain like surface structure b) SEM top-view image with higher
magnification c) SEM sideview image at 45° degree: the inner part between the
two microlectrodes are shown: the cross section is hardly to determine.
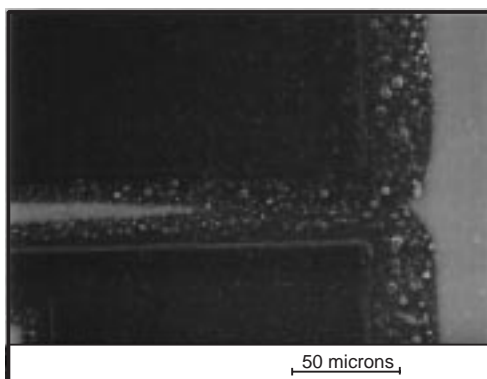
Figure 2.21: SEM image of a polythiophene film grown on top of a microelectrode
arrangement. The outer part (contact-pads) is shown. The lateral growth is faster
at the outer part producing shortcuts by connecting the two current contact pads
if film growth has not been stopped before. The polymer film grown on a SiO$_2$
surface has a more cluster-like structure.

Chapter 3

Electrochemical Template Synthesis of Nanowires

3.1   Introduction

There are different ways to create nanowires. The most usual method for creating metallic nanowires is the electron beam lithography (EBL), where a high-energy electron beam "writes" a structure in a sensitive resist layer. In combination with the selective dissolution of the exposed resist area, metal evaporation and a subsequent lift-off process, wires of the diameters down to 10 nm can be obtained.[1] An indirect method, using EBL to generate a suitable mask, is patterning a deposited film by sputtering techniques, thus obtaining a wire, arrays of wires or other structures, depending on the mask.

AFM and STM lithography is a quite new approach for producing nanowires or features as small as a few nanometers [62, 63, 64, 65, 66, 67, 68]. An elegant chemical approach for fabrication of nanowires and arrays of nanowires is the template synthesis[2], especially for materials which cannot be deposited by the evaporation, after a conventional lithographic process. This method can be considered as an alternative to the known lithograpic methods. Arrays of nanowires are obtained by filling a porous template containing a large number of straight cylindrical holes, the size distribution of which is narrow. The filling occurs in a solution by electrochemical deposition [69, 72, 73, 74, 77], other chemical methods [69] (e.g., polymerisation reactions), or by high-pressure injection of a molten material [75]. Useful templates are commercially available alumite membranes (anodized aluminum films)[3], commercially available track-etched polycarbonate

---

[1] For an introduction to lithographic methodes see Ref.[61].

[2] For a review see Refs.[69, 70, 71].

[3] Alumite membranes are available under the trade-mark name Anopore from e.g. Whatman Laboratory Division, Clifton, NJ.

membranes[4] [76] and nanochannel array glass [78, 79, 81] or mesoporous alumi-
nosilicate hosts (also called zeoliths [82, 83]). Such porous membrans can also be
used as a shadow mask, during sputtering for pattern transfer to other materials
[79, 80]. Historically, the method of template synthesis was introduced by Possin,
who prepared different metallic wires with diameters as small as 40 nm in pores
of etched nuclear damage tracks (produced by highly energetic accelerated nu-
clei) in mica [73]. This method was thereafter refined by Williams and Giordano,
who obtained Ag wires with diameters below 10 nm [74]. Membranes filled with
Co, Ni, or Fe are magnetic nanocomposites which have a strong perpendicular
magnetic anisotropy suitable for recording [84, 134, 136, 87, 88, 89].

Penner and Martin demonstrated a successful synthesis of CPs (polypyrrole
and polythiophene) using commercial screen membranes, which are polycarbon-
ate foils with pores obtained by etching nuclear damage tracks [77, 90, 91, 92,
93, 94, 95]. For small pore diameters the conductivity of these polymeric fibrils
was found to be almost an order of magnitude higher than in bulk polymer films
prepared under the same experimental conditions [90]. This has been attributed
to the polymer chains with an enhanced order, i.e. having less defects due to the
unidirectional growth imposed by the confined geometry. Instead of wires, it
is also possible to synthesize tubules [72]. In addition, pores have successfully
been filled with two different materials stacked alternatingly to form multilayers
[96, 97, 98]. Arrays of Bi nanowires can be obtained by template synthesis as
well, allowing interesting magnetotransport investigations [99, 100, 101, 102].

Applications of template synthesis comprise arrays of electron field emitters
(e.g., arrays of carbon nanotubes grown in Al_2O_3 membranes) [103], biosensors
[104, 105], micro- and nano-electrodes for electrochemical investigations and sen-
sor applications [106, 107, 108, 109, 110, 111], novel magnetic-recording materials
[84, 134, 136, 87, 88, 89], magnetic sensors based on the giant magneto-resistance
effect [96, 97, 98], anisotropic optical filters [112] and the synthesis of aqueous
dispersions of monodisperse metallic colloidal rods [113, 114].

The importance of synthesizing nanowires of CPs was indicated by the work
of Cai [90], where drastically enhanced conductivity of chemically template-
synthesized polypyrrole and polythiophene nanowires in polycarbonate mem-
branes with smaller pore sizes was observed (Fig. 3.1.). The conductivity mea-
surements were carried out on an array of fibrils using a two-contact method. The
fibril/polycarbonate composite membranes were contacted by a bottom electrode
(made of Ag-grains) and a top electrode (Au, with a well-defined contact area).
The conductivity of one fibril was deduced by taking into account the pore density
of the membranes used [115].

---

[4]Track-etched polycarbonate membranes are available from e.g. Nucleopore Corp., Pleasan-
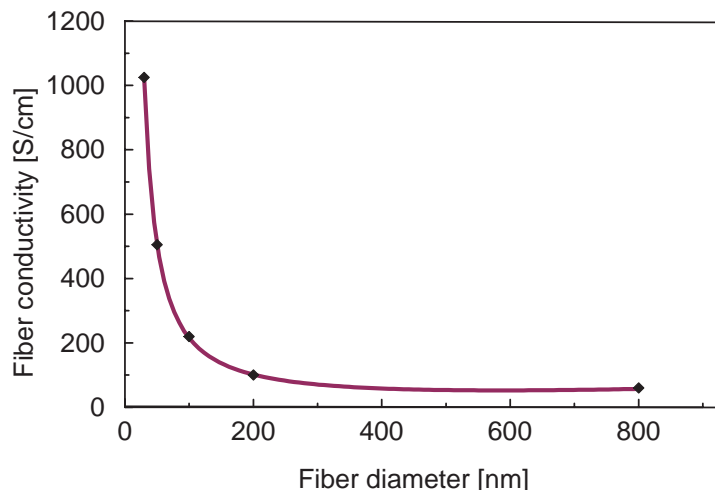ton, CA, or Poretics Corporation, Livermore, CA.

Figure 3.1: Conductivity of polypyrrole fibers versus fiber diameter. Polypyrrole was chemically synthesized in polycarbonate membranes having different pore diameters (see Ref.[90]).

In order to investigate the electric transport properties of a single polymer fiber, one has to develop a method for its selective contacting. This research was done in collaboration with the author's C. Terrier and A. Bachtold (see section 3.4.). First the formation of different metal wires (Ni, Co and Cu) using this template technique and electrochemical deposition within polycarbonate membranes of different pore sizes was carried out. In the second step a new method of contacting one or a few of this nanowires was developed (section 3.4.). Finally this approach was applied to the synthesis of polypyrrole nanowires.

3.2 Polycarbonate Membranes as Templates

The electrochemical growth of nanowires using commercially available polycarbonate track-etched membranes was studied in our group in collaboration with the Philips Research Laboratories in Eindhoven (The Netherlands). Most of the results were published in Ref. [116].

3.2.1 Experimental Conditions

PVP (polyvinylpyrrolidone) coated screen membranes were used for template synthesis (overall diameter 13 mm) with pore diameters d_N = 10, 30, 50, 80 and 200 nm (specified by the manufacturer, the Poretics Corporation), thereafter refered to as the "nominal diameter" d_N. Similar results have also been obtained
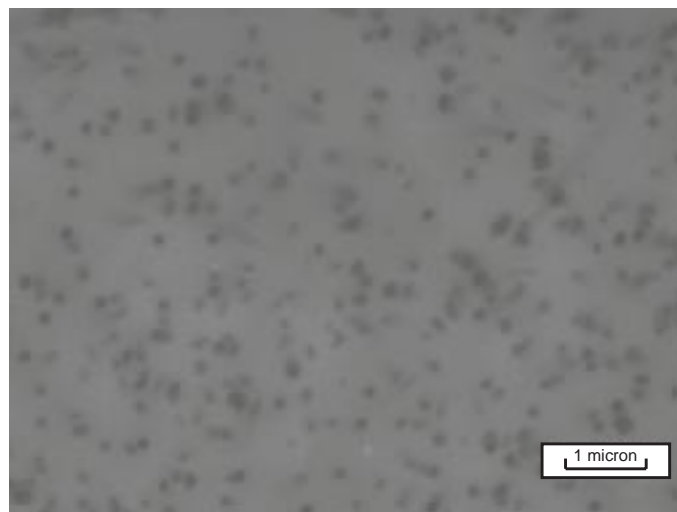
Figure 3.2: SEM image of a polycarbonate membrane surface with the nominal pore diameter of $d_N = 80$ nm. The pores are randomly distributed, with an average density of 4×10^8 cm^{-2}.

for membranes from suppliers, e.g. Nucleopore and Millipore, indicating that the findings are probably of a general nature. The membranes are 6 μm thick. A SEM picture of the surface of such membrane is shown in Fig. 3.2.. A metallic layer serving as the back electrode is evaporated onto one side of the membrane[5]. After evaporation the membranes are fixed with the electrode facing a conducting substrate (Cu or Au covered plate), using an adhesive sticker. The sticker leaves the central part of the membrane open over a diameter of 6 mm, which is the part that is exposed to the electrolyte.

Before mounting the pre-fixed membrane into the electrochemical cell, it is immersed into deionized water under ultrasonic agitation for two minutes. This step has turned out to be crucial for obtaining reproducible results and a homogeneous growth over the whole growing area. If this step is omitted, the growth starts in some pores first and the number of pores in which the growth proceeds may increase with time, which results in an increasing current at the potentiostatic mode. This current increase is an artifact and cannot be related to the effective pore diameter, since at no time is one certain about the number of pores in which the electroplating commences. After the ultrasonic treatment, the membranes are removed from the deionized water. A reliable test of successful pore

---

[5]A 20 nm thick adhesion layer of either Ti or Cr is deposited first, which is followed by the evaporation of a 0.5-1 μm thick Au film. The thicker layers are needed in case of the wider pores, in order to ensure that the electrode completely covers the pores.
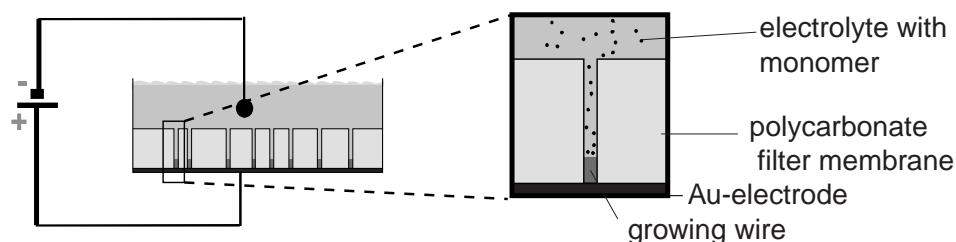
Figure 3.3: Schematics of electrochemical template synthesis within polycarbonate membranes. The membrane is fixed on an Au working electrode and exposed to an electrolyte containing the monomers and the dopant ions. By applying a certain voltage between the Au and the Pt counter-electrode the monomers of the CP are electro-polymerized, filling the pores and forming a wire growing upwards.

wetting is the requirement that the free membrane area is fully covered with a water droplet after the removal. If this is the case, the membrane is finally mounted into the electrochemical cell.

Electroplating is done in a teflon cell with the substrate (membrane) facing upwards. There is no separate compartment for the counter electrode, a Pt foil of $10\,cm^2$, nor is there any agitation (stirring) or heating. A saturated-calomel electrode (SCE) was used as a reference for the applied potential. This electrode is placed ~ 7 mm above the substrate. Using a conventional potentiostat, the current is measured during the electroplating at a fixed potential versus SCE, referred as V_{SCE}. The growth in pores has been studied for Ni, Co, Cu and Au. Conducting-polymer nanowires of polypyrrole and polythiophene can be synthesized successfully as well[6]. The principle of electroplating within the pores, leading to a nanowire, is indicated in Figure 3.3..

After electroplating, the membrane is inspected by using an optical microscope. If the growth has been interrupted while the pores where not completely filled, areas on the membranes covered with the nanowires appear black. If the pores were completely filled and the growth proceed on the whole membrane surface, a three-dimensional "bulk" film starts to cover the membrane. If this is the case, the membrane appears reflective in the case of metal deposits. These two

---

[6]The following aqueous electrolytes have been used: **Ni solution:** 515 g/l Ni(H_2NSO_3)*4H_2O + 20 g/l NiCl$_2$*6H2O + 20 g/l H$_3$BO$_3$; **Co solution:** 400 g/l CoSO$_4$*7H_2O + 40 g/l H$_3$BO$_3$; **Au solution:** 0.32 M gold(I)cyanide + 0.26 M citric acid and 0.65 M KOH (pH = 5-6); **Cu-solution:** 125 g/l CuSO$_4$*5 H$_2O$ + H_2SO_4 such that pH = 1; **pyrrole solution:** 0.5 M pyrrole (freshly destilled) + 0.1 M LiClO$_4$; **thiophene solution:** 0.2 - 0.5 M thiophene + 0.1 M LiClO$_4$ with propylene carbonate as solvent. **Typical deposition voltages are:** -1.2, -1.1, -1.0, -0.2, +0.8 and +1.9 V_{SCE} for Ni, Co, Au, Cu, pyrrole and thiophene, respectively.

simple observations allow one to test the degree of the growth homogeneity on the membrane. In order to measure the diameter of the wires, the polycarbonate membrane is dissolved in dichloromethane (CH_2Cl_2) at $40°C$, rinsed in fresh dichloromethane, chloroform and ethanol. This preparation procedure is sufficient for standard SEM inspection. However, high resolution images still suffer from electron-beam-induced charging effects caused by a residual organic (and insulating) layer on the wires. In the case of metal wires this organic coating can be removed by an oxygen-plasma treatment at $100°C$, whereas in the the case of conducting polymer wires this insulating layer cannot be removed, which leads to SEM images of reduced resolution.

3.2.2   Experimental Results for Metal Nanowires

The most comprehensive dataset has been obtained for the membranes with a nominal pore diameter of $d_N = 80$ nm. For this reason, we focus mainly on these membranes. In Fig. 3.4.a) are shown two electrical-current (I) versus time (t) characteristics (I-t characteristics) for the reduction of Ni^{2+} and Co^{2+} ions. These curves were obtained during the electrodeposition at a constant applied voltage (potentiostatically) across the membranes. In the same figure, two pores are schematically drawn in cross section and at three stages of the growth process. During the first stage (left schematics labeled I) the metal (shown hatched) is growing in the pores while the reduction current takes a value of ≈ 2 mA (the variation in the current will be discussed below). The growth proceeds in the pores until they are filled up to the top surface of the membrane (middle schematics). Beyond this, the growth can continue in three dimensions: hemispherical caps form on top of the wires (see also Figs. 3.5.a) and b)) and grow in size until coalescence on the membrane surface occurs. This is the transition region (labeled II), which starts at the position of the arrow in Fig. 3.4.a). Since the effective electrode area increases rapidly during this stage, the electrochemical current increases. In the following, the term "transition to bulk growth" will be used. Once the growth proceeds on the whole membrane surface (right schematics labeled III), the current approaches an asymptotic value. This value corresponds to the current measured on a metallic electrode of the same overall area and for the same applied voltage.

Fig. 3.4.b) shows a SEM image of the Ni wires after the dissolution of the polycarbonate membrane. In this example the deposition was interrupted before the transition to bulk growth. The wires, shown in Fig. 3.4.b) are oriented in a wide range of directions. This is not an artifact produced by the dissolution of the membrane, what could be suspected, because during the dissolution and drying mechanical forces tear on the wires. This is a property intrinsic to commercial screen membranes. The pores in these membranes are not aligned parallel but
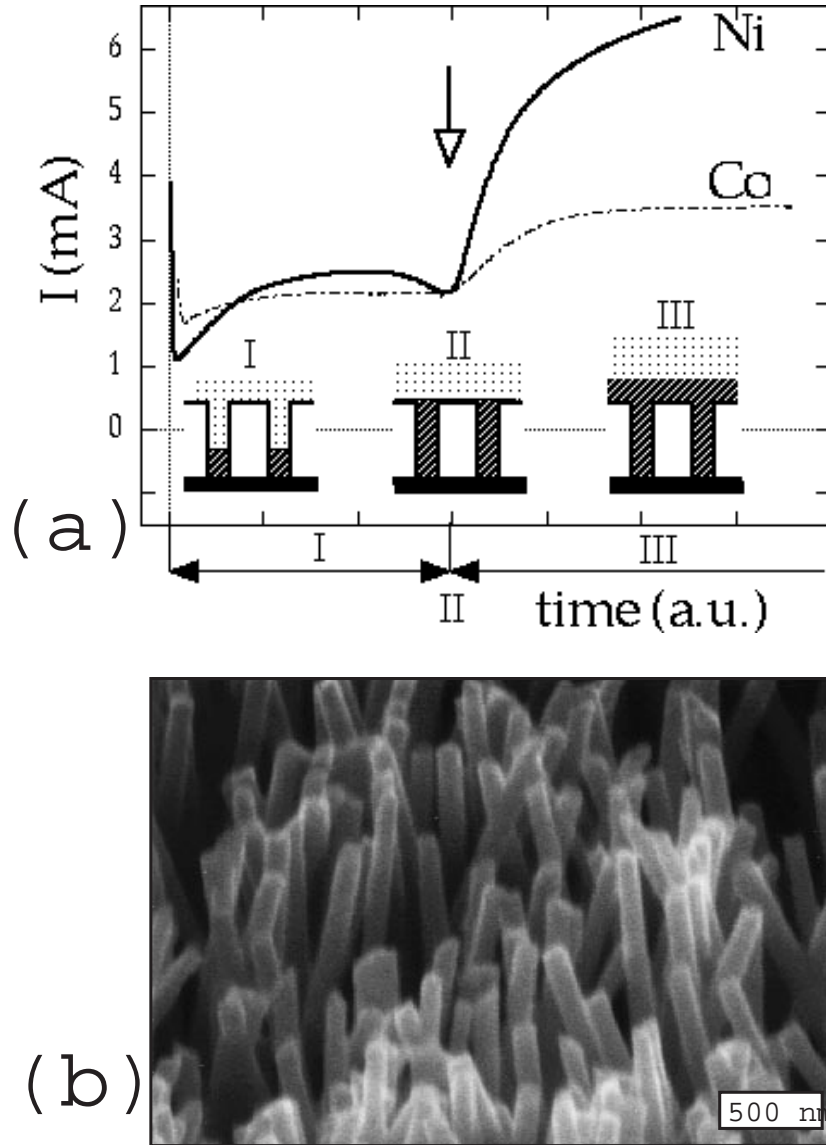
Figure 3.4: (a) Electrochemical reduction current as a function of time for the potentiostatic plating of Ni and Co (-1.1 V_{SCE} for Ni and -1.2 V_{SCE} for Co) in pores of polycarbonate membranes with $d_N = 80$ nm (nominal pore diameter). The schematic displays three different stages of the growth process: in region I, metal wires (hatched) grow in the pores; in region II, the pores are just completely filled (transition region to the bulk growth); in region III, the growth commences over the whole membrane (diameter 6 mm). (b) SEM image if the Ni deposit obtained after the dissolution of the polycarbonate membrane. Electrodeposition has been stopped in region I.

have a considerable angular distribution of $\pm\, 34°$ (Poretics production selection guide). For this reason the length of the pores across the membrane is not constant. Hence, even if the electrochemical deposition would proceed at an exactly constant rate, the instant of complete pore filling would still vary among different pores. This is the reason (of a fundamental origin) of the broadening the "sharp" transition to the 3D bulk growth observed in the I-t characteristics; another is the inhomogeneous growth: if some of the pores are initially poorly wetted, the number of pores in which the electrodeposition occurs can increase with time. This (1) results in a gradually increasing current and (2) leads to a considerable smearing-out of the transition to the bulk growth (not shown). A sharp transition, as the one shown in Fig. 3.4.a) is a good criterion for the homogeneous growth.

As shown in Fig. 3.4.a) a strong increase of the current is observed when the deposition starts to change from the growth in pores to the growth on the whole surface of the membrane. In the first approximation, this increase may be related to the changing effective electrode area. The membranes have a typical porosity of $\sim 5\,\%$ (using an effective electrochemical pore diameter, defined later), so that the electrode area increases by at least an order of magnitude. However, the observed current increases only by a factor 3-4 for Ni and ≈ 2 for Co.

The observed reduced current increase at the transition is attributed to the partial mass transport limitations (convection and diffusion). Though high ionic concentrations $\approx 1\,\mathrm{M}$ are used for all plating solutions, electroplating on the whole membrane surface is not ideal; i.e., it does not only depend on the electrode parameters (applied voltage and electrode area), but also to a certain extend on the transport of ions from the solution reservoir to the electrode region, where the ionic concentration is (partly) depleted. In order to test this, we applied electrolytes with a diluted concentration of Cu^{2+} ions. For low concentrations (1-10 mM) the current rise, observed at the transition to the bulk growth in highly concentrated electrolytes, completely disappears. The changing electrode area at the transition does not change the electrical current, because it is limited by the mass transport in the bulk electrolyte. Hence, we can conclude that the smaller electrical current rise at the transition to the bulk growth for Co when compared to Ni (seen in Fig. 3.4.a)) demonstrates that mass-transport limitation is more important for Co than for Ni[7]. While Fig. 3.4.b) displays a SEM image of Ni wires obtained from a growth process stopped before the transition to bulk growth, Fig. 3.5.a) corresponds to the situation after the transition, when the metallic deposit covers the whole membrane. Fig. 3.5.b) shows an example of the electrochemical growth being stopped just at the transition point. Small

---

[7]It is important to emphasize that highly concentrated electrolytes are prerequisite for monitoring the growth process with the aid of the I-t characteristic.

hemispherical caps have already been formed. In the following, the apparent wire diameter d_a deduced from SEM images of Ni and Co wires will be compared to the electrochemically derived effective wire diameter d_e. Up to now, the pores in polycarbonate membranes have been assumed to be cylindrical with an inner diameter that correspond to the one tabulated by the manufacturer (nominal diameter d_N). This assumption was questioned by Chlebny et al. [117] who found that the diameters of nanowires (analyzed by transmission electron microscopy (TEM)) could be larger by up to a factor of three compared to the nominal diameter of the nanopores.

First, the pore diameter and density of empty polycarbonate membranes are studied with SEM. In order to render electron microscopy possible, the membranes have been coated with a thin (10 nm) conducting layer. We measure the pore diameter of $d_s = 78 \pm 18$ nm ($d_s =$ "surface diameter") and the pore density of $n_p = 7 \times 10^8$ cm^{-2} in reasonable agreement to values specified by the manufacturer ($d_N = 80$ nm and $n_p = 4 \times 10^8$ cm^{-2}). Since the growing area is predetermined by the adhesive sticker (diameter $D = 6$ mm), the total number of pores N_p is known:

$$N_p = n_p D^2 \pi / 4. \tag{3.1}$$

The volume V_p of one completely filled pore, assuming an effective electrochemical diameter d_e, is given by

$$V_p = L d_e^2 \pi / 4, \tag{3.2}$$

where $L = 6$ μm is the thickness of the membrane (approximate for the maximum length of the wires). Using the molecular volume V_M of Ni or Co (almost identical), the total charge needed to fill all the pores up to the membrane surface is

$$Q = z F N_p V_p / V_M, \tag{3.3}$$

where $z = 2$ for the divalent Co^{2+} and Ni^{2+} ions and F is the Faraday constant. This charge Q is approximated by the experimentally obtained charge Q_t that has been transferred into the cell from the start of the growth up to the point of the transition to the bulk growth (Q_t is referred to as the transition charge). Here a 100 % current efficiency is assumed. This assumption has carefully been studied and confirmed for the Co bath, which is similar in concentration than the other applied electrolytes [118]. Since the transition charge Q_t for many experiments on Co and Ni deposits shows no difference within the accuracy of the measurements, a 100 % current efficiency for the Ni bath is justified as well. From ~ 50 samples (Ni and Co deposits), where the growth resulted in the whole exposed coverage-area, we obtain $Q_t = 0.7 \pm 0.13$ C. Using this value, an effective electrochemical diameter $d_e = 161 \pm 19$ nm is deduced (the error given includes the uncertainty in the wire length).
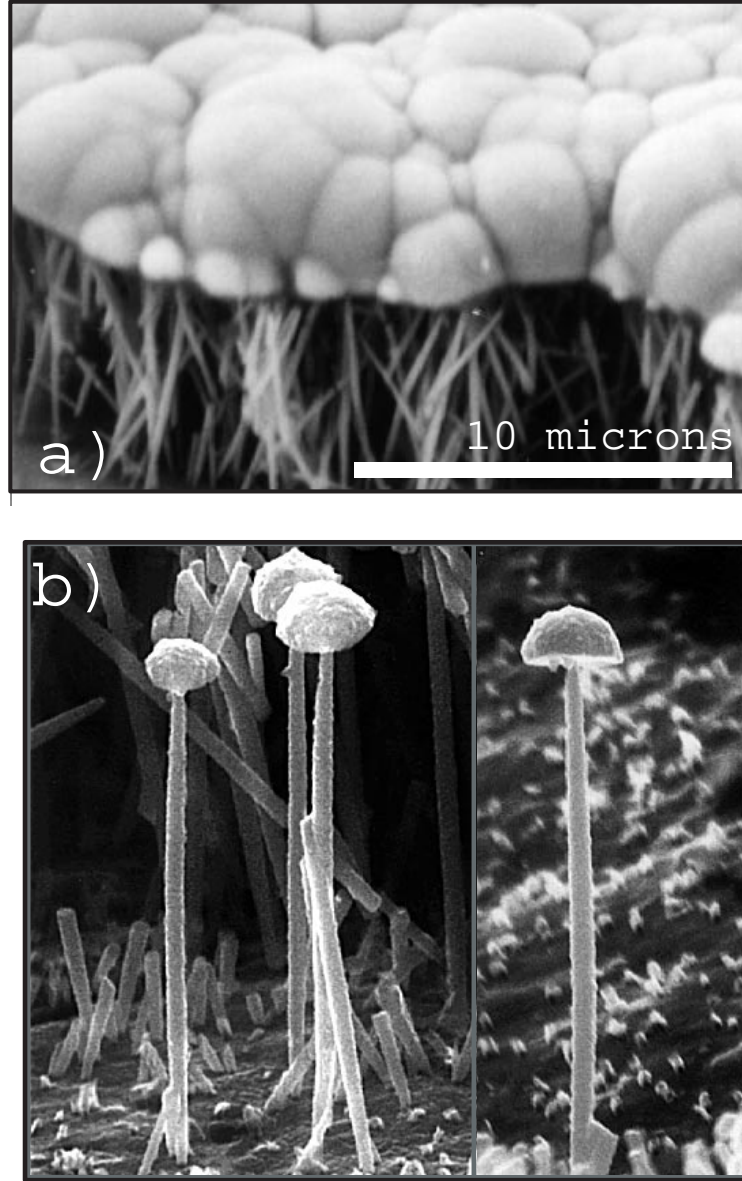
Figure 3.5: a) SEM image of the Ni deposit plated into $d_N = 80\,\text{nm}$ porous membranes after the dissolution of the polycarbonate membrane. Electrodeposition has been stopped long after the transition to the bulk growth (region III in Fig. 3.4.a)); b) SEM images of Ni wires grown in $d_N = 80\,\text{nm}$ membranes after dissolution of the membrane. The growth was stopped after the transition to the bulk growth, during which hemispherical caps were formed. The wires have a length of $\approx 6\,\mu\text{m}$ and an apparent diameter of $100\text{-}280\,\text{nm}$.

Figure 3.6: Three examples of the electrochemical reduction current $I(t)$ and the charge Q versus time t for potentiostatic Ni growth ($U = $-1.0 V_{SCE}) in pores of polycarbonate membranes with $d_N = 80$ nm. Inset: $I(t)$ for Cu (solid curve) and Co (dashed curve) at $U = $-0.1 and -1.1 V_{SCE}, respectively.
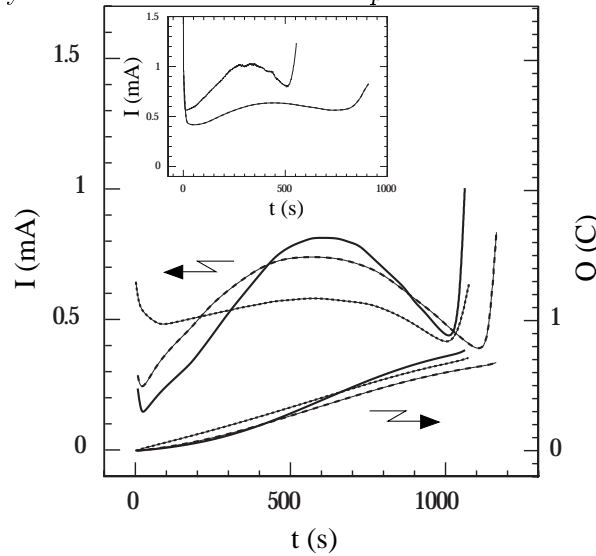
Similarly, from SEM images we obtain the apparent average diameter $d_a = 180$ $\pm$ 40 nm. These values for the diameter are in good agreement with the result of Chlebny et al. [117] who studied the diameter of similar wires with TEM and found a value of $d_a = 164 \pm 10$ nm. Both from electron-microscopy images of nanowires and electrochemically transferred charge, a considerable (a factor of two) larger wire diameter is found as compared to the nominal pore diameter d_N. The data for Cu and Au deposition (not shown) are in full agreement with the Co and Ni data.

In the region I (Fig. 3.4.a)) where the electroplating proceeds in the pores, the observed electrochemical current is not constant. Details of the I-t characteristic during this growing period are shown in Fig. 3.6.. Three I-t curves representative of Ni deposition at $U = $-1.0 V_{SCE} together with the integrated current, i.e., the charge $Q(t)$, are displayed. Growth proceeds in the pores up to $t \approx 1000$ - 1200 s when the rapid current increase signals the transition to the bulk growth. For these examples the transition charges are 0.65, 0.67, and 0.75 C, which are values in agreement with the average of $0.7 \pm$ 0.13 C. Starting growth in the pores, the current first increases with time, approaches a maximum after $\approx 1/2$ of the period needed to fill the pores up to the top membrane surface, and then starts to decrease significantly before the transition to the bulk growth.

In general, the current maximum is found to be more pronounced the sharper

the current rises at the point of transition, which is the case if almost all wires approach the top surface of the membranes simultaneously (ideal case). In the first approximation, the length l of the wires can be assumed to be proportional to the time t that has elapsed after the growth was initiated. Hence, when the wires have been grown to a length $\approx 1/2$ of the total pore length of $L \approx 6\,\mu$m, we can observe a deposition current up to a factor of six larger than the initial current. The decreasing reduction current with the progressive growth is quite unexpected: the electrochemical current is determined by the applied voltage and, if the mass transport is a limitation, by the diffusion of ions. Since the reference electrode is located in the bulk electrolyte (reservoir) above the membrane, there may be a voltage drop along the electrolyte in the pores which would result in a reduced electrochemical current. With the progressive growth, this voltage drop should decrease, however, since the wires are approaching the reservoir. Hence, the current is predicted to increase. A similar conclusion is drawn if the mass-transport limitation is considered. As a first-order approximation one could assume a constant ion concentration in the electrolyte (reservoir) above the pores. The concentration gradient, which determines the diffusion current, increases if the wires approach the top surface of the membrane, so that the diffusion current increases as well. The surprising current drop in the I-t behaviour is also observed for all the other electrochemical systems (Ni, Co, Au and Cu). These systems correspond to a wide range of deposition voltages ranging from -1.3 to -0.1 V_{SCE}. As an example, the inset of Fig. 3.6. shows I-t curves for Cu, grown at $U = $-0.1 V_{SCE} (solid line), and for Co, grown at $U = $-1.1 V_{SCE} (dashed line). In both cases, clear maxima are observed[8].

In addition to using different solutions, the deposition time for pore filling was also varied by changing the applied voltage. For the range $U = $-1.3 to -1.0 V_{SCE} used for Ni deposition, which corresponds to 120 - 1200 s, the maximum was always clearly observable.

Besides diffusion and migration, the electrochemical current is also proportional to the electrode area. The current maximum is due to an increased wire diameter in the middle section of the nanowires, as will be demonstrated. Fig. 3.5.b) shows high-resolution SEM images of Ni wires viewed from a direction almost perpendicular to the wires. These wires originated from a membrane which was electroplated a short instant beyond the point of the transition. The hemispherical caps on the top of the wires developed just after the pores were completely filled. The wire diameter is observed to be larger in the middle than at the bottom (where the growth started) and the top (immediately underneath the caps). This effect is even more pronounced in two extreme examples displayed in Fig. 3.7..

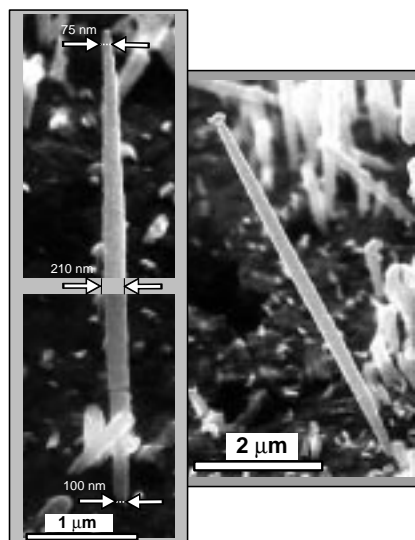[8]The maxima were less pronounced for Co, in general.

Figure 3.7: SEM images of Ni wires grown in $d_n = 80$ nm membranes after dissolution of the membrane. The growth was stopped immediately at the transition to the bulk growth. The two images to the left display the top and bottom $2\,\mu$m of the same wire (total length $\approx 6\,\mu$m). Note the remarkably increased diameter in the middle section of the wires.

In the left image of Fig. 3.7. the bottom and top $2\,\mu$m of the same wire are shown. The diameters are 100 and 75 nm close to the bottom and the top respectively, and 210 nm around the middle section. In the right image the diameters ≈ 100 nm close to the top and bottom and 240 nm in the middle. The wires are observed to be up to a factor 2.5 wider in the middle than at the base or top end. This increase in diameter, which amounts to a factor of ≈ 6 increase in area, is consistent with the I-t behaviour of Fig. 3.6.. The observed dimensions are also in agreement with the average of the effective electrochemical pore diameter of about 160 nm.

There are two possible reasons for the increased diameter. First, the pores may not be cylindrical (but wider inside), or second, the pores widen during the growth. The latter scenario can originate from the metal deposition, if the metal grows not only strictly along the direction of the pore axis but also to a certain extend radially, exerting pressure onto the polycarbonate membrane, which then causes a widening of the pores. Within this scenario a decreasing wire diameter with progressive growth would be difficult to understand, since the mechanical strain would relax much easier near the membrane surface. As a test, polymeric wires were also potentiostatically grown within these pores. Since the polymer is expected to have mechanical properties more similar to the template material
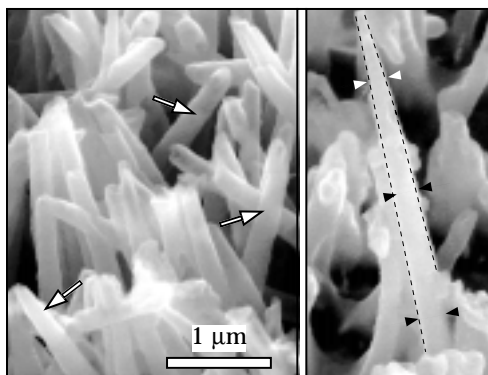
Figure 3.8: SEM images of polypyrrole fibrils grown potentiostatically in $d_N = 80$ nm membranes, after the dissolution (in part) of the membrane. Note that the polymeric wires are thinner at their ends (e.g., arrows on the left image). In the right image (identical magnification), the variation of the diameter d along the wire is emphasized with dashed lines that follow the border of the wire. In this case $d \approx 130$ nm at the top end and $d \approx 250$ nm in the middle section. The bottom section of the wire cannot be seen here.

("soft matter"), a widening imposed by the growing wires is not expected in this case. Fig. 3.8. shows two SEM images of the top part of polypyrrole wires after the dissolution of the polycarbonate membrane. Even though the image contrast is much poorer here, one can clearly see that the wires narrow at the top (see arrows). In the right image of Fig. 3.8. the boarder of a wire is highlighted by dashed lines. This wire has a diameter of 93 nm at the top and 250 nm in the middle section, in agreement with the results for metal wires[9].

We conclude that the pores themselves are in general not cylindrical with a constant cross section but are rather *cigar-like*. For the analyzed pores with the nominal diameter of $d_N = 80$ nm, the middle section of the pores is wider by up to a factor 3. This is not in contradiction to the SEM studies, in which the membrane surface and hence the pore diameter just at the surface are studied. This apparent diameter is comparable to the nominal one.

The observed current maxima in Fig. 3.6. directly reflect the shape of the pores. We mention that a similar maximum is observed in case of $d_N = 50$ and $d_N = 200$ nm membranes[10]. For smaller diameters, however, the I-t dependences show some differences (for details see Ref. [116]). They were not directly part of

---

[9]In the case of CPs the wetting agent (PVP) is still around the nanowires. This can effect the shape of the wires.

[10]This maximum is also (and with similar intensity) present in pores of membranes obtained from different suppliers (i.e., Poretics, Nucleopore and Millipore).
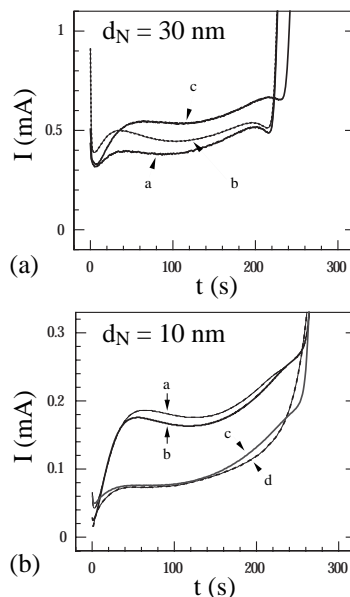
Figure 3.9: Electrochemical reduction current $I(t)$ versus time t for potentiostatic metal deposition in polycarbonate membranes with (a) $d_N = 30$ nm and (b) $d_N = 10$ nm pores. All curves correspond to Ni plating, except for the dashed one in (b), which corresponds to Co.

this thesis. The main results are summarized in the following paragraph.

The nanowires in 10 and 30 nm wide pores show the same behaviour like nanowires grown in 80 nm wide pores. The apparent wire diameter exceeds the nominal pore diameter by up to a factor of three. The wires are also not uniform in width, they are wider in the middle, whereas the top and the bottom end show the diameter of the nominal pore diameter d_N specified by the manufacturer. An effective electrochemical diameter is also derived from the transition charge $Q(t)$ obtained from the I-t curves. With respect to the effective wire cross section, the area is on average up to a factor of ten larger than what would be assumed if the nominal values were used. This can drastically influence physical parameters derived from measurements on these wires, for example conductivity measurements, where the geometrical factor plays a significant role.

For the smaller pore diameters the I-t characteristic shows an increase of $I(t)$ with time in addition to the geometrical dependence. In Fig. 3.9. characteristic I-t curves for the growth of Ni and Co wires in smaller pores are shown. This increase is very pronounced for $d_N = 10$ nm. Here the current has a gradually increasing component, because of which the transition of the bulk growth can hardly be discerned.

From the discussion of Fig. 3.4., we know that the mass transport is more a limiting factor for Co than for Ni growth. The dashed curve (d) in Fig. 3.9.b) is an example for Co growth in the narrowest pores. Apart from the initial rise and plateau, there is a smooth and gradual increase of $I(t)$, which extends beyond the transition to the bulk growth. The transition point cannot be determined unambiguously anymore.

We think that the increasing current is caused by the mass-transport limitation. The current increases close to the point of transition because the wire approaches the top membrane surface and, therefore, also the large electrolyte reservoir, in which the ion concentration is approximately constant. That the current is increasingly controlled by the diffusion for smaller pore diameters is consistent only if the diffusion coefficient for the active ion species is pore-size dependent. This has been found indeed [116].

Possible Origin of the Widened Pore Diameter

One can imagine that the origin of the pore widening in the middle of the membranes is caused by the highly energetic ion exposure during this production step. The direct impact interaction produces a damage zone along the ion track (damage track) [119]. The membrane is then etched in a solution with a high selectivity for damage tracks; i.e., the etching rate for a damaged zone is much larger than for the undamaged material. For polycarbonate this selectivity is found to be ≈ 400 [120]. During this process, a physical hole is opened in the membrane. As the etching proceeds, the hole is opened in the membrane.

Since the etching proceeds from the top and bottom surfaces, the pore is expected to have a shape with a thinner middle cross section. This is just the opposite of what is observed in our work. However, one has to keep in mind that the (primary) damage zone is localized within a very narrow region. A typical damage diameter is $10\,\mathrm{nm}$ [121, 122]. Once the pores are open, they widen progressively by the etching time. The ideal homogeneous process would result in the cylindrical holes. Possibly this is not the case, at least for the smaller pore diameters, $d \leq 200\,\mathrm{nm}$, because of a secondary effect which also modifies the membrane (polycarbonate).

Besides the primary damage, caused by the ion impact, a large number of secondary electrons are generated at any point along the track (electronic collision cascade) [119]. These electrons themselves have sufficient energy (already a few electron-volts are enough) to interact destructively with the polymer membrane by cleaving chemical bonds, (see Ref. [123]). The resulting smaller polymeric fragments are etched more easily than the original polymer, and since the rate of secondary electrons is large, the etch rate can also be enhanced at positions

away from the track center. This effect is very well-known in EBL [124][11]. A fundamental problem in EBL is the fact that the electrons resulting from the secondary emission in the substrate expose the resist as well and often even dominate the exposure. Since the secondary electrons can penetrate the polymer over rather long distances, the resist is effectively exposed laterally away from the position of the primary beam. In EBL this effect has been termed "proximity effect".

We propose that the pore widening is a consequence of the proximity exposure. This suggestion allows an understanding why the etched pores are in general wider inside than at the top and bottom ends of the membrane. Let us assume that the secondary electrons are generated isotropically at each point along the ion track in the membrane. Any point in the vicinity of the track, but sufficiently inside the membrane, receives exposure from the secondary electrons generated above and below this point. This is different for a point close to the membrane surface. On the top of the surface, for example, impinging secondary electrons can only originate from below this point, since the impacting ion moves through the vacuum above. For this reason, proximity exposure is reduced by approximately a factor of two close to the membrane surface. If etched, the pore will develop a smaller diameter at the top and the bottom of the membrane, compared to the regions inside.

3.2.3 Experimental Results for Polymer Nanowires

Nanowires of polypyrrole, polythiophene and poly-3-methyl-thiophene can also be successfully synthesized in polycarbonate membranes. Membranes with pore diameters of $d_N = 80$ nm and in some cases of $d_N = 30$ nm were mainly used for template synthesis[12]. After wetting the pores by ultrasonic treatment in pure water for a few minutes, this procedure has to be repeated using ethanol and propylene carbonate (including the supporting electrolyte) for solvent exchange. Polypyrrole was just destilled before use, all solutions were ultrasonically treated and purged with nitrogen before use, in order to avoid the influence of oxygen.

Fibers of polypyrrole synthesized in membranes with nominal pore sizes of $d_n = 80$ nm have already been shown in Fig. 3.8.. Additional SEM images are shown in Fig.3.10. of polypyrrole, polythiophene and poly-3-methyl-thiophene fibers.

---

[11] A focused medium-energy electron beam (≈ 10 - 100 keV) is used to expose a resist, which most often is PMMA. In the developing step (etching) the exposed material is dissolved.

[12] In the case of polypyrrole the synthesis was carried out in an aqueous solution with $LiClO_4$ as electrolyte (0.1-0.2 M) and concentrations of pyrrole up to 0.5 M at potentiostatic conditions ($V = +0.75$ V, $+0.8$ V or 0.85 V). Polythiophene and poly-3-methyl-thiophene fibrils were usually synthesized in propylene carbonate with $LiClO_4$ as electrolyte (0.1 - 0.2M) and concentrations of thiophene up to 0.5 M at potentiostatic conditions ($V = +1.8$ - 1.95 V).
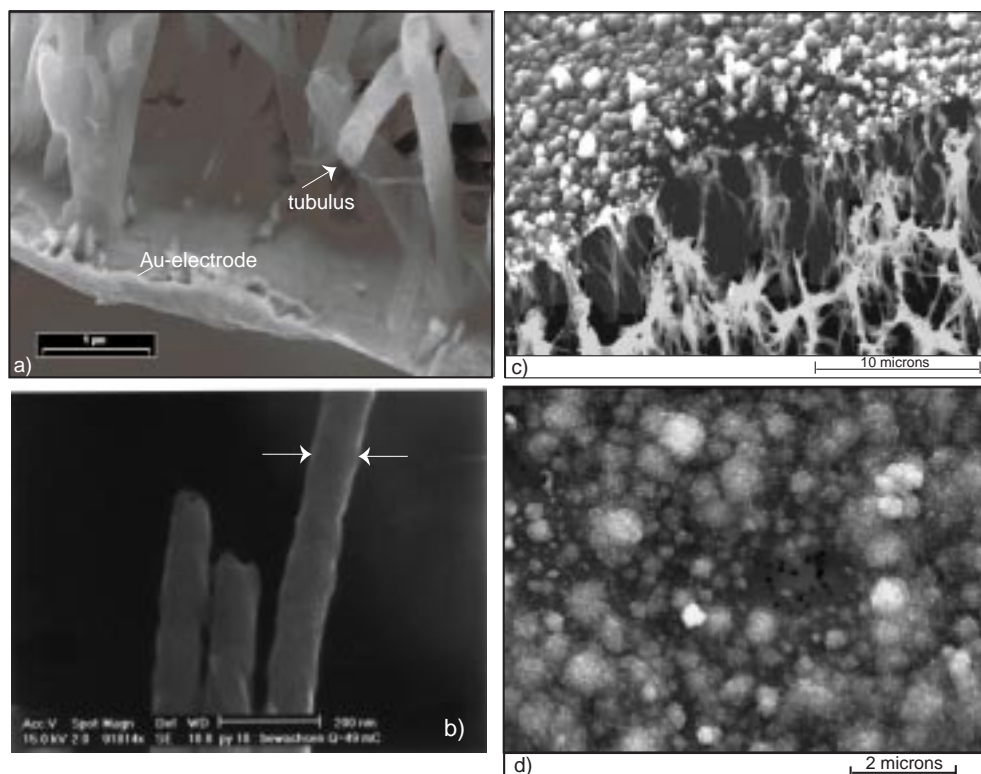
Figure 3.10: a) SEM image of polypyrrole fibers grown in $d_N = 80$ nm membranes in an aqueous solution at potentiostatic conditions after the dissolution of the membrane. The growth was interrupted before the wires could reach the surface. The fibers are connected to a Au electrode, were the initial growth starts. The arrow shows a fiber which indicates that we obtained tubes instead of wires. b) SEM image of polypyrrole fibers grown in $d_N = 30$ nm membranes in an aqueous solution at potentiostatic conditions. The wires are 2-3 μm long. The middle part is shown. The arrows demonstrate that the effective wire diameter is three times larger than the nominal one. c) SEM image of polypyrrole fibers grown out of the membrane forming a granular film on top of the membrane (cross-sectional image). The membrane is partially dissolved. d) SEM image of the polycarbonate membrane surface where polymer fibers of poly-3-methyl-thiophene are just grown out. Some pores in the middle part are not filled. Further growth would lead to the film formation, shown in c). The fibers were synthesized in propylene carbonate under potentiostatic conditions.

Fig. 3.10.a) shows a SEM image of polypyrrole fibers grown in $d_N = 80\,\text{nm}$ porous membranes after the dissolution of the membrane. As can be seen, in the bottom part the fibers are connected with the Au electrode, were the growth process starts. The fiber, indicated by an arrow, looks more like a tube than a wire. The diameters, measured from SEM images, are 2-3 times larger than the nominal pore diameter, in agreement with the results found for metallic wires grown by the same methode.

Fig. 3.10.b) demonstrates this behaviour also for polypyrrole fibers grown in $d_N = 30\,\text{nm}$ porous membranes. The middle part of the wires are shown, indicating a diameter of about 90 nm, three times higher than the nominal pore diameter. After the fibers are grown out of the membrane, they begin to build a homogeneous polymer film. In the beginning the growing caps of the wires form a granular film, as shown in Fig. 3.10.c) (cross-sectional image) for polypyrrole fibers and in Fig. 3.10.d) for poly-3-methyl-thiophene fibers (top-view image) grown in $d_N = 80\,\text{nm}$ pores, respectively.

In Fig. 3.10.d) the film formation process is just in its beginning state, the single caps are not grown together completely. There are even parts (in the middle) where no polymer is grown out of the membrane, unfilled holes can be clearly seen. During a complete film formation process on top of the membrane these parts will be closed by the lateral film growth, forming a homogeneous film. The different sizes of the polymer caps, representing the grains, indicate that the growth is not homogeneous.

The growth behaviour of CPs within the pores of polycarbonate membranes have not been studied as systematically as the growth of metals. However one can still conclude that the growth is quite much more inhomogeneous, which can be seen by optical investigations of the membrane surface after the electropolymerisation. Sometimes the areas where no polymer has been grown out of the membrane are relatively large, whereas at other areas of the same sample the film formation processes has just been started. The growth control is therefore very difficult. Electrochemical metal deposition is much better controlled than the deposition of CPs.

- A fixed ratio of charge and the amount of material deposited cannot established exactly for CPs.

- Additional charging and discharging effects due to the doping are difficult to be estimated. Two electrons are needed for the coupling process of two polymeric units and 0.2 - 0.5 electrons are correlated to the p-doped state.

- CPs do not have a unique density and posses a lower value of the diffusion coefficient because the monomer is not charged, therefore a main attractive driving force for the monomer to enter the electrode surface is missing.

- Interactions of the momomer or the polymeric units with the wetting agent PVP are more favourable for organic compounds than for metals and could also influence the growth process. For example, often can be seen, that we obtain tubes with a hollow inner part and not wires (indicated in Fig. 3.10.a). This phenomena have recently been investigated by Demoustier et al. [125].

The *I-t* curves of wire-growing processes within the polycarbonate membranes show less characteristic features for CPs because the wire growth and the film growth overlap due to the inhomogenious growth. There is no sharp transition between the wire growth within the pores and the film growth on top of the membrane surface, as found for metal wires (Fig. 3.4.a)). After an initial part of a wire-growing with a moderately increase of the current, the transition step is smeared out due to the overlap of both processes. The current increases due to the increased area exposed to the ionic solution. The more flat wire-growing part shows not the characteristic shape representing the geometrical situation of the pore as it was shown for metal wires. At the end the current begins to saturate when the grown film covers all of the surface, and the area exposed to the ionic solution does not grow any more as it was observed for the bulk film formation on macroscopic Au electrodes (Fig. 2.9.a). The curves are more similar to the *I-t* curves for Co deposition in pores with $d_N = 10$ nm, where the current is controlled by diffusion effects. This indicates that in the case of CPs the diffusion limitation of the current during the wire-growing step seems to play a major role. In Fig. 3.11. a typical *I-t* curve for the deposition of polypyrrole in polycarbonate membranes with $d_N = 80$ nm is shown.

For the polypyrrole wires grown potentiostatically at $V_{SCE} = +0.8$ V shown in Fig. 3.11. the transition point was estimated at $t = 58$ s with a deposited charge of 9.08 mC. The whole deposited charge was 100.8 mC. The surface after the deposition looked grey and was relatively homogeneously covered with a thin film. At some outer parts small black areas were seen due to an increased film thickness. In polypyrrole films grown under identical conditions in polycarbonate membranes of $d_N = 80$ nm, one finds a broader range for the transition point. Comparable samples showed average values for the transition time between 21 s and 115 s with 42 s and for the deposited charge between 1.67 mC and 9.08 mC with 4.48 mC. The theoretically expected charge for complete pore filling can be deduced from the charge/volume ratio of obtained bulk films grown under identical experimental conditions. In the case of the polypyrrole/ $LiClO_4$ system one obtains a mean value of 9.04×10^5 mC/cm^3 for the bulk film formation, assuming 100 % efficiency of the charge. By taking into account the pore density of the membrane, the area which is exposed to the electrolyte and the volume of one pore, one can calculate the volume for the complete pore filling. For an
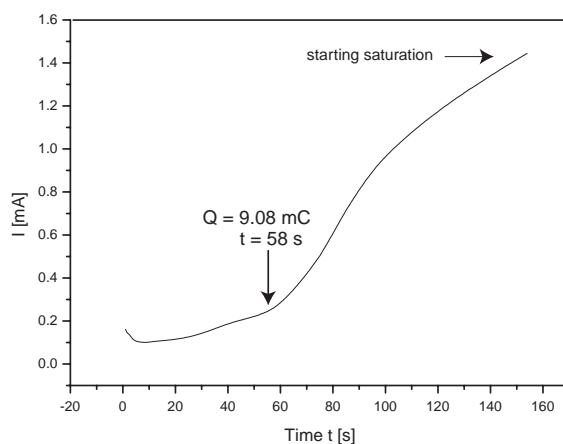
Figure 3.11: Typical *I-t* characteristic for the potentiostatic growth at $V = +0.8$ V_{SCE} of polypyrrole (0.1 M in aqueous solution with 0.5 M LiClO$_4$ as the dopant) in a polycarbonate membrane with $d_N = 80$ nm. The initial period (up to $\approx$ 58 s and 9.08 mC deposited charge) is dominated by the wires growing in the membrane. The current increases moderately. Between 68 s and about 95 s after starting the electrochemical growth, the current increase is much higher due to the beginning of the film-growth at some areas. The transition is not as sharp as for the metal-wire deposition in membranes of the same diameter (Fig. 3.4.). 95 s after the start the curve becomes more flat due to the saturation of the current. The hole surface of the membrane is covered by a polymer film. The area which is exposed to the electrolyte does not increase very much during the further film-growth.

area of $0.25\,\mathrm{cm}^2$ one obtains an effective charge of $0.868\,\mathrm{mC}$ for $d_N = 80$ nm and 10.9 - 24.55 mC for an estimated pore diamter of 2-3 times larger than d_N.

In reality probably not all the pores are filled completely, so the effective volume and the effective charge is reduced. Therefore the mean value of 4.48 mC for reaching the transition state is a roughly-estimated lower limit, which would increase if the "lost volume" of not or not completely filled pores could be taken into account. But it is even still higher than the calculated value for $d_N = 80$ nm of 0.868 mC. This indicates that the effective pore diameter must be higher than the nominal one, in agreement with SEM image analysis of the grown wires and in agreement with the data found for the electrochemical grown metal wires in subsection 3.2.2.

3.2.4   Conclusion

The results obtained show that the geometrical factor of the template synthesized fibrils for conductivity measurements is different then expected, which would affect the calculations of Cai et al. who found an enhanced conductivity of polypyrrole and polythiophene fibers of a smaller diameter (Fig. 3.1.). Recent results and investigations about the tubulus formation in dependence to chemical synthesis conditions have been published [125, 126, 127]. Conductivity measurements done on polypyrrole tubules even show an enhancement in conductivity for the narrowest tubules. Taking into account the correction for the geometrical factor because of tubules formation, conductivity values an order of magnitude lower were found in comparison to the values of Cai et al..

3.3   Porous Alumina Membranes as Templates

3.3.1   Introduction

Commercially available porous alumina membranes (for instance Anopore, Alltech Assoc.) have a limited range of pore diameters. The membranes can also be prepared by anodization of aluminum in an aqueous acidic electrolyte. The aluminum metal (Al) is converted into aluminum oxide (Al_2O_3, a ceramics called alumina) through the following anodic electrochemical reaction $2\,Al + 3\,H_2O \rightarrow Al_2O_3 + 3\,H_2$. Fig. 3.12. shows an idealized porous alumina membrane prepared by the anodization.

The membrane consists of a packed array of hexagonal cells [128, 129, 130, 131, 132]. The centre of the hexagonal cell is formed by cylindrical uniformly-sized pores. The steady-state evolution of the porous structure results from the balance between two competing processes across the barrier- layer: oxide formation at the metal-oxide interface and field assisted oxide dissolution at the oxide-
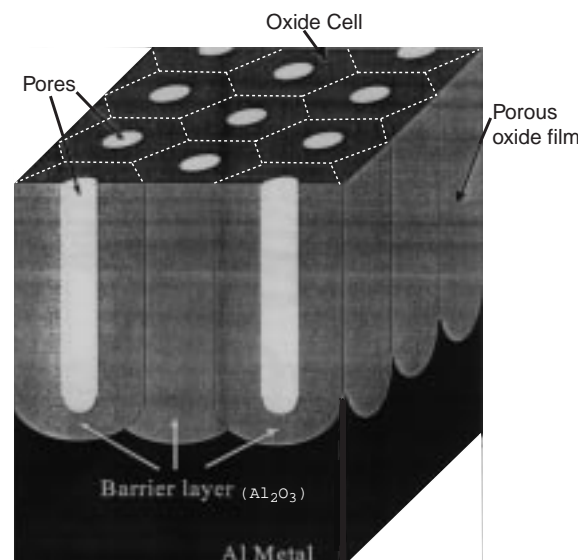
Figure 3.12: Schematic of an idealized porous anodic alumina film.

electrolyte interface [133]. Al always has an oxide layer (e.g. the barrier-layer) whose thickness depends on the applied voltage. The barrier-layer thickness is forced to remain constant during the growth at a constant voltage. Due to slow dissolution of the alumina at the alumina-electrolyte interface, formation of alumina occurs at the aluminum-alumina interface leading to a pore surrounded by an alumina wall of a constant thickness. The pore diameter is mainly determined by a field-assisted dissolution process at the bottom of the pores and depends on the electrolyte (nature of the anion, concentration, pH, temperature). It is independent of the applied voltage [129, 132]. The current lines are diffracted at the bottom because water is a better conductor than alumina. Therefore, chemical dissolution is enhanced at the bottom of the pores leading to well-defined cylindrical pores which are oriented parallel. The spacing between the pores and therefore the pore density is controlled by the applied voltage. The pore density decreases with increasing voltages [129]. The initial pore diameter can be increased by slow post-synthetic dissolution of alumina in a 1v/v % phosphoric acid solution (H_3PO_4) [134, 135, 136].

As an alternative to polycarbonate membranes, alumina membranes with pore diamters down to 9 ± 1 nm were synthesized. Ni-wires were successfully grown within these pores. Initially these systems were used for developing a method to make electrical contacts to at least one single wire (Section 3.4.). First attempts to grow polymeric wires within these pores were not successful, probably because the hydrophobic monomers can hardly enter the pores because of the strongly

electrolyte	voltage	pore diameter	pore density
H_3PO_4 (2%)	60 V	40-60 nm	$1.4 \times 10^{10} cm^{-2}$
H_2SO_4 (15%)	15 V	9 nm $\pm$ 1 nm	$5 \times 10^{14} cm^{-2}$
H_2SO_4 (15%)	10 V	9 nm $\pm$ 1 nm	$8 \times 10^{14} cm^{-2}$

Table 3.1: Values for the pore diameters and the pore densities obtained after anodization of Al in respect to the applied voltage and the used electrolyte.

hydrophilic pore walls. Chemical treatment of the pore walls with hydrophobic silylating agents could make electrochemical deposition of CPs possible. Further attempts in this direction were not done. Because of the lower pore density of polycarbonate membranes, we focussed on this type of membrane for developing a contact method for one single wire (Section 3.4.).

3.3.2 Experimental Conditions for the Synthesis of Alumina-Membranes

15 x 15 mm^2 pieces of a silicon wafer[13] were washed first in aceton and then in pure water using ultrasonic treatment for a few minutes. After drying and treatment in oxygen plasma, 20 nm of Ti[14], 60 nm of Au, and 500 - 1000 nm of Al were evaporated onto the silicon-wafer surface. For anodization of Al a constant voltage was applied between the Au electrode and a Pt counter-electrode. The substrate was mounted in the teflon cell, mentioned in subsection 2.4.1. with the Al facing up and being the working electrode. Only the center part of Al was exposed to the electrolyte constrained by an 0-ring seal (A $=0.38$ cm^2). There was no stirring of the solution during the anodization process. The current between the working and the counter electrode was measured as a function of time. The time scale to anodize 1 μm of Al was between 1.5 and 2 minutes, depending on the conditions of the synthesis. The anodization process was stopped immediately at the moment when strong gas evolution occured (strong increase in the current) due to the reduction of water. With different experimental conditions, different pore diameters and pore densities were obtained, as summarized in Table 3.1.

A SEM image of the surface of a synthesized alumina membrane is shown in Fig. 3.13.. Anodization was done in H_2SO_4 (15%) at $V_{Anodic} = 15.0$ V. Typical pore openings with about 9 nm in diameter can be clearly seen.

---

[13]Si (100), 300 μm in thicknesss, with 400 nm SiO$_2$-layer.

[14]Ti ensures the adherence of Au (working electrode) to the silicon substrate.
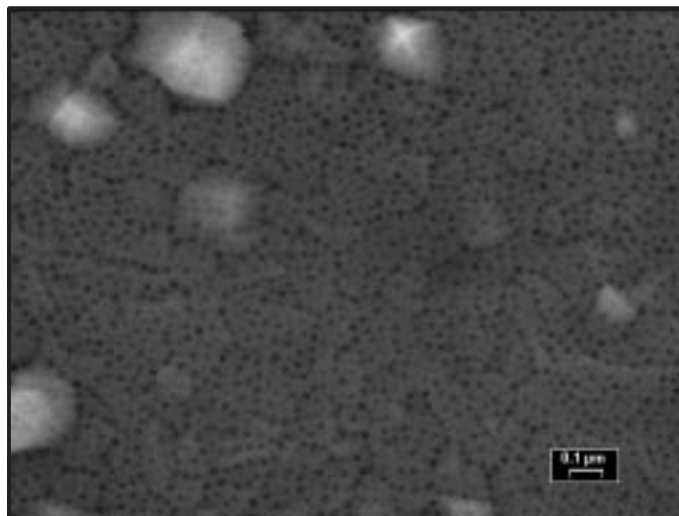
Figure 3.13: SEM surface image of a self-made alumina membrane at $V = +15.0$ V in 15 v/v % H_2SO_4. The pore density is 5×10^{14} m^{-2} and the pore diameter 9 ± 1 nm.

3.3.3   Electrodeposition of Ni within Alumina Membranes

For the deposition of Ni within alumina pores, the Ni-bath described in subsection 3.2.1. was used. The deposition was usually done at -1.0 V_{SCE}. The current was measured as a function of time. A steep current increase from about 0.5 - 1 mA up to a few mA indicated the lateral growth on the alumina surface when the wires were grown out. The transition is very sharp, indicating a homogeneous growth of the Ni-wires. In Fig. 3.14. a typical *I-t* curve for the deposition of Ni in alumina membranes is shown. There are three characteristic regions:

- During the first stage (I) the nickel was deposited in the pores.

- In the region II the pores are completely filled and electrodepostion proceeds in three dimensions, resulting in hemispherical caps and a strong increase in the current. The transition step occurs between 80 and 120 s after starting the deposition.

- In the region III the growth over the whole membrane area commences. A constant current is retained.

An important detail for successful pore filling is that the pores must be kept wet after the synthesis in pure water. Additional treatment with 1 % H_3PO_4 for one minute increases the possibility for successfull pore filling. Without H_3PO_4
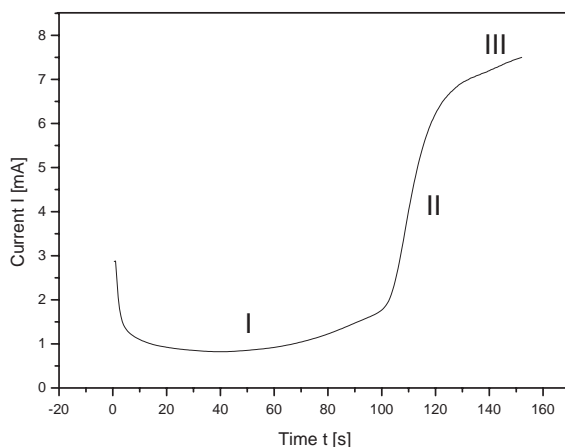
Figure 3.14: Characteristic *I-t* curve for the deposition of Ni in $9 \pm 1\,\text{nm}$ pores of alumina at -1.0 V_{SCE}. Three regions during the growth period are indicated. In region I the electrodeposition in the pores occurs with essentially no change of the current. In region II there is a steep increase of the current due to the three-dimensional growth of the Ni wires after growing out of the membrane, building hemispherical caps. In region III the current begins to saturate because the hemispherical caps grow together building a homogeneous film on top of the alumina membrane.

treatment only 2-5 % of the pores can be filled, wheras 10-25 % of the pores can be filled after this additional step. Fig. 3.15.a) shows an example for the Ni deposition in pores which were not additionally treated after the synthesis, and Fig. 3.15.b) shows an example of the Ni deposition in pores after treating the alumina membrane in 1 % H_3PO_4 for one minute. The number of successfully filled pores increases significantly. For contacting one single in an array of wires it is much better that the number of the filled pores is not to high; therefore no effort was done to increase the number of the filled pores by the " H_3PO_4" treatment presumably for a longer time. During the H_3PO_4 treatment, the possible remaining barrier layer of Al_2O_3 is dissolved to enable contact of the Au electrode with the Ni bath.
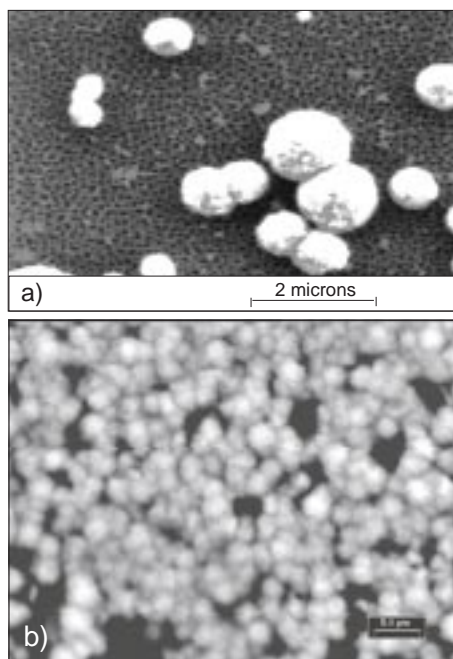
Figure 3.15: a) SEM image of Ni-wires growing out of an alumina membrane with about 40 nm pore diameter and a pore density of $1.4 \times 10^{10}\,\mathrm{cm}^{-2}$. The membrane was not treated with H_3PO_4 after synthesis. The number of the filled pores are quite low (below 2 %). b) SEM image of Ni-wires growing out of an alumina membrane with about 9 nm pore diameter and a pore density of $8 \times 10^{14}\,\mathrm{cm}^{-2}$. After synthesis the alumina membrane was treated in 1 v/v % H_3PO_4 for one minute. Deposition of Ni at -1.0 V_{SCE} was just stopped at the beginning state of region III where the caps begin to connect to each other and film formation starts. More than 10 % of the pores were filled.
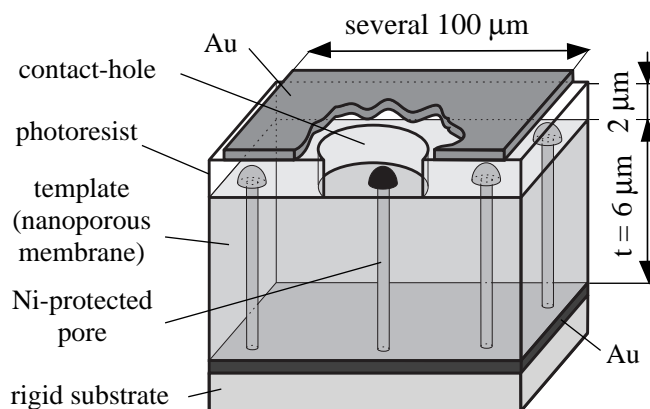
Figure 3.16: Schematics (not to scale) showing a completely structured device before the dissolution of the Ni in the pore selected by the contact hole.

3.4 Contacting Single Template Synthesized Nanowires for Electric Measurements

3.4.1 Introduction

In this section is outlined a method of electric contacting of the template-grown nanowires. Its success is demonstrated for Ni wires grown in polycarbonate templates with a nominal pore diameter $d_N = 80$ nm, membrane thickness $t = 6\,\mu$m, and mean pore length of $6.5\,\mu$m. The mean pore length is $\geq t$ because of the angular spread of the pore axis of $\pm 30°$. The contacts enable electrical measurements on one nanowire. The method comprises a combination of chemical methods and EBL. Main parts were published in Refs. [19, 137]. The work was done together with A. Bachtold and C. Terrier.

3.4.2 Device Fabrication

Due to the high density of pores, which are in average separated by 300 nm apart, contacting one nanowire demands a method based on high resolution lithography. CPs are sensitive to environmental conditions and should certainly not be exposed to a developer. Having this in mind, our process has been designed thus that the final nanowire is grown in the last step, subsequent to *all* lithographic processes. With reference to the schematics in Fig. 3.16., the process is outlined in what follows:

- A gold layer, thick enough to close the pores, is deposited on one side of the membrane (membrane diameter 1 cm). This layer serves as the bottom

electrode for all electrodeposition steps as well as for electric measurements.

- Then, Ni is electrochemically deposited into all pores. The growth is stopped at the instant when spherical Ni caps start to nucleate on top of the membrane [116]. This initial filling of the pores protects the pores from all lithographic processes that follow.

- To make spin coating possible, the membrane is permanently fixed onto a rigid substrate with the Au layer facing the substrate. Then a resist layer is spin-coated on top of the membrane. A positive Novolak-based photoresist was selected instead of PMMA, because of its higher chemical resistance.

- Using EBL, a contact hole ($\approx 500\,$nm in diameter) is opened in the resist selecting one or a few pores. Similary to the above mentioned protection of the pores, electrochemically plated Ni is also used to fill the contact hole for protection (not shown in Fig. 3.16.).

- To complete the process a top electric contact pad has to be defined. This is done as follows: a homogeneous Au layer of thickness $100\,$nm is evaporated over the whole sample. Then, a second positive resist (PMMA-MA copolymer) is spin coated and structured with EBL. The structure consists of a) an opening of size $\approx 10\,\mu$m centered above the previously made contact hole, and b) open lines separating the central area (several $100\,\mu$m) from the rest. The parts of the Au layer which are exposed through the openings of the structured PMMA-MA mask are now removed by chemical wet-etching using KI. Finally, the PMMA-MA resist is stripped-off, completing the structure.

A very important aspect of the process outlined is the protection of the pores, which is maintained during all processing steps. Due to the permanent protection, the devices may be stored at this stage until a final nanowire, a conducting polymer nanowire, for example, is required for measurements. Then, the Ni protection is selectively removed through the contact hole. This is done electrochemically using sulphuric acid (H_2SO_4). Next, the opened pores are refilled with the material of interest. This time, however, the electrochemical growth is continued until the pore and the contact hole are filled as well as the gap between the contact hole and the Au pad, as shown in Fig. 3.17.a).

An important aspect for the reliable filling of the pores in our scheme is the fact that the opened pores are automatically wetted by an aqueous solution due to the preceeding dissolution of Ni (wet etching), which proceeds from the top contact down to the bottom of the pore. This is very advantageous since electrochemical plating into dried pores can be quite unreliable due to wetting
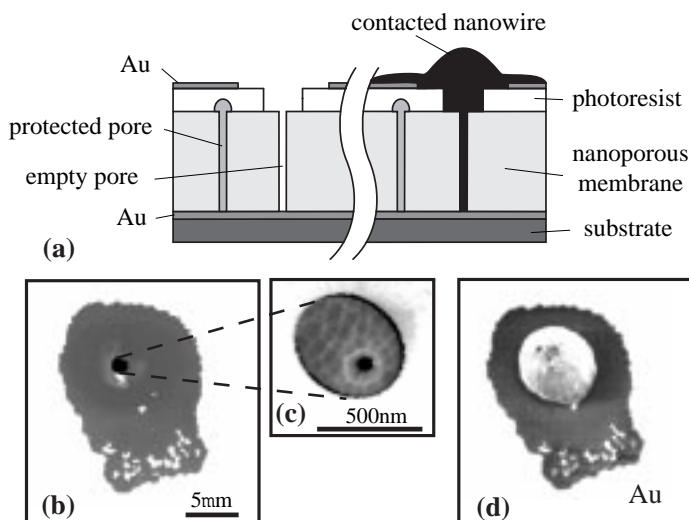
Figure 3.17: (a) shows one selected pore with dissolved Ni protection (on the left) and on the right refilled with the desired material forming electric contact to the top Au layer. The SEM images are top views of one and the same device obtained after the dissolution of Ni (b,c) and after (partial) refilling (d).

problems. Fig. 3.17. serves to illustrate the step in which the final electrically-contacted nanowire is formed. The left part of Fig. 3.17.a) shows one pore after the dissolution of Ni used for protection. In the right part, the previously opened pore has now electrochemically been refilled with the material of interest. The filling is stopped once the material has established contact to the gold pad. The three SEM snapshots, in Fig. 3.17.b)-d), have been taken for one and the same device at different times: Fig. 3.17.b) and Fig. 3.17.c) after the dissolution of the Ni protection, and Fig. 3.17.d) after refilling the pore (in this case using also Ni).

The two images in Fig. 3.17 b) and c) illustrate nicely the hierarchy of three levels of holes: the nanopore of the template can be seen in Fig. 3.17.c) within the contact hole of size 500 nm. This contact hole is seen in Fig. 3.17.b) to be located within a larger opening in the Au layer of $\approx 10\,\mu$m. The ragged border of this hole is due to unavoidable underetching in the Au etch step. Fig. 3.17.d) demonstrates that the same pore can sucessfully be refilled. The bright 'blob' centered above the contact hole is freshly plated Ni that has filled the pore and grown out of the contact hole. For visualization purposes, the plating was stopped before the Ni could make contact with the Au surrounding.
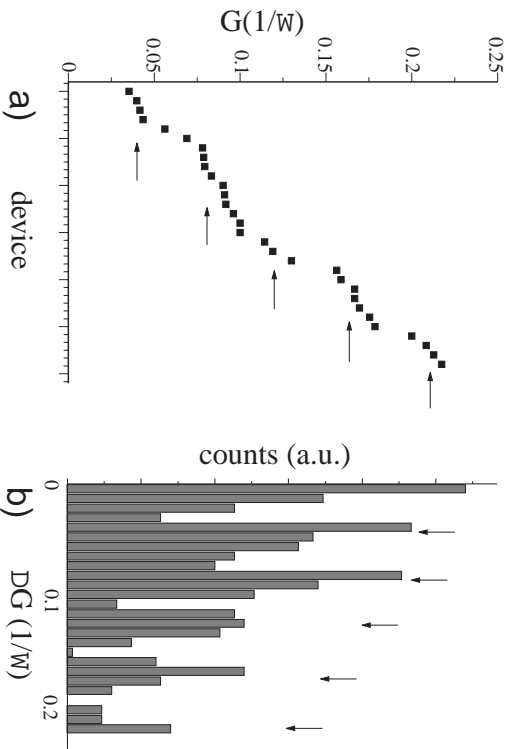
Figure 3.18: a) Conductance values of 30 devices with Ni wires represented in ascending order. b) Histogram for the difference in conductance of different devices.

3.4.3 Electric Measurements

Our goal is to measure the intrinsic electric resistance of nanowires formed by template synthesis. For this to be possible, we need to know the number of wires which are contacted. Since the nanopores are randomly distributed on the surface of the polycarbonate membrane, the number of pores being selected by the arbitrarily placed contact hole in the photoresist change for every device (from zero to a few wires). In order to evaluate this number, a statistical analysis of the measured conductance G is used. This is demonstrated in what follows.

In Fig. 3.18.a) the conductances G, measured at $T = 300\,\mathrm{K}$, are shown for 30 identically prepared devices consisting of pores filled with Ni. Each point corresponds to one device. The horizontal axis, the device number, has been arranged thus that the G-values appear in ascending order. If all pores were exactly identical sharp steps would appear. We noticed an accumulation of the points (in particular) around the G-values of 0.042 S, 0.084 S, and 0.168 S (arrows). Since there are no conducting devices found with $G \leq 0.03$ S, the smallest conductance of ≈ 0.042 S has to correspond to one single nanowire. This 'unit' of conductance can more accurately be derived from the histogram in Fig. 3.18.b) representing the difference in conductance ΔG for different devices. This histogram shows pronounced equidistantly spaced peaks, the distance of which is a measure of the mean conductance for one single nanowire. For the mean resistance $R = 1/G$ a value of $R = 23\,\Omega$ is deduced. Using the measured specific
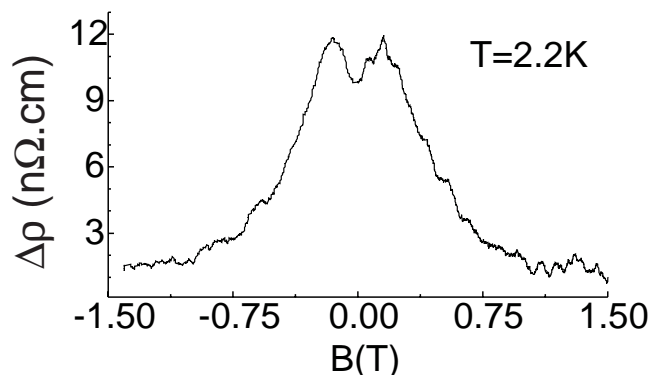
Figure 3.19: Magnetoresistance of four contacted Ni nanowires measured at $T = 2.2\,\mathrm{K}$ with the magnetic field B directed $\perp$ to the Ni nanowire.

resistance of $\rho = 7.7\,\mu\Omega\,\mathrm{cm}$ for electrodeposited Ni films, the average inner pore diameter of $160\,\mathrm{nm}$ [116], and the mean pore length of $6.5\,\mu\mathrm{m}$, a single Ni wire should have an average resistance of $25\,\Omega$, in excellent agreement with the present experiment. This result also proves that contact resistances can be neglected for Ni-wires.

Finally, Fig. 3.19. shows a first magnetoresistance measurement, demonstrating that the nanowires – contacted according to the description given above – can be used for electric transport studies.

3.5   Conclusion

Conducting nanowires are electrochemically fabricated in templates consisting of a large and dense array of nanopores. Electric contacts to one or a few nanowires have successfully been made using a newly developed multilevel process. First electric measurements on a set of Ni nanowires demonstrate that the conductance of one single nanowire can be measured if a statistical analysis is applied. After this analysis, the devices with only one contacted Ni wire may further be used, for example, for growing alternative materials like Bi and CPs after successful dissolution of the Ni wire.

3.5.1   Comments

By combining chemical methods and high-resolution EBL in a multilevel process, a successful contacting method allows to select one wire. Although being successful, we have later identified the following problems:

- The fabricated contact-hole is not self-aligned to one pore automatically.

- Attaching macroscopic wires to the Au contact pads by ultrasonic bonding does not work, because of the softness of the polycarbonate membrane.

- Four-terminal measurements, which are needed if intrinsic electric properties are to be obtained unambiguously, are impossible to be realized.

- The volume of the pores are a priori not known, as we have shown that the pore diameters are neither as specified by the manufacturer nor constant along the pore axis. Since the geometry of the pore has to be accurately known in order to determine the resistivity from the measured resistance, an extensive investigation has to precede any electric measurement for each new pore diameter.

- We found an incompatibility of organic solvents to the resists used, therefore the method would be interesting only for the synthesis of polypyrrole wires, which can be realized in aqueous solution.

This has been tried for polypyrrole[15]. The Au pad was sometimes grown with polypyrrole, as is shown in Fig. 3.20., but no reliable resistances can be measured by contacting the pad and the Au electrode with prober tips. The resistance of eight devices were measured. Resistances of 50 Ω, 710 Ω, 2.2 kΩ, 2.4 kΩ, 3.9 kΩ, 4.3 kΩ, 1.38 MΩ, 6 MΩ and 12 MΩ were obtained. By taking the best conductivity values and the geometrical shape into account one would expect resistances in the range of 42-43 kΩ for the polypyrrole/p-toluenesulfonic acid system. The lower measured resistances are probably due to the shortcuts to not-fully-dissolved Ni wires. However it is difficult to apply this contact method to CP wires to get reliable contacts. To apply statistics to CP wires is very difficult because of the non-unique values for the conductivity even in bulk samples. The fabrication of devices is also very time-consuming. In a next step we decided to develop an alternative contact methode for ensuring four-terminal contacts together with a better control of the wire formation by using self-made pores in a polyimide resist, laterally aligned to the surface. The results are described in the following section.

3.6 Fabrication of Lateral Nanopores in Polyimide as Template

3.6.1 Principle of Achieving Lateral Nanopores

There is a big advantage in using lateral nanopores for template-synthesis purposes. For instance many surface-structuring techniques are well known, and

---

[15]Synthesis: 0.1 M pyrrole with para-toluenesulfonic acid (0.1 M) as dopant in aqueous solution at $V_{SCE} = +0.8$ V.
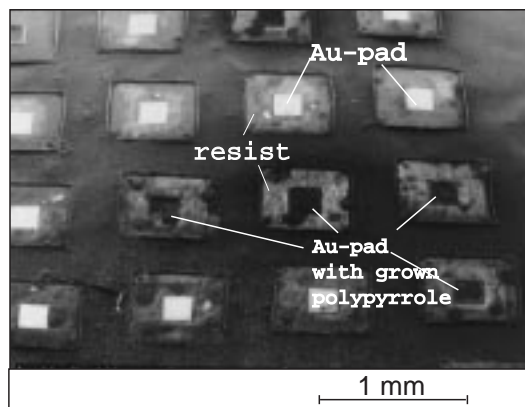
Figure 3.20: SEM image (topview) of an array of different devices after dissolution of the Ni-wire and electroploymerisation of polypyrrole in order to get contacted polypyrrole nanowires. In some cases polypyrrole was grown on top of the Au-pads. No reliable resistances can be measured.

one in general has a better control on making electrical contacts, the devices are more stable against mechanical stress, and interconnects or branched networks are much easier to achieve. By using optical lithography, four macroscopic Au pads[16] are defined on top of a Si/SiO$_2$ wafer[17] These pads are used for bonding the contact wires in the end. The device configuration is shown schematically in Fig. 3.21.a) (top-view) and Fig. 3.21.b) (cross-section). The outer left and right pads are used as the current contacts. The two inner pads are used to measure the voltage drop, thereby realizing a true four-terminal measurement. These inner Au pads are attached to the central part via Au fingers fabricated by EBL. The part which will define the final pore is made from Ni (or Cu) deposited on top of the four-terminal configuration. Here an additional high-resolution EBL step is used to structure a Ni nanowire connecting the left and right Au pads[18]. A polyimide layer is spin-coated over the whole device with a following hard baking process[19].

---

[16]Details about the optical lithography and metal evaporation are mentioned in Appendix B.

[17]The Si/SiO$_2$ wafer pieces (1.5 cm x 1.8 cm) were cleaned before use as described in Appendix B.

[18]Details about EBL and Ni evaporation are mentioned in Appendix B.

[19]The polyimide(PI 2570) was delivered by DuPont. It was spin coated on top of the silicon wafer device at 1000 rpm (from 0 to 1000 rpm in 4 seconds) for 5 seconds and at 2000 rpm (from 1000 rpm to 2000 rpm in 4 seconds) for 50 seconds. During the following 10 seconds the rotation speed was reduced continuously from 2000 rpm to 0. The thickness was between 2.7 and 3 μm. A following hard baking process of the resist was done with a certain temperature profile for the baking. At first the temperature was increased to $200°C$ (temperature increase $\leq 4°C$ / minute) and held for 30 minutes at this temperature (pre-baking step). After this step the temperature was increased from 200 to $350°C$ (temperature increase $\leq 2.5°C$/minute).
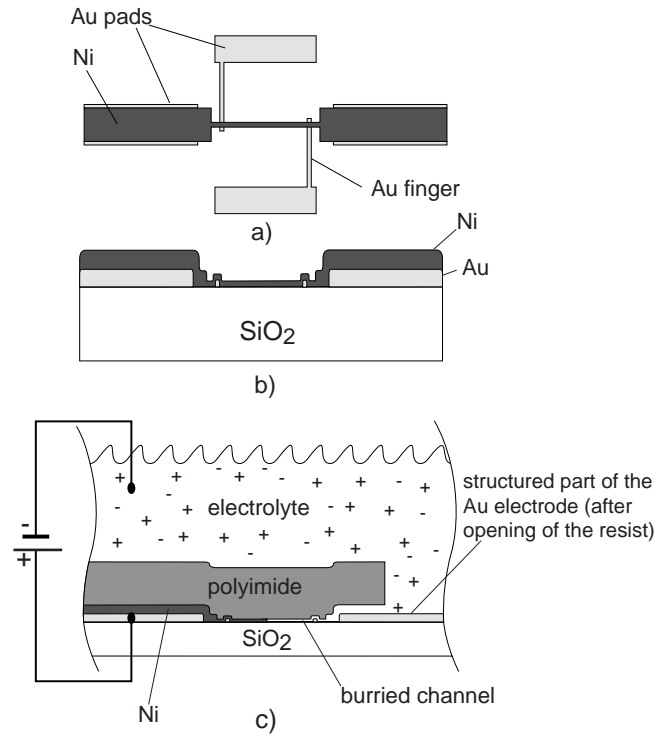
Figure 3.21: a) Top-view of a particular device configuration designed for four-terminal electric measurements. b) Cross section of the device described in a). c) The device after covering the central part with polyimide as an insulating layer. On the right side the polyimide is opened by RIE. The Ni is partially electrochemically dissolved, resulting in a burried channel in between the Au contacts.

Finally a large opening (400μm x 400μm) in the polyimide at one side of the device is structured by reactive ion etching (RIE)[20] at one side of the device, e.g. just over the outer right Au contact pads. An additional PMMA resist layer (3-4 μm in thickness)[21] is therefore used as sacrificial layer, structured by a third EBL step[22]. Through this opening the Ni is electrochemically (at $V_{SCE} = +0.2$V) and /or chemically dissolved with H_2SO_4 (98%)/H_3PO_4 (42%) = 1:5 leaving a *burried nanochannel* underneath the polyimide isolation layer, as shown in Fig. 3.21.c)[23].

The nanochannel runs from the left to the right outer Au pads. After dissolving the Ni, the channel can be refilled by other materials like Bi or CPs using electrochemical synthesis. Now, only one nanopore is obtained and automatically aligned to the macroscopic electric contacts. In Fig. 3.22.a) a SEM image of a Ni wire is shown. The wire was fabricated over two Au fingers used as electrical voltage probes. Fig. 3.22.b) shows a SEM image of a Ni wire fabricated over a Ti/SiO_2 gate electrode (30 nm Ti / 60 nm SiO_2) with SiO_2 being the insulating layer. This opens a possibility to deposit a CP wire over a large gate electrode. Such a device would be an organic field-effect transistor in which the active channel is an organic nanowire. Since CPs behave like semiconductors, a large field effect is expected.

The dimensions of the deposited Ni wires were typically 100 - 200 nm in width, 100 nm in thickness, and 6 μm in length. The structures shown in Fig. 3.22.a) and b) were not covered with the polyimide insulating layer. The polyimide has been found to be pinhole-free, so that the Ni wire is attacked chemically. It is also compatible to the use of organic solvents, which should make deposition of a variety of CPs possible.

To make electrical contacts during the electrochemical procedures, the pads at the outer parts were set free from polyimide by reactive ion etching and contacted with an In-wire, pressed over the Au contact lines. During RIE the inner parts which were exposed to the liquid were covered.

This temperature increase and the following hold at $350°C$ (hard baking step) for one hour was done in a nitrogen atmosphere (oven was purged continuously with nitrogen). Cooling down to room-temperature was done over night in a nitrogen atmosphere.

[20]RIE was done with CHF_3 / O_2 = 10 : 30 (100 watt and a base pressure of 0.05 mbar) for about 20 minutes to set a square structured opening on the Au pads free. The remaining thickness of the polyimide resist varied between 1 and 1.5 μm.

[21]A 9 w/w % solution of PMMA in chlorbenzene was spin-coated twice on top of the polyimide resist with 2000 rpm for 45 seconds, respectively.

[22]Focussing and exact alignment was hard to realize because of the thickness of the organic resist layers but could be done with sufficient accurancy.

[23]The dissolution needed a lot of time (usually some hours) and was not unique for 5 devices aligned in parallel on the same substrate and treated under the same experimental conditions.
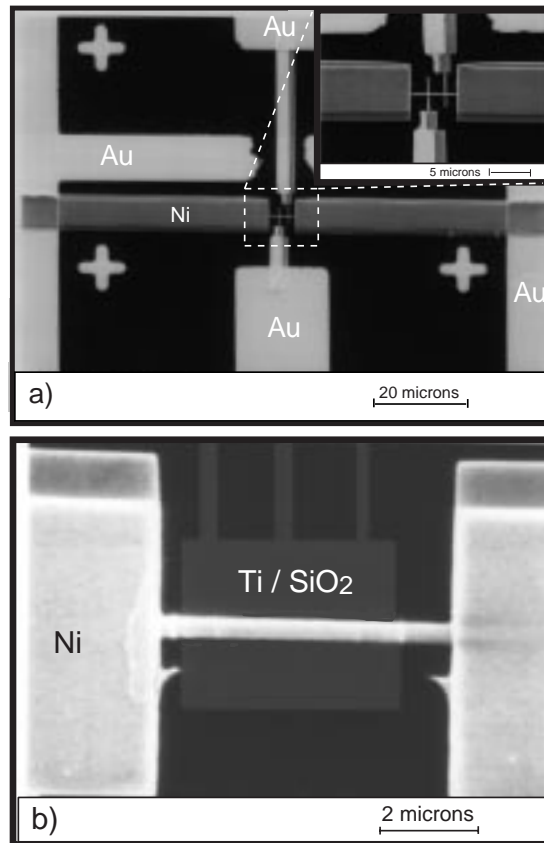
Figure 3.22: a) SEM image of a Ni nanowire fabricated over two gold fingers. b) SEM image of a Ni nanowire fabricated over a large gate electrode (20 nm Ti/60 nm SiO_2). In both cases the shadow evaporation technique was used in order to achieve thin wires (Ni wire and Au fingers) together with thicker leads making contact to the Au pads. The angle used for the thicker parts was $20°$ with respect to the e-beam evaporation source.
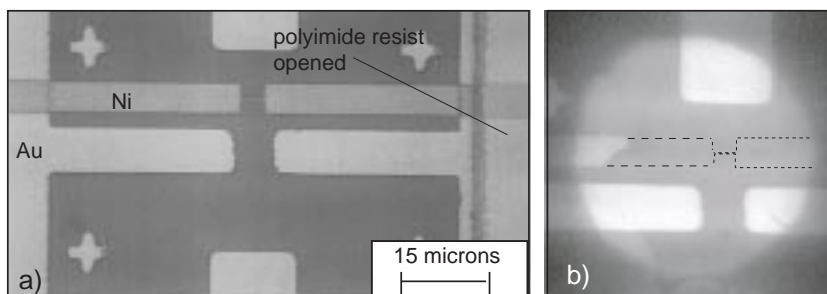
Figure 3.23: a) Optical microscope image of a Ni nanowire over a structured Au electrode; an inert polyimide resist is spinned on top. At the right side the resist was opend by RIE in order to dissolve the Ni wire. b)Optical microscope image of a lateral channel, indicated by the lines. The channel is created by electrochemical dissolution of the Ni wire in H_2SO_4/H_3PO_4 1:5. Both images have the same magnification.

3.6.2 Experimental Results and Discussion

We succeeded in producing such devices as described in the previous chapter. To estimate the reliability of the method we first realized two-contact devices. On dissolving Ni a single pore is formed. This can be observed by optical microscopy, albeit with low resolution only. However, the resolution was sufficient to see that the front between the solution and solid Ni is moving back, resulting in the formation of a pore. Fig. 3.23.a) shows an optical-microscope image of a Ni wire and Fig. 3.23.b) a generated pore just after dissolution of the wire. In both cases the structures are covered with polyimide.

For further use it is important that the pore remains wetted with pure water. Changing the solution from the electrochemical solvent to the plating bath, without allowing the pore to dry out, a metal or a CP could be deposited electrochemically in the pore. This way we have fabricated Bi wires[24] as well as CP wires (poly-3-methyl-thiophene, polypyrrole and polythiophene)[25] Since there is a relatively thick insulating layer (about 2-3 μm of polyimide) over the structure, it is difficult to image the final devices with SEM in order to view at a high magnification. In Fig. 3.24.a) the successful refilling of the pore with Bi is shown on an optical-microscope image. We measured the electric resistance as a function of magnetic field for such wire at three different temperatures, showing that electrical transport measurements are possible. This is shown in Fig. 3.24.b).

---

[24]The deposition of Bi was done in a concentrated $HClO_4$ solution (2.3g Bi_2O_3 in 100 ml $HClO_4$) at $V_{SCE} =$ -0.4 V.

[25]For the deposition of the conducting polymers similar conditions of synthesis were used as described for the bulk films (section 2.4.).
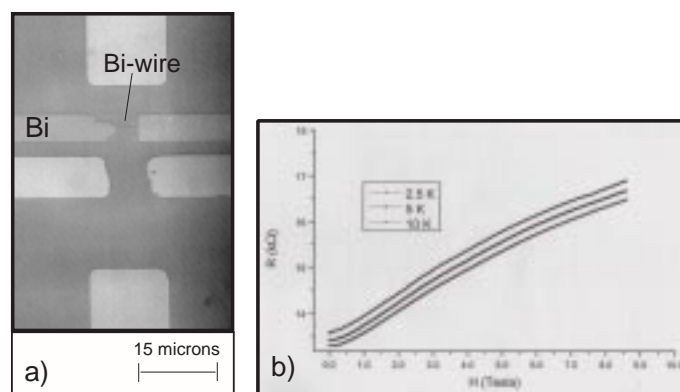
Figure 3.24: a) Optical microscope image of a Bi wire obtained by template synthesis in a single pore which has been fabricated *inplane* before. b) Electric resistance as a function of magnetic field for such a wire at three different temperatures.

In the case of CPs it is difficult to image a successful filling of the pores by optical microscopy and even by confocal optical microscopy. In some cases polymer wires were grown out of the pore channel, covering the contact pad. In Fig. 3.25.a) a multi-device structure is shown. Five devices were fabricated on a Si wafer simultaneously. After dissolving the Ni wire, conducting polymer was deposited in the pores. Some contact pads were grown with the CP after a while, resulting in an increase of the current during the electrochemical deposition. Fig. 3.25.b) shows an optical-microscope image of the inner part of the device after electropolymerisation of polypyrrole (0.1 M) in aqueous solution at $V_{SCE} = +0.8$ V with p-toluenesulfonic acid (0.1 M) as the dopant.

It was concluded that the pores could be filled with CPs. Resistance measurements were carried out successfully, but showed relatively high resistivities[26] in the range of a few MΩ. The *I-V* characteristic showed non-ohmic behaviour: i.e. with increased current the resistance dropped. Taking the geometrical factor into account, one would obtain values for the conductivity below 1 S/cm for the polymer systems which have much higher conductivity values in bulk films (70 - 120 S/cm). It was not clear wether the measured conductivity was linked to the polymer or the ionic solution remained in the pore.

Up to this state only two terminal contacts were applied, therefore the contact resistances could be very high. As mentioned in subsection 2.4.5. the growth

---

[26]Resistance measurements were done DC with a Digistant Typ 4405 calibration source (used as voltage source in combination with a 10 MΩ resistance) and a HP-Nanovoltmeter at a prober station.
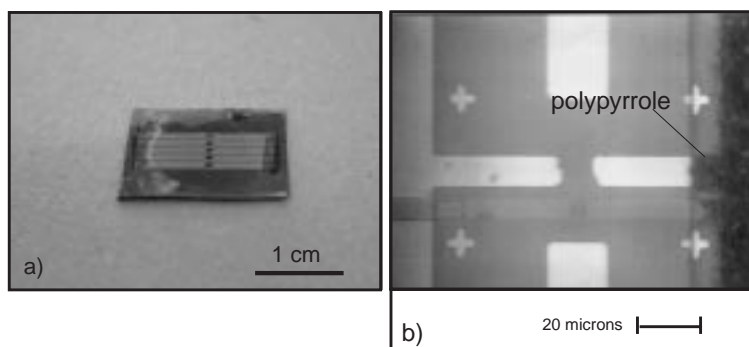
Figure 3.25: a) optical image of 5 Devices aligned parallel on top of a silicon wafer. Polyimide resist is spin-coated on top. The resist was opend (square structures at the right), Ni was dissolved to achieve a lateral nanochannel and polypyrrole was tried to deposited in the channel. At some devices the polymer is grown out covering the electrode areas were the polyimide resist was removed. b) Optical microscope image of the inner part of such an device. The channel was refilled with polypyrrole (0.1 M) in aqueous solution at $V_{SCE} = +0.8V$ with p-toluenesulfonic acid (0.1 M) as the dopant.

of CPs on top of SiO_2 is much different. The polymer forms more granular structures, which can affect the physical properties like conductivity dramatically. This would be a good explanation for the high resistivities measured.

First attempts to produce four-terminal-contacted polymer wires were not completely successfull. After the dissolution of a Ni wire and refilling of the pore with a CP the polymer often grew on top of the finger structure, indicating that there is a free space between the polyimide and the Au finger structure, resulting in the macroscopic-film formation. The shortcuts often caused by pinholes on top of the Au fingers. Several low-ohmic samples in a four-probe configuration have resistances in the range of a few kΩ after electropolymerisation of polypyrrole within the opened channel, but it was not clear, wether the short-cuts were responsible for this values (low resolution of the optical microscope). During this time we got in contact with another type of CP, with a well defined structure, dimensions in the nanometer range by itself without any additional techniques for nanostructuring. This lead us into the fascinating field of carbon nanotubes, which can relatively easy contacted to two- and even four- terminal leads, by methods we were experienced, making electric transport measurements possible. Therefore no further effort was done to improve this method for contacting lateral nanowires. Results and experiments with multiwalled carbon nanotubes are described in chapter 4.

Chapter 4

Carbon Nanotubes as Molecular Wires

4.1 Introduction

Until the 1980s only two crystalline forms of carbon were known, diamant and graphite. The diamant is sp^3-hybridized forming a three-dimensional network by binding to four neighbouring carbon atoms, graphite is sp^2-hybridized forming a two-dimensional layer of hexagons. In the latter case the carbon atom is bound to three neighbouring carbon atoms in the plane, forming one graphene sheet. Between adjacent sheets of carbon the fourth valence electron can move freely building a delocalized π- electronic system. These structural differences strongly affect the chemical and physical properties of diamant and graphite: diamant is an insulator with a large energy band gap, extremely hard and stable against chemicals; graphite is soft, less stable to chemical reactions and conducting. The resistivity of graphite is anisotropic. It is relatively large within the x-y plane (0.4-0.5 x $10^{-4}\Omega$cm), where the electrons can move, and low in the z-direction perpendicular to the graphene sheets (0.2-1.0 Ωcm). Both structures are shown in Figs.4.1.a) and b).

Because of the delocalized electronic system graphite should show metallic behaviour in the x-y direction. Indeed, the hexagonal symmetry of the flat graphene sheet causes the band structure to be that of a zero-gap semiconductor. Graphite shows semi-metallic behaviour, its conductivity is relatively low compared to metals due to the small number of electrons at the Fermi level. Arc-grown and single-crystalline graphite display a metallic behaviour, i.e. the resistivity decreases with decreasing temperature. More disordered graphitic materials where the graphene planes are randomly stacked (so called turbostratic graphite) show a non-metallic temperature dependence of the resistivity [142]. Many intercalation compounds of graphite with e.g. alkali metals are well known and show a
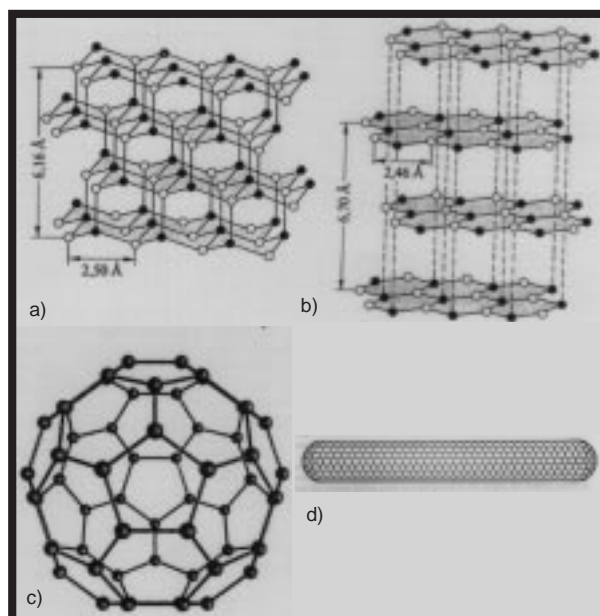
Figure 4.1: Three modifications of carbon: a) diamant structure of carbon; b) graphite structure of carbon; c) structure of the fullerene C_{60}; d) schematics of a carbon nanotube structure regarded as an elongated fullerene.

better electrical conductivity than graphite itself.

In 1985 Kroto discovered a new crystalline modification of graphite, the C_{60} fullerene molecule [143], with a "molecular soccer ball" (so-called "buckyball"[1] structure, as shown in Fig.4.1.c). These balls form a fcc crystal lattice. The discovery mentioned and subsequent synthesis in large quantities in 1990 [144] opened a new field of chemistry and physics of carbon. These fullerene molecules are structures of closed hollow networks ($10\,\mathring{A}$ in diameter) constructed mainly from five- and six rings of carbon (Fig.4.1.c). In contrast to many other molecules, C_{60} and other fullerenes retain their chemical reactivity in the crystalline form resulting in a rather extended solid state chemistry. From 1991 alkali-doped fulleride compounds attracted considerable interest since a number of them are superconducting "synthetic metals" with transition temperatures superseded only by perovskites[2].

While working on the characterization of fullerenes in 1991 Iijima discovered a cylindrical form of the "buckyball", the "buckytube", better known as carbon

---

[1]C_{60} was called buckminster fullerene after its discovery, the name originates from the architect Buckminster Fuller who built up domes in the shape of these "buckyballs" (of course, half of them).

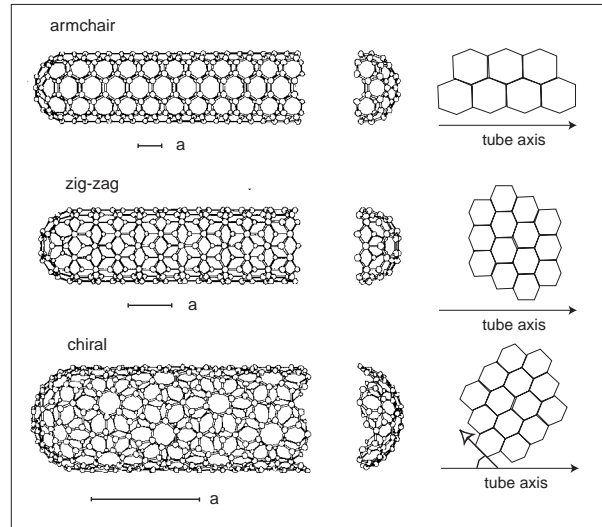[2]For a review about superconductivity in fullerene compounds see Ref.[145].

Figure 4.2: Schematics of three different (single-walled) nanotubes. The length corresponds to the primitive translation vector in the nanotube axis. a) Armchair nanotube: the two C-C bonds on opposite sides of each hexagon are perpendicular to the tube axis. b) Zig-zag nanotube: the two bonds on opposite sides of each hexagon are parallel to the tube axis. c) Helical structure: the C-C bonds lie at an angle to the tube axis.

nanotube (CN) in 1991 [146]. CNs can be regarded as an elongated fullerene (see Fig.4.1.d)[3]. CNs consist of concentric hexagon rich cylinders of sp^2- hybridized carbon, as in graphite, and terminated by end-caps arising from the presence of 12 pentagons (six per end). One can think of a CN as a hexagonal graphene sheet rolled-up into a cylinder. This can be realized in different ways. Two of these are "non-helical" in the sense that the graphite lattices at the top and the bottom of the tube are parallel. These arrangements are termed "armchair" and "zig-zag". In the armchair structure two C-C bonds on opposite sides of each hexagon are perpendicular to the tube axis, whereas in the zig-zag arrangement these bonds are parallel to the tube axis, as indicated in Figs.4.2.a) and b). In all other conformations the C-C bonds lie at an angle to the tube axis and a helical structure results (indicated in Fig.4.2.c)).

The nanotubes discovered by Iijima in 1991 were of the multi-walled type (multiwalled carbon nanotubes; MWNTs) and consisted of several concentric shells with diameters betweeen 2 and 20 nm and several micrometers in length. Multi-shell fullerenes were reported in 1992 and called carbon onions [147]. Sin-

---

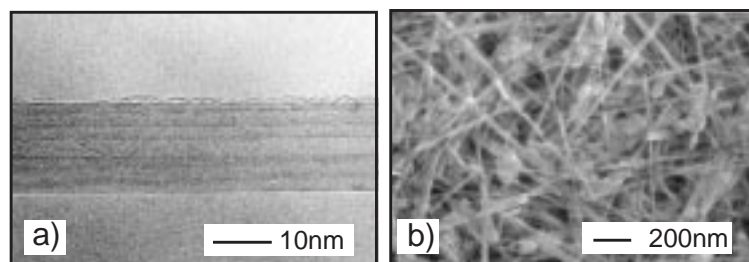[3]For general reviews about CNs see Refs.[138, 139, 140, 141].

Figure 4.3: a) TEM image of a typical MWNT. b) SEM image of a powder of purified MWNTs produced by the group of L. Forró (EPFL Lausanne).The images are taken from Ref.[19]

gle walled carbon nanotubes (SWNTs) were reported 1993 [148] with diameters between 0.7 and 1.6 nm and several microns in length. It took a few years, until 1995, before it became possible to produce clean carbon nanotubes consisting of only one shell in large practical quantities[4][149]. These discoveries marked a new area in the physics and chemistry of carbon nanostructures.

Much of work has been done to develop purification methods for the synthesized tubes and to isolate them from amorphous carbon and other graphitic residues ("onions" etc.). Nanotubes tend to form bundles. For our investigations we used MWNTs synthesized by the arc-discharge method in the group of L. Forró from the EPFL in Lausanne (CH). A transmission electron microscope image of a typical MWNT is shown in Fig.4.3.a). The nanotubes investigated have a diameter between 10 and 20 nm and consist of 10 to 30 shells. In Fig.4.3.b) an SEM image of a powder of purified MWNTs is shown. It is a challenge to select one of these molecules, to attach for example electrical contacts and to use them as molecular wires for electrical transport measurements.

The first electrical conductance measurements on an individual MWNT [154, 155] and an individual SWNT [17, 157] were done in 1996 and were a breakthrough in the field of molecular electronics. Even a room-temperature transistor

---

[4]Carbon nanotubes can be produced in several different ways. One is the arc-discharge method where a current of the order of 70 to 100 A passes through a graphite rod (anode) to a graphite cathode in a He atmosphere. A rod-shaped deposit is formed on the cathode containing bundles of MWNTs. SWNTs can be produced using a variation of this method, by replacing the graphite anode with a hollow graphite tube filled with graphite powder with small amounts of transition metal (i.e. Mn, Cr, Fe, Co, Ni, Cu) and a rare-earth metal (Y, La, Gd, Hf) catalysts [148]. Laser ablation of a graphite target impregnated with a transition metal catalyst in a He atmosphere is an alternative for SWNT production. Another possibility for nanotube production is the thermal decomposition of hydrocarbons in the presence of a catalyst [150]. In this methode the catalyst can be structured on a substrate allowing the selective growth of single nanotubes and aligned nanotube films [151, 152, 153]. Nanotubes with a length exceeding 100 μm can be obtained by this method.
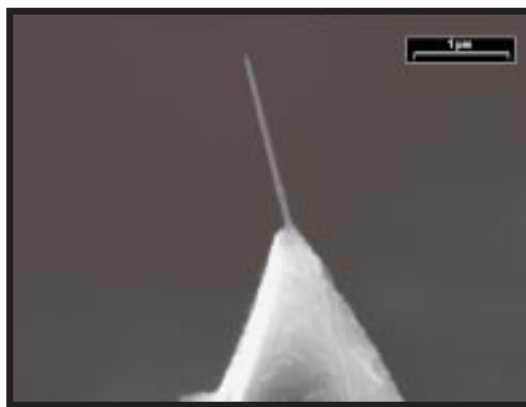
Figure 4.4: A MWNT (bundle) fixed on a Si cantilever by a glue: these tips are extremely sharp and stiff. The image is taken from Ref.[162].

based on a single carbon nanotube can be realized [156]. Besides the use of CNs as molecular wires in nanoelectronic devices, due to their good conductance and the variety in their electronic properties they have a large potential for many different applications. They are not only an interesting model system for fundamental studies of one-dimensional systems but also equally-well or even more attractive for applied researchers and industries due to a large variety of potential applications: They can be used e.g. as a balance for weighing small particles in the fg regime [158], as sharp and well-defined AFM cantilever tips because of their outstanding mechanical properties [159] (an example is shown in Fig.4.4), or as a wire-based planar magnetic switch which has recently been demonstrated [160]. In bulk amounts they can be used as electron field emitters [158] in long-living lamps and for flat-panel displays, as high-strength fiber materials because of their exceptionally high Young's elastic modulus of the order E = 1 Tpa [161], or as a storage medium for H_2, a possible fuel gas [163].

CNs are ideal examples of molecular wires for studying electrical transport through a single molecule. They have exceptional electrical and mechanical properties and they can be manipulated and contacted much easier than other molecules. They are believed to be chemically inert and low-ohmic contacts are easily achievable, which is crucial for the investigation of the intrinsic electrical properties of CNs and for their use in nanoelectronic devices. This explains a large and growing number of publications on electrical transport through single nanotubes or single ropes of nanotubes within the recent years.
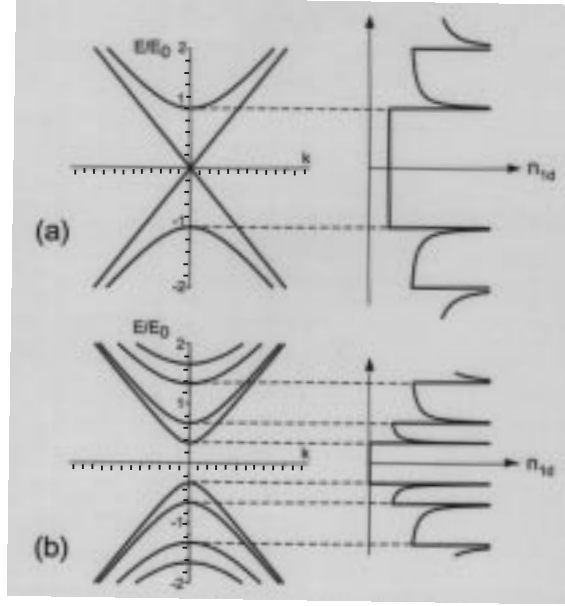
Figure 4.5: Approximate dispersion relations (left) for the one-dimensional bands and corresponding DOS (right) of metallic (a) and semiconducting (b) SWNTs close to the Fermi energy. The energy scale is in units of $E_\circ = 2hv_f/2\pi d$

4.2 Electronic Properties of Carbon Nanotubes

4.2.1 Introduction

Theoretical calculations predict that electronic properties for a SWNT vary as a function of its diameter and helicity [164, 165, 166, 167, 168, 169][5], and that the tube may behave as a semiconductor or a metallic conductor. Measurements by scanning tunneling spectroscopy (STS) have nicely confirmed this prediction [170, 171]. In general 1/3 of the SWNTs should be metallic and 2/3 semiconducting. All armchair tubes are metallic, zig-zag tubes are either metallic or semiconducting. In Fig. 4.5.a) and b) the dispersion relation for the one-dimenional band structure and the corresponding DOS of a metallic and a semiconducting SWNT is shown.

CNs are giant molecular wires in which the electrons can freely propagate, as in a ordinary metal. This strongly contrasts with conventional "conducting polymers" (Chapter 2) where the electrons localize. CPs are actually insulators and become conductors only if they are doped. As mentioned in the introduction, a SWNT can be estimated as a rolled-up graphene sheet. Graphite is a "zero-gap"

---

[5]For reviews about the electronic properties of CN see Refs.[172, 173, 174].

semiconductor. This peculiarity renders the electronic states very sensitive to additional boundary conditions, such as the periodic boundary condition along the circumference of a CN. A stationary electron wave can develop only, if the circumference of the tube is a multiple of the electron wavelength. This removes the peculiarity mentioned and turns nanotubes into either true metals or semiconductors. A perfect metallic nanotube is supposed to be a ballistic conductor. A ballistic conductor is the best (normal electron) conductor an engineer can dream of, and is beaten only by a superconductor. If an electron is injected from a contact into a ballistic wire with ideal contacts, the electron will end at the drain contact with certainty. There is no back-scattering in the wire, which is the source of intrinsic electric resistance and leads to Ohm's law. The theory predicts for a SWNT two independent eigenmodes independent of the diameter. The electric conductance is then expected twice the fundamental conductance $G_\circ$ ($G_\circ = 2e^2/h$) [177]. In contrast to classical resistors and to Ohm's law, the resistance is independent of the length of the wire. In reality, impurities, defects (pentagons and heptagons instead of hexagons), as well as "bad" contacts makes it difficult to investigate the expected ballistic behaviour.

4.2.2 Electronic Properties of Multiwalled Carbon Nanotubes

Because MWNTs consist of several concentrically arranged SWNTs, one would expect that MWNTs do not qualify as one-dimensional conductors. If adjacent carbon shells interact as in graphite, electrons may not be confined to one shell only. Recent results show that the current in MWNTs mainly flows through the outermost shell [175, 176]. In this respect, studying electric transport in MWNTs is similar to studying transport in a large diameter SWNT. MWNTs have some advantages:

- They have larger contact areas because of their larger diameters making low-ohmic contacts possible.

- Their large diameter enables the investigation of quantum interference phenomena in a magnetic field. Recently the Aharonov-Bohm effect in MWNTs has been demonstrated[176].

- Arc-discharge grown MWNTs do not contain magnetic impurities and contain less defects.

Electric transport measurements on single MWNTs have been performed in two different ways:

- Metallic leads are attached to a single tube on top of a Si wafer. This can be done by microfabrication technology [176, 154, 178, 155]. Contacts can
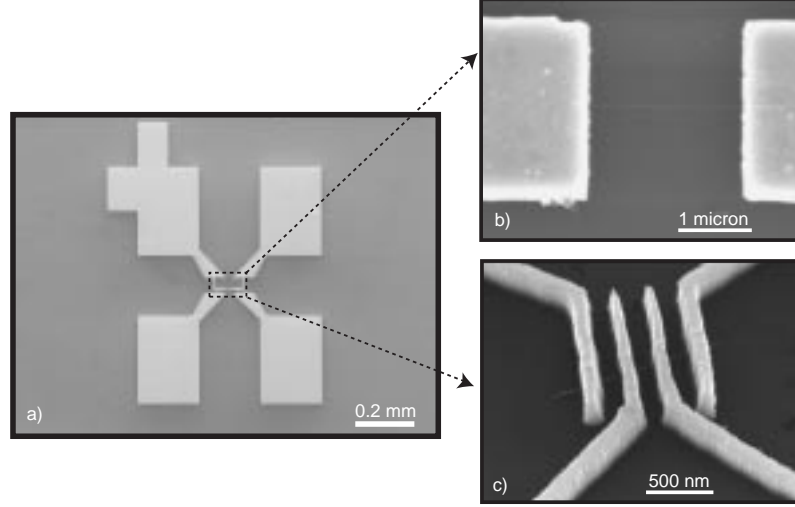
Figure 4.6: a) SEM image of one single device of a contacted CN. b) SEM image of a two-terminal contacted CN c) SEM image of a four-terminal contacted CN.

be fabricated on top of the tubes (leading to low contact resistances R_c between 0.1 and 20 kΩ with an average of 4 kΩ [173]) or below the tubes. In the latter case the yield of the successfully contacted tubes is quite low and the contact resistances are quite large ($\sim$ 1 MΩ). R_c has been determined from comparing the two-terminal (R_{2t}) with the four-terminal (R_{4t}) resistance according to $R_c = (R_{2t}\text{-}R_{4t})/2$. In our case we fabricated contacts on top of the nanotubes by EBL[6]. The SEM image in Fig.4.6.a) illustrates one contacted nanotube. The SEM image of Fig.4.6.b) shows a characteristic two-terminal contacted single MWNT and the SEM image shown in Fig.4.6.c) represents a four terminal contacted single MWNT.

 – A different method was reported by Frank et al.[175] where a macrobundle of MWNTs was fixed onto a movable manipulator, which is steered above a beeker containing a liquid metal (e.g. Hg) and then

---

[6]Onto an oxidized Si wafer an array of contact pads (four-terminal or two-terminal) together with alignment marks was patterned by EBL and Au evaporation. On the wafer (usually 2cm x 2cm) 49 such contact-pad assemblies were fabricated. After an ultrasonic treatment for 15 minutes a droplet of a dispersion of CNs in CHCl$_3$ was spread on top of the contact-pad arrangement by spin-coating. After adsorbing the NTs the samples are imaged in SEM in order to locate suitable NTs. Having notified the coordinates (using the alignment marks) the electrodes can be structured directly onto the respective NTs with high precision. One additional EBL- and Au evaporation step is necessary to fabricate the contact leads to the tube. Within this second Au evaporation step no Ti adhesion layer was used, otherwise the contact resistances were found to be high-ohmic, with increasing R_c in time.
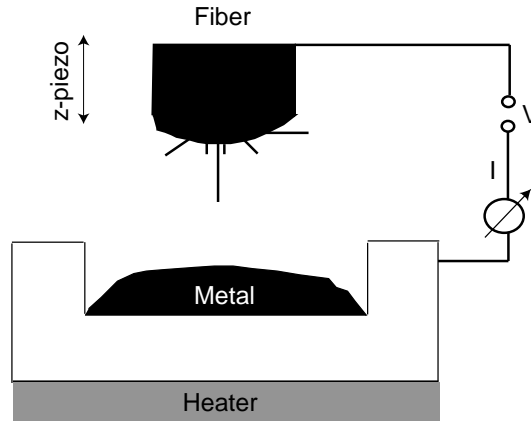
Figure 4.7: Schematic diagram of the contacting apparatus of Frank et al. The fiber is moved into the liquid metal while the conductance G is being measured.

gently lowered into it. Thereby, a single MWNT is making contact to the liquid metal first, enabling conductance measurements on a single tube. A schematic diagram of the contacting apparatus is shown in Fig.4.7.

They measured the conductance G while the fiber is being moved into the liquid and found that G increased in steps of magnitude close to the quantized conductance $G_0 = 2\mathrm{e}^2/\mathrm{h}$. Each step is due to an additional MWNT coming into a contact with the liquid. The nearly equal conductance of $\approx G_0$ for each MWNT has been taken as evidence for quantum ballistic transport. The fact that large electrical currents could pass through a single MWNT without heating-up the tube and destroying them strongly suggests ballistic transport as well.

Other experiments like magnetoresistance measurements on a single MWNT[154], recently observed Aharonov-Bohm resistance oscillations in a single MWNT [176], and observed electron-electron interactions at low temperatures [174] indicate that the transport is diffusive or at least quasi-ballistic. The question whether a MWNT is a ballistic wire with no backscattering effects or a diffusive wire is still open. The origin of the observed backscattering phenomena is not known at the present. Nonetheless, both the experiment of Frank et al. and the observed Aharonov-Bohm effect in MWNTs indicate that the current in MWNTs is carried by the outermost conducting shell.
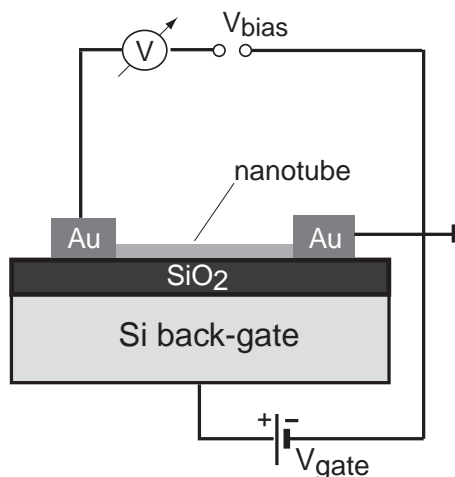
Figure 4.8: Schematic side-view of a TUBEFET device. A single nanotube is contacted by two electrodes. The doped Si substrate, covered by a layer of SiO_2, acts as the back-gate electrode.

4.2.3   Doping the Carbon Nanotubes

Doping is an important tool to modify electronic properties of materials. For example, p- and n-doped Si is the basic for many microlectronic devices. B and P atoms are built into the lattice as electron acceptors or donors, respectively. Doping of some fullerides by intercalation of alkalimetal atoms lead to metallic behaviour and even to superconductivity in some cases [145]. Changing the charge carrier concentration leads to a shift of the Fermi level. Doping of CPs described in Chapter 2 changes the electrical properties, e.g. the electric resistivity, over a several orders of magnitude. The change of the carrier concentration can also be achieved electrostatically by applying an electric field using an additional gate electrode. Doped Si separated from the device by an insulating oxide layer can be used as gate electrode. The first room-temperature transistor based on a single SWNT was described by Tans et al.[156] who used a doped Si back-gate electrode. A semiconducting SWNT was connected to two metal electrodes. By applying a voltage to the gate electrode, the nanotube could be switched from a conducting to an insulating state. A schematic of a so called "TUBEFET" device is shown in Fig.4.8. This was a real breakthrough, since the operation of such a field-effect transistor (FET) works at room-temperature, which is an important requirement for possible applications and an important step towards molecular electronics.

The question are then CNs intrinsically doped has recently attracted considerable attention, in particular for SWNTs. Already in 1994, Song et al. found a positive value of the Hall coefficient R_H by studying the electronic properties of macrobundles of MWNTs [179]. This suggests that nanotubes are hole-doped. Much more evidence for the hole doping was derived from the thermoelectric-power measurements, both for SWNT- and MWNT ropes [180, 181, 182], where the thermoelectric-power was found to be positive. Most recently, it has been shown that the magnitude and even the sign of the thermoelectric-power can be changed by annealing the nanotubes in vacuum. It is believed that such a treatment removes oxygen which may act as the dopant [183, 184, 185]. This indicates that nanotubes might be more sensitive to the environmental conditions than initially believed. Extrinsic doping would make it impossible to investigate intrinsic electrical properties. This could be an explanation for the conflicting results on electric transport measurements on single MWNTs. Scattering effects observed, leading to the diffusive transport behaviour in nanotubes might be caused by dopants which are adsorbed on the surface of the nanotubes und suppress the expected ballistic transport.

Recent results of Kong et al. demonstrate the sensitivity of CNs to environmental conditions [186]. By exposure of a single SWNT to NO_2 and NH_3 the tubes were found to behave as a hole-doped semiconductor. After the exposure to the gases the chemical gating effect and the conductance changed up to around three orders of magnitude. This indicates a shift of the valence band away from the Fermi level, induced by the charge-transfer interactions of the gases and the tube and leading to chemical gating. This gating effect was found to be reversible. In the following our experimental results on the doping of MWNTs by different techniques are described.

Doping of a Single MWNT by a Si Back-Gate Electrode

Highly doped Si [7] with a 400 nm SiO_2 layer on top was used as a substrate for creating four-terminally or two-terminally contacted single MWNT devices. Measurements of the resistivity versus the applied gate voltage V_g were carried out at room temperature. The resistance was measured by a lock-in technique. A characteristic R-V_g diagram observed for a single four-terminal contacted MWNT is shown in Fig.4.9.: a) is an example of a low-ohmic sample, and b) for a higher ohmic sample [8].

---

[7] Boron doped Si with $\rho \leq 0.02$ Ωcm.

[8] Resistances between 1.4 kΩ and 12.5 kΩ for the four-terminal contacted MWNTs were observed. Most of the MWNTs had resistances betwen 2 kΩ and 5 kΩ. The distance between
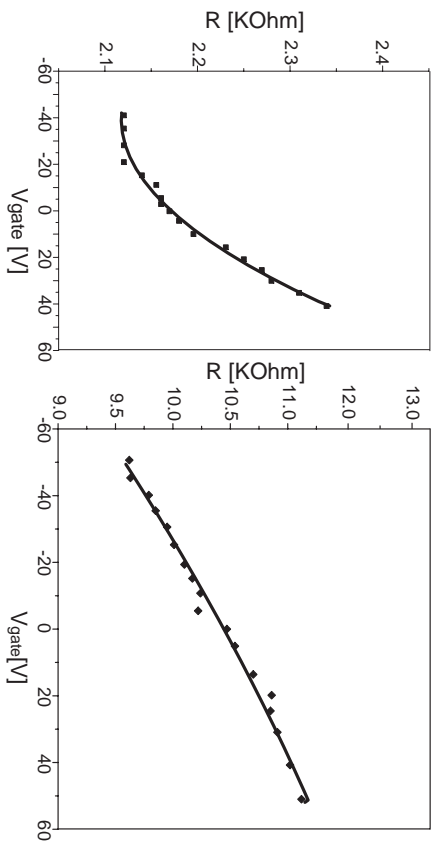
Figure 4.9: Characteristic R_{4t}-V_g diagrams for two different samples: a) a lower ohmic (2.24 kΩ at V_g = 0 V) and b) a higher ohmic one (10.43 kΩ at V_g = 0 V). The curves are reversible for the forward and backward scans.

At room temperature we found a weak dependence of the resistance on the applied gate voltage for both the low-ohmic and high-ohmic samples. By changing V_g of the Si back-gate between -50 V and +50 V the resistance changed within 5-20% (in most of the cases within 10 %). This indicates a metallic-like behaviour, because for semiconducting tubes one would expect a more strongly pronounced dependence of the resistance to V_g. By applying a positive voltage to the Si back-gate electrode the resistance increases, whereas the negative voltage leads to a decrease of the resistance. This was found for all the samples investigated, indicating that the MWNTs we used were originally p-doped[9]. The slope of the decrease at negative V_g was usually lower than for the increase at positive V_g, sometimes leading to a saturation at high negative voltages, as seen in Fig.4.9.a).

In the case of the two-terminal contacted MWNTs the same resistance behaviour was observed as a function of the applied V_g. Usually a hysteresis was observed due to the change of the the contact resistance as a function of V_g. An example of a two-terminal measurement is shown in Fig.4.10. The separation of the electrodes was in this case around 500 nm. The resistance change observed in two-terminal contacted samples between V_g = -50 V to +50 V was 50-100% indicating the additional change of R_c.

---

[9] For negative V_g an accumulation of holes occurs leading to a decrease of the resistance, whereas for a positive V_g the holes are depleted, yielding a higher resistance.
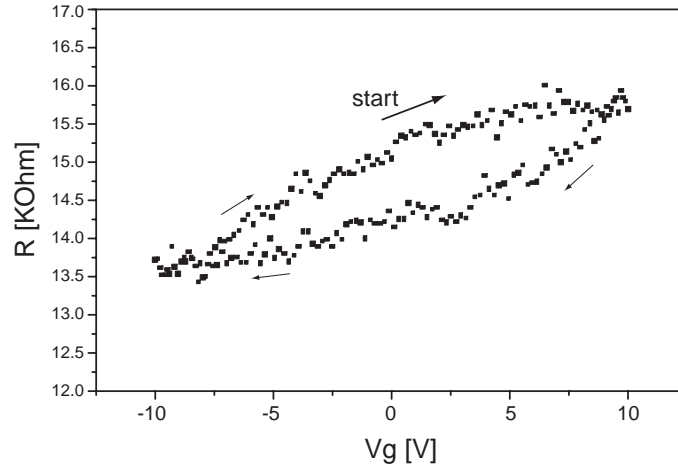
the two voltage leads was usually about 300 nm and 350 nm.

Figure 4.10: Characteristic R-V_g diagram for a two-terminal contacted single MWNT between V_g = -10 V and +10 V. The arrows mark the direction of the measurement. A hysteresis is observed.

Electrochemical Doping of MWNTs

By using a single contacted MWNT as an electrode itself, one can place a droplet of an ionic solution onto the MWNT and apply a voltage between the tube electrode and a counter electrode. The charged surface of the tube attracts ions of opposite charge and repels ions of like charge. An electric double-layer is built-up, which can be interpreted as capacitor. The surface charge and therefore the electric field between the oppositely charged layers can be varied by the applied voltage. Now we have the situation equivalent to a back-gate electrode. By changing the electric field one can modulate the doping state of the nanotube. But now much larger electric fields can be easily achieved because the distance between the two charged layers is reduced to one or a few nanometers in comparison to 400 nm SiO_2 layer of the Si back-gate[10]. The resistance can be investigated as a function of the voltage applied between the tube and a Pt counter electrode (V_{PT}). A schematics demonstrating the electrochemical doping is shown in Fig.4.11.[11]

---

[10]The voltage which could be applied to the Si back-gate electrode was limited to about 70-80 V, at higher voltages an electrical breakdown occured leading to a current flow through the oxide layer.

[11]The measurements were carried out at a probing station (shown in Appendix C). Positioning of the droplet and controlling its shape during the measurement was done using an optical microscope. The size of the droplet was between 50 and 200 μm, wetting also parts of the leads. This did not affect the resistance measurements of the tube, since it was found that the resistance of a droplet on top of the used elctrode arrangement is much higher (several MΩs
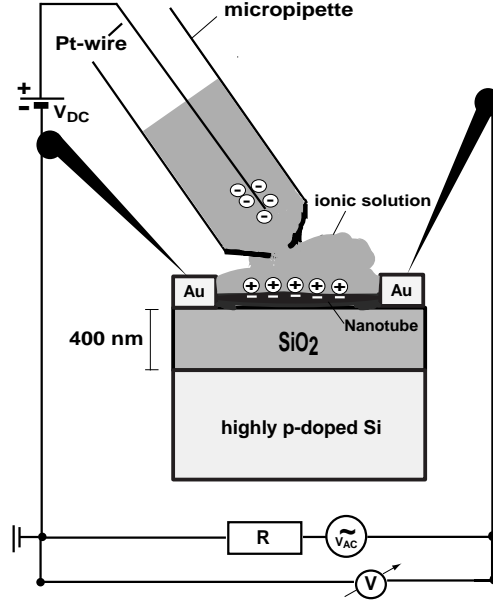
Figure 4.11: Schematics of the electrochemical doping of a single MWNT. A droplet of an ionic solution is applied by a micropipette and a microliter syringe on top of the nanotube using a micromanipulator. The resistance of the tube was measured by a lock-in technique ($I = 100$ nA at frequencies between 15 and 30 Hz) as a function of the applied voltage V_{DC} between the tube and the Pt wire (counter electrode). Measurements were usually carried out in the range of 0 to +1.8 V (with respect to the ground potential). A charged double-layer is established on the nanotube surface due to V_{DC}, influencing the electronic properties by changing the electric field. Further remarks are given in the footnote 11, photographs of the arrangement for measuring the electrochemical gate effect are given in Appendix C.

One would expect that electrochemical gating would be more effective than a conventional Si back-gate electrode. We indeed observed a drastic change of the nanotube resistance, namely between 50 and 500%, as a function of the applied voltage V_{Pt} between the counter electrode (Pt) and the tube

---

depending on the droplet size and the concentration of the ionic solution). The DC current between the nanotube and the Pt counter electrode in the solution is dominated by the contact of the solution with the Au electrode arrangement. This DC current (below 1 nA for lower values of V_{DC} to about 100 nA for high values of V_{DC}) was measured as well and does not affect the AC current in the tube. The method developed is suitable for good conductors as CNs, otherwise the measurements are affected by the ionic conductivity.
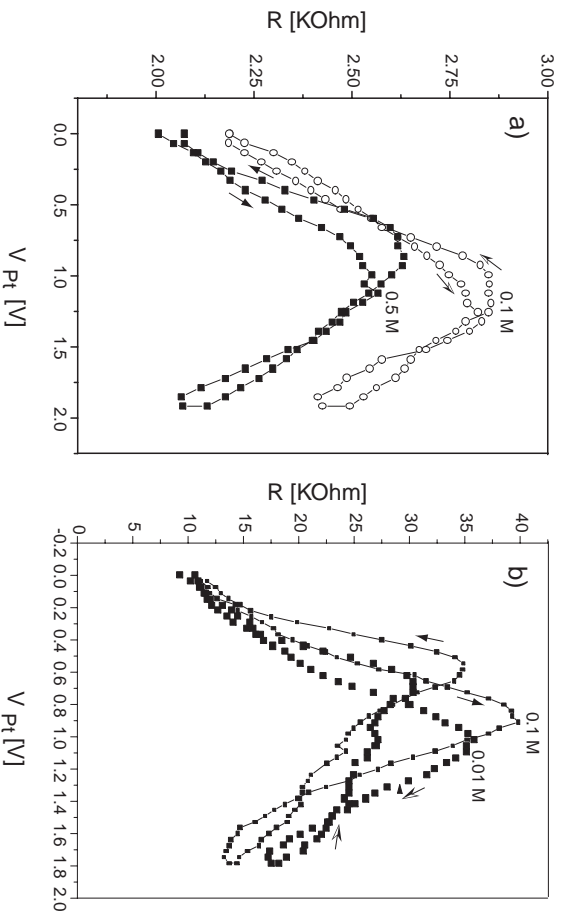
Figure 4.12: Characteristic R-V_{Pt} diagrams obtained by electrochemical doping with LiClO$_4$ for four-terminal contacted single MWNTs. Different concentrations of LiClO$_4$ were used. A peak shift to the left to lower values of V_{Pt} can be seen for higher concentrations of LiClO$_4$. The forward and backward scans are marked by the arrows. a) The behaviour of a low-ohmic sample is indicated (see also Fig.4.9.a)). b) The behaviour of a high-ohmic sample is indicated as well (see also Fig.4.9.b)).

electrode. MWNTs are hole conductors if left unpolarized. By applying a positive voltage to a counter electrode a resistance peak which signals the transition from hole to electron conduction occurs. In Fig. 4.12.a) and b) characteristic R-V_{Pt} curves of one single MWNT electrochemically doped with LiClO$_4$ are shown. The same MWNTs as those in the backgate measurements (Fig.4.9.a) and b)) were used for the electrochemical doping. The general results obtained by electrochemical doping of single MWNTs are summarized as follows:

— After wetting the MWNT with a LiClO$_4$ solution the resistance usually dropped for around 10-15%. By excluding the ionic conduction the ClO$_4^-$ anion seems to change the charge on top of the CN surface by a specific adsorption or an electron transfer between the tube and the anion (charge transfer process or a redox reaction), thus increasing the p-doped state.

— In most of the cases an increase of the electrolyte concentration shifts

the peak to the lower values of V_{Pt}. This is demonstrated in Fig.4.12.a) and b), where two measurements with different electrolyte concentrations are shown, respectively. This represents qualitatively what would one expect: The Debeye length λ, which can be regarded as a measure of the thickness of the ion atmosphere at the charged surface double layer, represents the distance of the oppositely charged layers [187]. λ depends strongly on the concentration c and the charge of the electrolyte ($\lambda \propto c^{-1/2}$), varying from hundreds of water-molecule diameters in dilute solutions to a distance of the order of one water molecule diameter in concentrated solutions of highly charged ions. Therefore an increase of the ion concentration leads to lower values of λ and to a reduced potential V_{PT} for reaching the maximum of the peak.

The observed shifts of the peak to lower potentials with higher concentrations is much less pronounced then expected: the concentrations we used were relatively high (0.4-0.5 M), and the simple picture of of the electric double layer is still valid. It is also important to note that it is difficult to control the concentration within a droplet. By evaporation of water the concentration of the ionic solution within the droplet increases. The deposits of salts on the tube after one measurement are unavoidable, therefore after changing the concentration of the solution these residues can change the concentration of the droplet in a second measurement.

— The peak obtained by a forward scan is usually not as high as the peak obtained by the backward scan. Sometimes a pronounced hysteresis was observed, as can be seen in Fig. 4.12.b). This suggests that electrochemical doping is a time dependent process. Why some samples show more pronounced time dependence on the doping than the other samples under the same experimental conditions is not clear.

— By driving the potential to the higher positive values of $V_{Pt}(\geq +2.0$ V) or to the negative potentials ($V_{Pt} \leq$ -0.5 V) the resistance increases drastically. But even now a pronounced resistance peak can be observed at the similar potential and with an increase of equivalent order in magnitude. An example is shown in Fig.4.13.a)and b). At higher oxidation or reduction potentials redox reactions of the tube with, e.g. water, could be induced leading to defects. This could be an explanation for the observed increase of the resistance.

— It should be remarked that the resistance in general increased slightly with the increasing number of experiments done on the same tube. Also the relative increase of the resistance to the initial value becomes
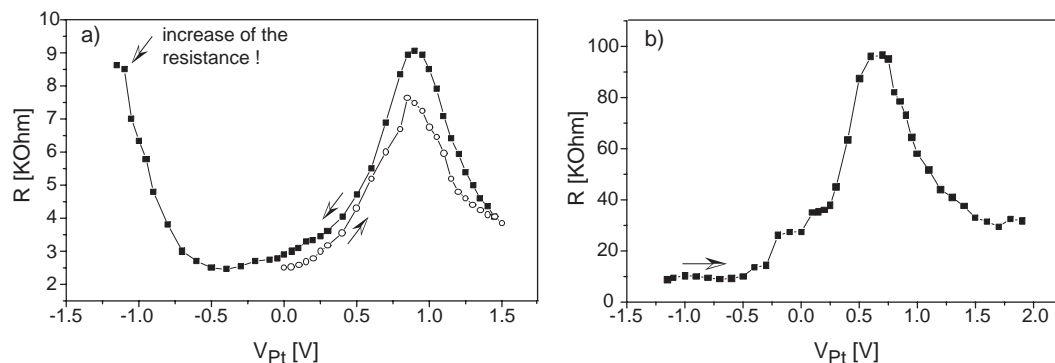
Figure 4.13: a) R_{4t}-V_{Pt} diagram of a single MWNT doped in a 0.4 M LiClO$_4$ solution. The forward and backward scans are indicated by the arrows.The peak occurs at around +0.9 V. By reaching a negative potential of around -0.5 V the resistance begins to increase significantly. b) R-V_{Pt} diagram after the resistance change to higher values. A peak could also be observed at around $V_{Pt} = +0.7$ V. The magnitude of the resistance increase (around 250-300%) at the top of the peak is quite similar to the one shown in a).

more pronounced. In Fig.4.14.à schematic of the R-V_{Pt} diagram observed for the same tube shown in Fig.4.9.a) is demonstrated after holding the tube at a high reduction potential ($V_{Pt} = 1.9$ V) for about ten minutes. The initial resistance at V_{Pt}=0 V has increased from 2.17 kΩ(curve a) in Fig.4.14.) to 3.6 kΩ (curve b) in Fig.4.14). The doping was carried out in a 0.01 M solution of LiClO$_4$. After the backward scan a resistance of 3.21 kΩ was observed, indicating a partial regeneration of the resistance. For comparison, the graph of the initial measurement carried out under identical experimental conditions is shown in addition (curve a). It can clearly be seen that the relative peak height has increased (the magnitude changed from about 50 to about 100%). After removing the solution and exposure to air the resistance dropped to 2.26 kΩ, near to the initial value. Since the measurements shown in Fig.4.14 were four-terminal measurements, changes of the contact resistances can be excluded.

At higher oxidation or reduction potentials redox reactions of the tube with e.g.water could be induced, leading to defects. Electrochemical doping should be completely reversible if electrochemical reactions or adsorbtion phenomena can be excluded. The slight increase of the resistance in time suggests some irreversibility. Structural changes within the tube by electrochemically-induced reactions
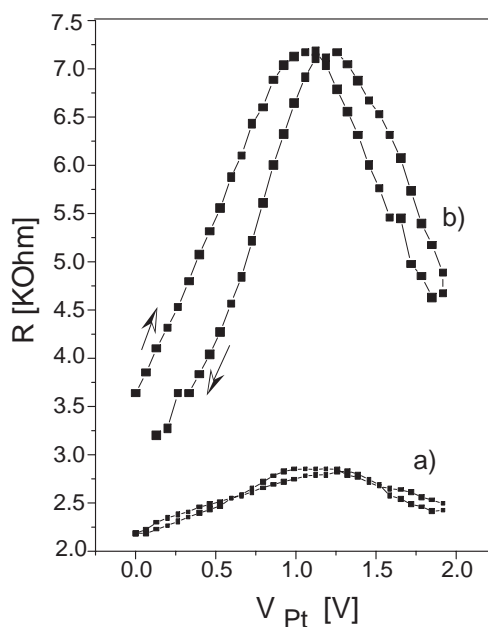
Figure 4.14: R-V_{Pt} diagram of a single four-terminal contacted MWNT doped in a 0.01 M LiClO$_4$ solution after holding the tube at a high reduction potential for about ten minutes (curve b). It is the same tube which was used for the measurements described in Fig.4.9.a). The resistance has increased from 2.17 to 3.6 kΩ. During the measurement after the backward scan the resistance dropped to 3.21 kΩ. The relative height of the peak has increased compared to the initial measurement (curve a). After removing the ionic solution and the air exposure the resistance dropped to 2.26 kΩ, near to the initial value.

of the nanotube would lead to an irreversible increase of the resistance as it was found e.g. at higher positive and negative voltages (Fig.4.13.b)). But this would not explain the partial regeneration of the resistance after removing the solvent and exposure to the air observed in the sample treated at high reduction potentials for a few minutes (e.g.shown in Fig.4.14.). If the originally p-doped state of the MWNTs is caused by the adsorbed oxygen, an additional scenario has to be be taken into account. With the increasing reduction potential the possibility of oxygen reduction on the surface of the nanotube, due to the following chemical reaction, must be taken into account: $O_2 + 2\,e^- + 2\,H^+ \longrightarrow H_2O_2$. This reaction is an irreversible process leading to a loss of the hole-doping. After removal of the solution and exposure of the nanotube to air, oxygen could be adsorbed again by the nanotubes and act as dopant. The resistance would be at least partially restored.

It was reported recently that improved charge transfer at CN electrodes can favour the reduction of oxygen more easily when compared to other carbon materials as graphite [188]. To explore a possible influence of oxygen to the doping state of CNs additional experiments have to be done, e.g. to desorb the possible adsorbed oxygen on the tube in the vacuum at higher temperature and to investigate the resistance change during the desorption process followed by the adsorbtion process after air (oxygen) exposure in time. Preliminary results of this kind will be presented briefly in the following section.

– The resistance peak usually occured between $V_{PT} = +0.8$ V - $+1.1$ V, with a mean value of about $+0.9$ V. In most of the cases the concentration of LiClO$_4$ was 0.4 M. The curves themselves were sometimes broader and it was difficult to determine the voltage value V_{Pt} of the peak. If hysteresis occured a V_{Pt} value for the forward and for the backward scan could be determined. The given V_{Pt} values represent in this case mean values of the two observed values of the forward and the backward scans. By using KCl (0.01 M) as the electrolyte the resistance peak was observed at $V_{PT} = +1.0$ V.

– By using KMnO$_4$ as the electrolyte a peak shift to higher positive potentials of V_{PT} was observed, as shown in Fig.4.15. After wetting the CN with the ionic solution the resistance dropped about 30-40% within five minutes. For a KMNO$_4$ concentration of 0.1 M (pH = 5-6) V_{Pt} of the peak could not be determined precisely, but it was $\geq +1.5$ V. At higher voltages the resistance increased irreversibly. For a 0.01 M solution the resistance peak occured at $V_{Pt} = +1.2$ V. The peak
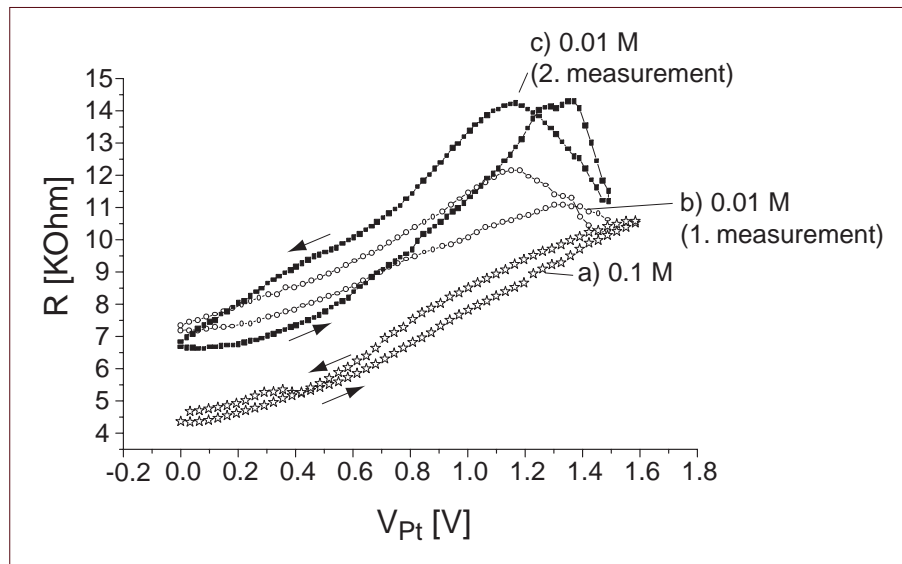
Figure 4.15: R-V_{Pt} diagrams: curve a) a single two-terminal contacted MWNT doped in a 0.1 M KMnO$_4$ solution. By driving V_{Pt} to higher positive potentials an irreversible increase of the resistance was observed. Curve b) represents the situation of a single two-terminal contacted MWNT doped in 0.01 M KMnO$_4$. By repeating the experiment an increase in the peak height was observed, but no significant peak-shift to the left to lower potentials V_{Pt} (curve c). The arrows indicate the direction of the voltage scan.

height increased in time without changing V_{Pt} of the peak and using the same concentration of the electrolyte. Besides the electrochemical gating, induced by the ions, an additional chemical gating effect of the oxidizing $MnO_4{}^-$ anion occurs, increasing the hole doping and shifting the resistance peak to higher positive potentials. By using the higher concentrations of $KMnO_4$ the additional hole doping is increased by the increase of the oxidizing effect.

– Electrochemical doping using H_3PO_3[12] as the electrolyte which is a strong reducing agent, leads to a peak shift of the resistance to lower values of V_{Pt} (Fig.4.16.). The additional chemical gating leads to a reduction of the hole doping. The resistance peak therefore shifts to the left, to lower positive potentials. By wetting the MWNT with the H_3PO_4 solution (0.01M) the resistance increased of about 10-15%. The height of the peak inreases by time as well as the peak shifts to the lower values of V_{Pt}. This is shown in Fig.4.16. in a R_{4t}-V_{Pt} diagram of a four-terminal contacted single MWNT.

In the first measurement (a) we observed a resistance peak at +0.7 V for the forward and at +0.3 V for the backward scan. The second measurement, performed just after the first one, some minutes later, demonstrates an increase in the height of the peaks of about 50% and a shift to +0.55 V for the forward and to +0.2 V for the backward scan.

The time dependence of the peak shift is very interesting, since this was not observed using the oxidizing electrolyte ($KMnO_4$). This implies an additional chemical reaction changing the tube (structural change by a reduction process) or its surrounding (surface). Structural changes would probably lead to higher resistivities without reaching the original value after the measurement as it was observed (Fig.4.15.). If oxygen is adsorbed at the surface, changing the electronic properties of the tube by doping, one would expect a peak shift to a lower value of V_{Pt} if oxygen is removed. Since H_3PO_3 is a strongly reducing agent one can think about the following reaction which could occur easily at higher reduction potentials: $H_3PO_3 + H_2O \longrightarrow H_3PO_4 + 2\ H^+$. This reaction would lead to a decrease of the pH in time. Now the reduction of oxygen can follow more easily: $O_2 + 2\ e^- + 2\ H^+ \longrightarrow H_2O_2$, on the surface of the tube. By the decrease of the pH one would expect a peak shift to lower values of V_{Pt} due to the irreversible removal of oxygen.

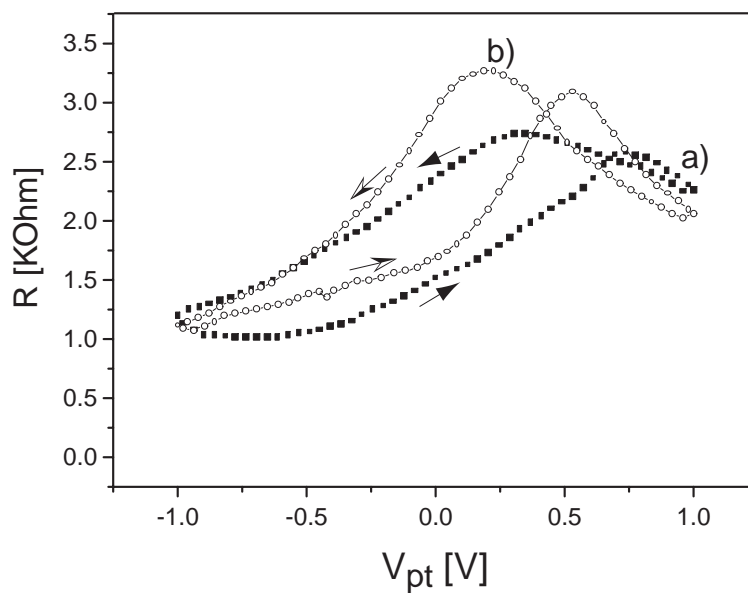[12]KOH was added to the solution until a pH of 6 was obtained.

Figure 4.16: R-V_{Pt} diagrams of a four-terminal contacted MWNT doped in a 0.01 M H_3PO_3 solution. The resistance peaks for the forward and backward scans are shiftet to lower values for V_{Pt}. This shift is time-dependent. In addition the height of the peaks are increasing in time. Curve a) represents the first measurement and curve b) the second one detected just a few minutes later.
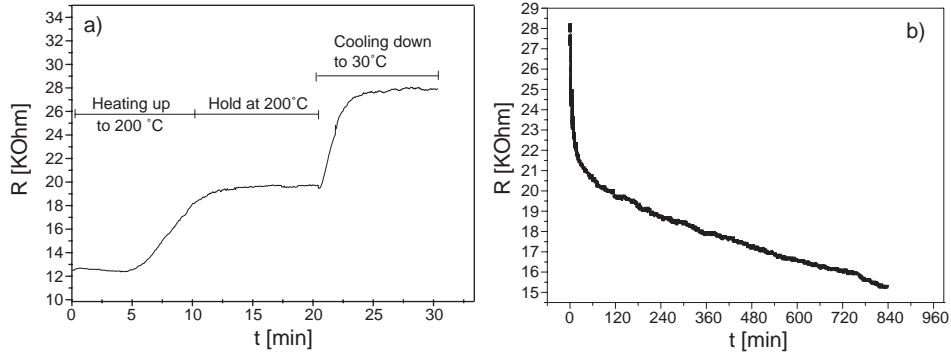
Figure 4.17: a) R_{2t}-t versus time during the annealing sequence. After R_{2t} increases the vacuum treatment and heating to 200°C, it saturates. By cooling down to 30°C an additional increase is observed. b) Exposure of the MWNT device to air at normal pressure afterwards. The resistance decreases in time.

Annealing a Contacted MWNT in Vacuum

A preliminary experiment was carried out on a single two-terminal contacted MWNT in order to investigate the resistance changes by the annealing in vacuum[13]. The initial resistance R_{2t} was 12.05 kΩ. After putting the device in a low pressure of 8 mbar for one hour the resistance slightly increased to 12.6 kΩ. By heating-up the device for ten minutes to 200°C the resistance increased to 19.7 kΩ and saturated. After cooling-down the sample to 30°C at the same pressure the resistance increased to 27.6 kΩ. The two-terminal resistance R_{2t} as a function of time t is shown in Fig.4.17.a). After the exposure to air the resistance decreased again as a function of time but needed much longer time to saturate at 15.2 kΩ. The original value of 12.05 kΩ was not achieved again. By repeating the annealing experiment described above for a second time the starting resistance of 15.2 kΩ can be restored. This is shown in Fig. 4.18., where the experiment was repeated after room-temperature exposure to air over two days. The decrease within the first two hours was quite strong and afterwards the slope of the R_{2t}-t curve became flat. The inset to Fig.4.18. shows the annealing step with the increase of R_{2t}.

---

[13]An Annealing Oven AZ 500 of MBE Komponenten GmbH (Germany) was used. The distance of the two Au contacts of the sample was 1.4 μm. A single MWNT device was fixed onto a macor plate. Contacting the Au pads was done by bonding Al wires to the silver-painted areas on the SiO$_2$ surface. The macroscopic contacts were obtained by contacting these areas by larger wires. Because of the sensitivity of single MWNTs to charging effects a good ground contact had to be realized during contacting and putting the device in the oven.
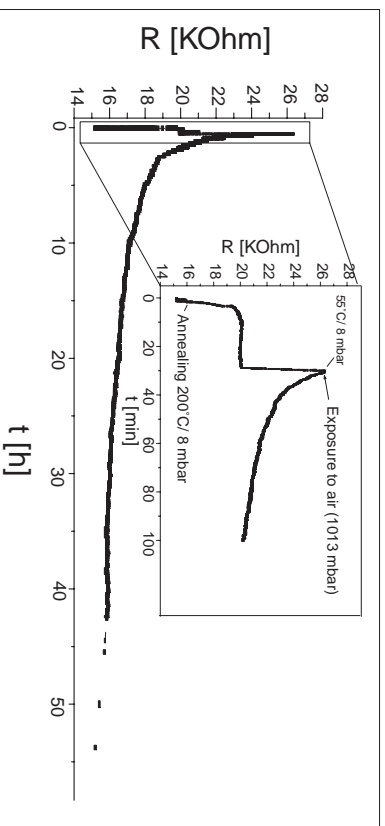
Figure 4.18: The R_{2t}-t behaviour by repeating the annealing sequence for a second time is shown. After air exposure R_{2t} dropped in this case to the value where annealing has been started. The inset shows the annealing part within the first 100 minutes.

After the second measurement the device has been taken out from the oven. The resistance was measured again but directly on the contact pads, e.g. without additional wiring in between. A value of 13.56 kΩ was obtained instead of 15.2 kΩ indicating that additional wiring and connection via silver-paint contacts lead to higher contact resistances of the circuit. Probably heating up to 200°C effects silver-paint contacts by effecting the organic binder of the silver paste [189]. The reversibility of the second measurement shows that the contact resistance of the Au contacts to the tube are not affected by heating significantly. One can conclude that the resistance increase of the MWNT (about 85%) by annealing in vacuum and the resistance decrease after exposure to air is due to the change of the environmental conditions. Heating of the tube would lead to a decrease of the resistance, as it is shown that cooling-down the tube increases R_{2t}.

Since annealing in the vacuum is supposed to remove adsorbed oxygen the resistance increase is correlated to hole depletion. Exposure to air probably leads to the adsorbtion of oxygen again, leading back to the p-doped state of the tube, since there is no other possible dopant around[14]. Hence, the resistance decreases again due to the restored p-doped state of the MWNT.

---

[14]Nitrogen, the noble gases and CO_2, the other parts of air are inert and non-oxidizing species without the possibility to induce doping effects in the MWNT.
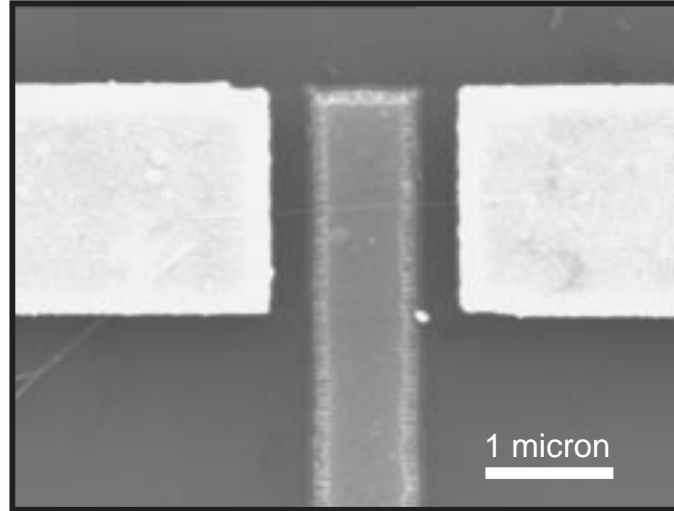
Figure 4.19: SEM picture of a single two terminal contacted MWNT with a Al-gate electrode on top between the two Au contacts.

Doping of a Single MWNT by a Nearby Al-Gate Electrode

We found the Al makes "bad" contacts to our MWNTs. This can be used to fabricate an Al-gate electrode on top of a single two-terminal contacted MWNT[15]. In Fig.4.19. a SEM picture of such a nanotube device is shown. In most of the cases there were no shortcuts observed from the Al to the Au contacts[16]. The distance betwen the Au contacts was usually about 1.4 μm and the width of the Al-gate 1 μm, so about 70% of the tube surface was covered with Al. The two-terminal resistances R_{2t} measured, varied between 6.2 kΩ and 34.5 kΩ with a mean value of about 14.5 $\pm$ 6 kΩ. Because the Al-gate is placed just on the top of the tube one would expect a similar gate effect observed by electrochemical doping of the MWNTs. A resistance peak should be observable and the changing of the doping state possible. This indeed could be observed. The resistance of the MWNT can be changed as a function of the applied gate voltage in a controlled and reversible way. A characteristic R_{2t}-V_g diagram is demonstrated in Fig. 4.20. The main features, observed at about twenty different samples, are summarized in the following, comparing the results with the results of the electrochemical doping (ECD):

---

[15]The Al gate was fabricated in a first step by EBL. Afterwards two Au contacts were produced by an additional EBL step.

[16]High contact resistances, from several MΩ to even larger values were found.
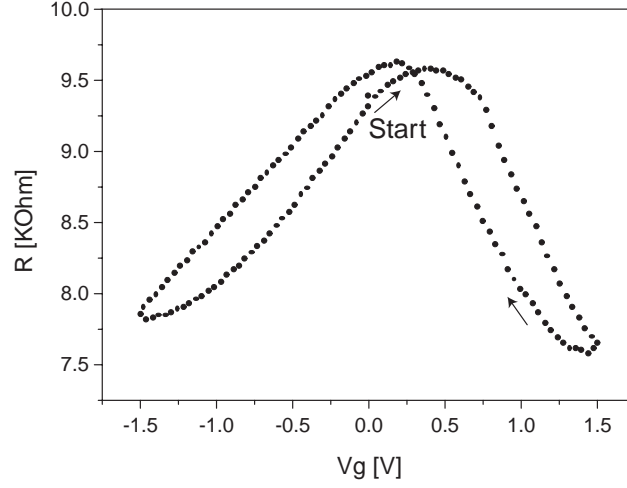
Figure 4.20: Change of R_{2t} of a single MWNT as a function of the applied voltage V_g of a nearby Al-gate on top of the tube. A resistance peak could be observed. The arrows indicate the scan direction.

- The characteristic resistance peak was observed in all the samples. In comparison to the ECD, the peaks were shifted at $V_g = 0$ to the left, indicating a hole depletion in same cases even n-doping. The peaks were usually observed between $V_g = $ -0.5 V to +0.5 V, often around $V_g = 0$. Since Al tend to react with oxygen one can imagine that during the evaporation Al can react with possible oxygen residues adsorbed on the tubes. This would probably affect the doping state. Al is a reducing agent as H_3PO_3 used for ECD, and we observed a similar peak shift to the left, in the direction of the neutral state of the CNs, and sometimes even more far to the n-doped state of the CNs. In addition oxygen could partially removed in vacuum. It seems that evaporation of Al protects the tube from adsorbing oxygen again and stabilizing a hole-depleted state.

- The peaks were generally broader when compared to ECD. The magnitude of the resistance change by the doping varied between 15 and 70% [17] and was lower than the resistance change observed by ECD.

- The hysteresis between the forward und backward scans observed indicates a time-dependence of the doping. It has been indicated that the hystereses vanishes by sweeping V_g very slowly during several hours for one scan between $V_g = $ -1.5 V and + 1.5 V. (as shown in Fig.4.22.a)

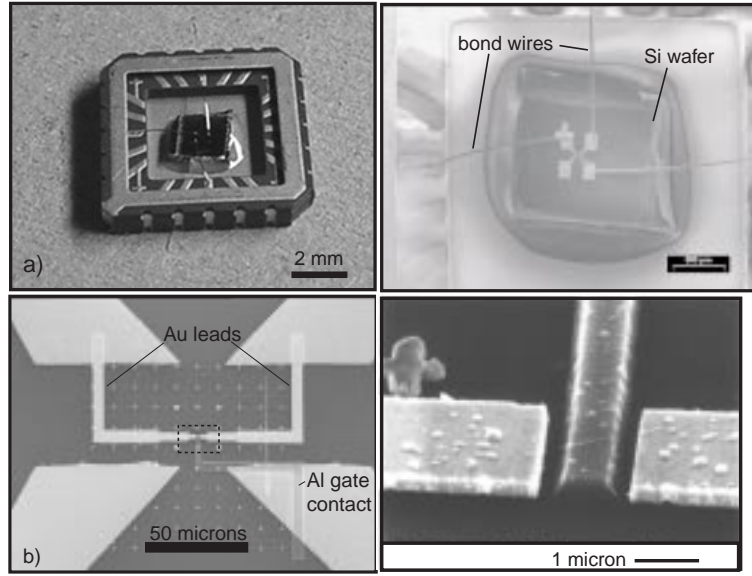[17]One has to keep in mind that R_{2t} was measured.

Figure 4.21: SEM images of a contacted device of one single MWNT: a) left: optical image of a MWNT device bonded in a chip carrier prepared for low-temperature mesurements. right: SEM image with larger magnification; bonding from the Au contact pads to the contact pads of the chip-carrier can clearly be seen. b) Left: SEM image of the inner part of the MWNT device with two Au leads and one Al lead for the gate contact. Right: sideview (45 degree) of the inner part: a 300 nm thick Al gate is on top of the single MWNT.

 — Our preliminary measurements of the doping using an Al-gate electrode have shown advantages over the conventional Si back-gate electrode approaches. Namely, much lower gate voltages are required in the present case, which leads to an enhanced sensitivity of the measurements. In Fig. 4.21. we show a device used in these measurements and in Fig. 4.22.a)-f) the results obtained (all measured in the R_{2t}-V_g configuration). It can be expected that this or a similar method might contribute to investigate the physics of MWNTs in the near future.

The devices were found to be very sensitive to electrical charging. In Fig. 4.23.a) a R_{2t}-V_g plot of a forward-and-backward sweep of V_g at 300 K is shown. The mesurement was carried out extremly slowly, i.e. over several hours. The hysteretic behaviour observed at higher sweep rates almost vanished and the resistance peak occured at $V_g = + 0.25$ V. By decreasing the temperature a fine structure developed (Fig.22.4. a)-e)). Significant resistance peaks as a function of V_g were observed. The highest resistance
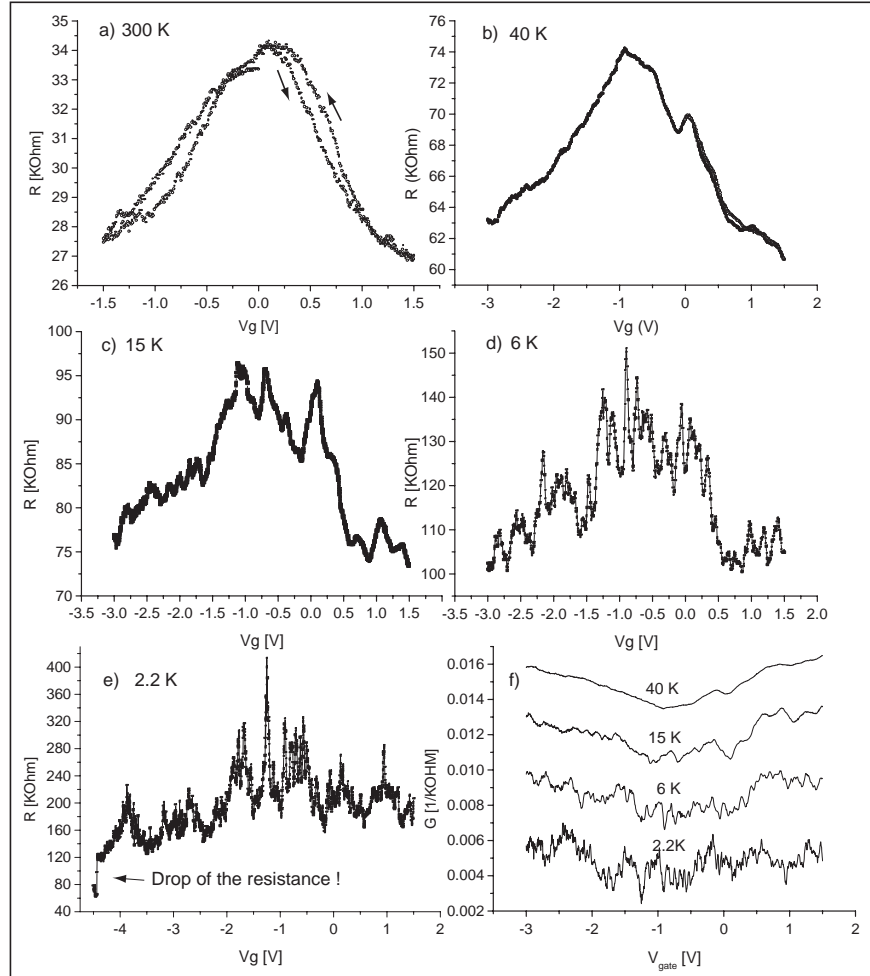
Figure 4.22: The temperature dependence of R_{2t} as a function of the applied gate voltage V_g for a two- terminal contacted single MWNT with an Al gate electrode on top, for five different temperatures. a) A forward-and backward sweep at 300 K. The measurement was done over several hours, the hysteretic behaviour observed at higher sweep rates vanished. b)-e) With decreasing the temperature a fine structure developed. Substantial resistance changes as a function of V_g are present. f) The electric conductances as a function of V_g for several temperatures.
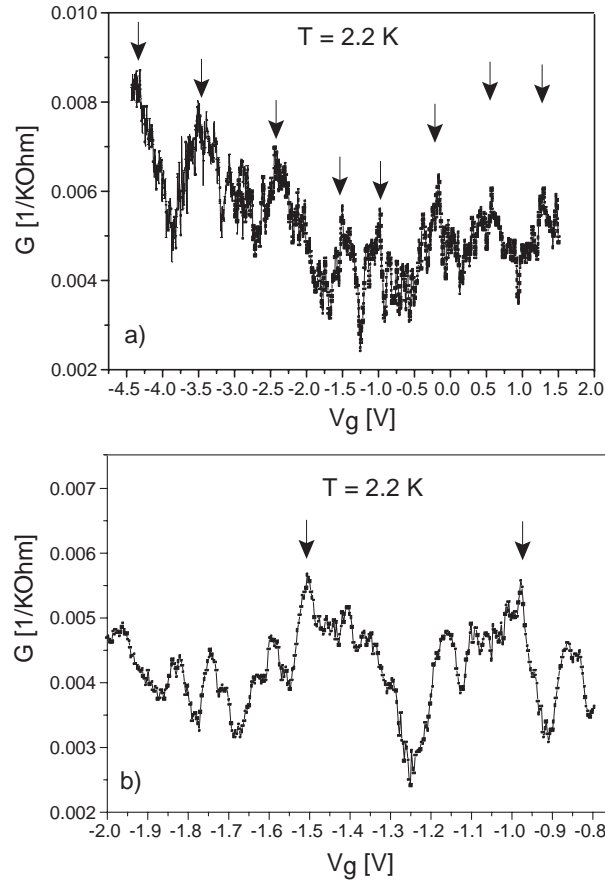
Figure 4.23: a) The conductance at $T = 2.2$ K as a function of V_g . The arrows indicate the peaks in the conductance. The peaks seem to group somehow to larger assemblies and are qualitatively equidistant. b) A magnified view of the inner part of the diagram shown in a), around the deepest dip in the conductance. The left and the right parts around the dip are fairly symmetric.

peak at 2.2 K was found to be around V_g = -1.25 V. In Fig. 4.22.f) are plotted the conductances as a function of V_g for several temperatures. The occurence of increasing changes of the conductance as a function of V_g with decreasing temperatures could be observed. In Fig. 4.23.a) the conductance as a function of V_g at 2.2 K is shown in more detail. As indicated in Fig.4.23.a) the conductance peaks seem to group in larger assemblies at specific gate voltages. The single peaks are qualitatively equidistant. A magnified view on the deepest dip in the conductance (around $V_g = $ -1.25 V), shown in Fig. 4.23.b), indicates fairly symmetric behaviour. The assemblies

are possibly correlated to the sub-band features. Since one sample was measured only further research is required in order to draw more elaborated conclusions.

4.3   Summary and Conclusions

It has been demonstrated that the doping of single MWNTs can be achieved by different methods. The doping modifies the electronic properties of CNs. Beside the doping using a conventional Si back-gate electrode with SiO_2 as barrier there are two more efficient methods. Rough calculations indicate that the changing can be 50 or 100 times more efficient with respect to the Si back-gate electrode for both the electrochemical doping and doping by the use of a nearby Al gate electrode. In both cases a resistance peak as a function of the applied voltage is observed, indicating a transition from hole to electron doping. The peak can be shifted if oxidizing and reducing agents are present during electrochemical doping.

We found that the MWNTs used in our measurements were intrinsically p-doped. Electrochemical doping with H_3PO_3 as the reducing agent and a time-dependent peak shift, as well as a preliminary annealing experiment of a single MWNT at 200°C and 8 mbar indicate strongly that oxygen is responsible for the intrinsic doping of CNs. Hence, extrinsic effects seem to play an important role by influencing the intrinsic properties of MWNTs. This sensitivity to environmental conditions could perhaps be used to build a molecular sensor. One could think about gas sensors where reducing or oxidizing gases influence strongly the conductivity of the tube, which could then be correlated to a specific concentration of a gas. Even a possibility of constructing a molecular pH sensor could be considered provided that the resistance peak observed in electrochemical doping can be shifted reversible as a function of pH. This method would be superior to electrochemical sensoring methods like cyclic voltammetry. Namely the measured resistance is a function of the molecule itself and can be measured very precisely in a wide range, whereas in the cyclic voltammetry the detected current as a function of the applied voltage is not determined only by the material of the electrode.

Chapter 5

Outlook

With respect to several topics this thesis can be considered as a starting point towards molecule electronics. Normally there are still many questions left open, as follows, but answering them might be an exciting and challenging task. For example, to what extent can the Al nearby gate electrode be used to investigate the electronic properties of CNs ? Is this a promising method for fabricating a whole class of controllable and reliable nanoelectronic devices? Reversible extrinsic chemical or electrochemical doping of CNs could be useful for developing highly sensitive chemical sensors. An advanced version of the template synthesis might be a method for aligning the nanotubes or other suitable molecules in highly-orderd arrays which would be useful in large scale applications of CNs, e.g. as field- emitters. Perhaps CNs could be used as molecular electrodes for creation of hybride-materials by the deposition of electroactive materials (metals or CPs) on to them.

It is not unrealistic to think about using two closely faced nanotubes as electrodes for trapping other molecules, building-up more complex molecular devices. Since the current in MWNTs is transported by the outermost metallic shell one can possibly use an inner shell, separately contacted, as gate electrode to modify the electronic properties of the MWNT.

Bibliography

[1] W. H. Brattain, J. Bardeen Phys. Rev. **74**, 230 [1948]

[2] H. Queisser, *Quristallene Krisen*, Piper-Verlag München (1985)

[3] P. Frommherz, A. Offenhäuser, T. Vetter, J. Weiss Science **252**, 1290 (1991)

[4] H. W. Fink, C. Schönenberger Nature **398**, 407 (1999)

[5] D. Porath, A. Bezryadin, S. de Vries, C. Dekker Nature **403**, 635 (2000)

[6] B. J. van Wees *et al.*, Phys. Rev. Lett. **60**, 848 (1988).

[7] A. Aviram, C. Joachim, M. Pommerantz Chem. Phys. Lett. **146**, 490 (1988)

[8] L. A . Bumm, J. J. Arnold, M. T. Cygan, T. D. Dunbar, T. P. Burgin, L Jones II, D. L. Allara, J. M. Tour, P. S. Weiss Science **271**, 1705 (1996)

[9] M. F. Crommie, C. P. Lutz, D. M. Eigler Science **262**, 218 (1993)

[10] T. A. Jung, R. R. Schlittler, J. K. Gimzewski Nature **386**, 696 (1997)

[11] J. van Ruitenbeek in *Quantum point contacts between metals in Mesoscopic Electron Transport, Ed. L. L. Sohn, L. P. Kouwenhoven, G. Schön*, Kluwer Academic, Dordrecht (1997)

[12] J. M. van Ruitenbeek, A. Alvarez, I. Pineyro, C. Grahmann, P. Joyez, M. H. Devoret, D. Esteve and C. Urbina, Rev. Sci. Instrum. **67**, 108 (1995)

[13] E. Scheer, N. Agrait, J. C. Cuevas, A. L. Yeyati, B. Ludoph, A. Martin-Rodero, G. R. Bollinger, J. M. van Ruitenbeek, C. Urbina Nature **394**, 154 (1998)

[14] H. Ohnishi, Y. Kondo, K. Takayanagi Nature **395**, 780 (1998)

[15] M. A. Reed et al., Science **278**, 252 (1997)

[16] C. Kergueris, J.-P. Bourgoin, S. Palacin, D. Esteve, C. Urbina, M. Magoga, C. Joachim Phys. Rev. B **59**, 19 (1999)

[17] S. J. Tans, M. H. Devoret, H. Dai, A. Thess, R. A. Smalley, L. J. Geerligs and C. Dekker Nature **386**, 474 (1997)

[18] T. W. Ebbesen, H. J. Lezec, D. Hiura, J. W. Bennett, H. F. Ghaemi and T. Thio Nature **382**, 54 (1996)

[19] A. Bachtold, Thesis, University of Basel (1999)

[20] Morpurgo et al. Appl. Phys. Lett. (1999)

[21] A. Bezryadin, C. Dekker, G. Schmid Appl. Phys. Lett. **71**, 1273 (1997)

[22] D. J. Berets, D. S. Smith Trans. Faraday. Soc. **64**, 823 (1968)

[23] M. Hatano, S. Kambara J. Polym. Sci. **51**, 26 (1961)

[24] T. Ito, H. Shirakawa, S. Ikeda J. Polym. Sci. Chem. **12**, 11 (1974)

[25] H. Shirakawa, T. Ito, S. Ikeda Polym. J. **4**, 460 (1973)

[26] H. Shirakawa, E. J. Louis, A. G. MacDiarmid, C.K. Chiang, A. J. Heeger J. Chem. Soc., Chem. Commun. 578 (1977)

[27] C. K. Chiang, M. A. Druy, S. C. Gau, A. J. Heeger, E. J. Louis, A. G. MacDiarmid Phys. Rev. Lett. **39**, 1098 (1977)

[28] C. K. Chiang, M. A. Druy, S. C. Gau, A. J. Heeger, E. J. Louis, A. G. MacDiarmid, Y. W. Park, H. Shirakawa J. Am. Chem. Soc. **100**, 1013 (1978)

[29] H. Naarman Synth. Metals **17**, 223 (1987)

[30] J. Tsukamoto, A. Takahashi, K. Kawasaki Jap. J. Appl. Phys. **29**, 125 (1990)

[31] T. A. Skotheim, R. L. Elsenbaumer, J. R. Reynolds *Handbook of Conducting Polymers 2nd Edition, Chapter V: Applications of Conducting Polymers*, MARCEL DEKKER INC., New York (1998)

[32] S. Curran, A. Stark - Hauser, S. Roth *Handbook of Organic Conductive Molecules and Polymers, Volume 2, Chapter 1: Polyacetylene, Ed. H. S. Nalwa*, J. Wiley and Sons, 1997

[33] S. Roth *One Dimensional Metals, VCH Weinheim* 1996

[34] A. P. Monkman *Physics of Conductive Polymers in Introduction to Molecular Electronics, Ed. M. C. Petty, M. R. Bryce, D. Bloor* E. Arnold 1995

[35] W. P. Su, J. R. Schrieffer, A. J. Heeger Phys. Rev. Lett. **42**, 1698 (1979)

[36] R. E. Peierls *Quantum Theory of Solids*, Oxford University Press, London (1955), p.108

[37] C. O. Yoon, M. Reghu, D. Moses, A. J. Heeger Phys. Rev. B **49**, 10851 (1994)

[38] J. W. Gardner, P. N. Bartlett Nanotechnology **2**, 19 - 32 (1991)

[39] J. Heinze *Electronically Conducting Polymers in Topics in Current Chemistry* Vol 152 (1990)

[40] G. P. Evans *The Electrochemistry of Conducting Polymers in Advances in Electrochemical Science and Engineering Vol 1 Ed. H. Gerischer, Ch. W. Tobias*, VCH Weinheim (1990)

[41] L. Zuppiroli, M. N. Bussac, S. Paschen, O. Chauvet, L. Forro Phys. Rev. B **50**, 5196 (1994)

[42] C. Schmid, diploma thesis, University of Basel, 1996

[43] P. Novak, B. Rasch, W. Vielstich J. Electrochem. Soc. **138**, 3300 (1991)

[44] T. L. Tansley, D. S. Maddison J. Appl. Phys. **69** 7711 (1991)

[45] F. Beck, P. Braun, M. Oberst Ber. Bunsenges. Phys. Chem. **91** 967 (1987)

[46] Masa-aki Sato, Susuma Tanaka, Kyoji Kaeriyama, J. Chem. Soc. Chem. Commun. 713 (1985)

[47] N. F. Mott, E. A. Davis *Electronic Processes in Non-Crystalline Materials*, 2nd ed., Clarendon press, Oxford, (1979)

[48] T. Kunugi, H. Okuzaki Journal of Polymer Science **34** 1269 (1996)

[49] M. Yamamura, T. Hagiwara, K. Iwata Synthetic Metals **26** 209 (1988)

[50] L. J. van der Pauw, Philips Res. Reports **13** 1 (1958)

[51] L. J. van der Pauw, Philips Techn. Rundschau **20** 230 (1958/59)

[52] Kohlrausch - *Praktische Physik Bd. 2 ed. by G. Lautz, R. Taubert* Stuttgart, B. G. Teubner Verlag, 1968 p.305

[53] R. Menon *Charge transport in Conducting Polymers in Handbook of Organic Conductive Molecules and Polymers Vol.4 Ed. H. S. Nalwa*, John Wiley and Sons, 1997

[54] R. Menon, C. O. Yoon, D. Moses, A. J. Heeger *Metal-Insulator Transition in Doped Conducting Polymers in Handbook of Conducting Polymers, Ed. T. A. Skotheim, R. L. Elsenbaumer, J. R. Reynolds*, Marcel Dekker, Inc., 1998

[55] M. Ahlskog, R. Menon, J. Phys.: Condens. Matter **10**, 7171 (1998)

[56] A. Aleshin, R. Kiebooms, R. Menon, F. Wudl, A. Heeger Phys. Rev. B **56**, 3659 (1997)

[57] K. Lee, R. Menon, A. J. Heeger, K. H. Kim, Y. H. Kim, A. Schwartz, M. Dressel, G. Grüner Phys. Rev. B **61**, 1635 (2000)

[58] R. S. Kohlman, A. Zibold, D. B. Tanner, G. G. Ihas, T. Ishiguro, Y. G. Min, A. G. MacDiarmid, A. J. Epstein Phys. Rev. Lett. **78**, 3915 (1997)

[59] P. Phillips, Hong-Lu Wu, Science **252**, 1805 (1991)

[60] D. S. Maddison, T. L. Tansley J. Appl. Phys. **72**, 4677 (1992)

[61] S. M. Sze, *VLSI Technology*, McGraw-Hill (1988)

[62] F. K. Perkins, E. A. Dobisz, S. L. Brandow, J. M. Calvert, J. E. Kosakowski, C. R. Marrian Appl. Phys. Lett. **66** 976 (1996)

[63] T. C. Shen, C. Wang, J. W. Lyding, J. R. Tucker Appl. Phys. Lett. **66** 976 (1995)

[64] M. J. Lercel, G. F. Redinbo, H. G. Craighead, C. W. Sheen, D. L. Allara Appl. Phys. Lett. **65** 974 (1994)

[65] E. S. Snow, P. M. Campbell Science **270** 1639 (1995)

[66] M. Wendel, S. Kuhn, H. Lorenz, J. P. Kozzhaus, M. Holland Appl. Phys. Lett. **65** 1775 (1994)

[67] A. Majumdar, P. I. Oden, J. P. Carrejo, L. A. Nagahara, J. J. Graham, J. Alexander Appl. Phys. Lett. **61** 2293 (1992)

[68] Y. Kim, C. M. Lieber Science **257**, 375 (1996)

[69] C. R. Martin Science **266** 1961 (1994)

[70] G. A. Ozin Adv. Mater. **4**, 612 (1992)

[71] A. Huczko Appl. Physics A **70**, 365 (2000)

[72] C. J. Brumlik, V. P. Menon, C. R. Martin J. Mater. Res. **9** 1174 (1994)

[73] G. E. Possin Rev. Sci. Instrum. **41** 772 (1970)

[74] W. D. Williams, N. Giordano Rev. Sci. Instrum. **55** 410 (1984)

[75] C. A. Huber, T. E. Huber, M. Sadoqi, J. A. Lubin, S. Manalis, C. B. Prater Science **263** 800 (1994)

[76] R. L. Fleisher, P. B. Price, R. M. Walker *Nuclear Tracks in Solids*, Univ. of California Press: Berkley 1975

[77] R. M. Penner, C. R. Martin J. Electrochem. Soc. **133** 2206 (1986)

[78] R. J. Tonucci, B. L. Justus, A. J. Campillo, C. E. Ford Science **258** 783 (1992)

[79] D. H. Pearson, R. J. Tonucci Adv.Mater. **8** 1031 (1996)

[80] D. Crouse, Y. H. Lo, A. E. Miller, M. Crouse Appl. Phys. Lett. **76**, 49 (2000)

[81] D. H. Pearson, R. J. Tonucci Science **270** 68 (1995)

[82] C. G. Wu, T. Bein Science **264** 1757 (1994)

[83] C. G. Wu, T. Bein Science **266** 1013 (1994)

[84] S. Kawai, R. Ueda J. Electrochem. Soc. **121** 32 (1975)

[85] N. Tsuya, T. Tokushima, M. Shiraki, Y. Wakui, Y. Saito, S. Hayano, A. Furugori, M. Tanaka IEEE Trans. Magn. MAG-22, 1140 (1986)

[86] K. I. Arai, H. K. Kang, K. Ishiyama IEEE Trans. Magn. MAG-27, 4906 (1991)

[87] H. Daimon, O. Kitakami J. Appl. Phys. **73** 5391 (1993)

[88] T. M. Whitney, J. S. Jiang, P. C. Searson, C. L. Chien Science **261**, 1316 (1993)

[89] W. Xu, J. Wong, C. C. Cheng, R. Johnson, A. Scherer J. Vac. Sci. Technol. B 13**6**, 2372 (1995)

[90] Z. Cai, C. R. Martin J. Am. Chem. Soc. **111**, 4138 (1989)

[91] L. S. van Dyke, C. R. Martin Synthetic Metals **36**, 275 (1990)

[92] L. S. van Dyke, C. R. Martin Langmuir **6**, 1118 1990

[93] C. R. Martin, L. S. van Dyke, Z. Cai, W. J. Liang J. Am. Chem. Soc. **112**, 8976 (1990)

[94] M. Granström, O. Inganäs Synthetic Metals **55-57**, 460 (1993)

[95] M. Granström, O. Inganäs Polymer **36** 2867 (1995)

[96] A. Blondel, J. P. Meier, B. Doudin, J. Ph. Ansermet Appl. Phys. Lett. **65**, 3019 (1994)

[97] L. Piraux, J. M. George, J. F. Despres, C. Leroy, E. Ferain, R. Legras, K. Ounadjela, A. Fert Appl. Phys. Lett. **65**, 2484 (1994)

[98] P. R. Evans, G. Yi, W. Schwarzacher Appl. Phys. Lett. **76**, 481 (2000)

[99] Z. Zang, X. Sun, M. S. Dresselhaus, J. Y. Ying Appl. Phys. Lett. **73**, 1589 (1998)

[100] D. Gekthman, Z. B. Zhang, D. Adderton, M. S. Dresselhaus, G. Dresselhaus Phys. Rev. Lett. **82**, 3887 (1999)

[101] K. Liu, C. L. Chien, P. C. Searson, K. Y. Zhang Appl. Phys. Lett. **73**, 1436 (1998)

[102] J. Heremans, C. M. Thrush, Y. M. Lin, S. Cronin, Z. Zhang, M. S. Dresselhaus, J. F. Mansfield Phys. Rev. B **61**, 2921 (2000)

[103] J. Li, C. Papadopoulos, J. M. Xu, M. Moskovits Appl. Phys. Lett. **75**, 367 (1999)

[104] C. G. J. Koopal, B. de Ruiter, R. J. M. Nolte J. Chem. Soc. Chem. Commun., 1691 (1991)

[105] M. Yoshida, M. Tamada, M. Asano, H. Omichi, H. Kubota, R. Katakai, R. Spohr, J. Vetter Radiation Effects in Solids **126**, 409 (1993)

[106] C. J. Miller, M. Majda J. Am. Chem. Soc. **107**, 1419 (1985)

[107] C. J. Miller, M. Majda J. Am. Chem. Soc. **108**, 3118 (1986)

[108] A. M. Bond, D. Luscombe, K. B. Oldham, C. G. Zoski J. Electroanal. Chem. Interfacial Electrochem. **249**, 1 (1988)

[109] K. Morita, Y. Shimizu Anal. Chem. **61**, 159 (1989)

[110] Y. Shimizu, K. Morita Anal. Chem. **62**, 1498 (1990)

[111] C. J. Brumlik, C. R. Martin Anal. Chem. **64**, 1201 (1992)

[112] C. A. Foss, G. L. Hornyak, J. A. Stockert, C. Martin J. Phys. Chem. **98**, 2963 (1994)

[113] B. van der Zande, M. R. Bömer, L. G. J. Fokkink, C. Schönenberger J. Phys. Chem. **101**, 852 (1997)

[114] B. van der Zande *Colloidal dispersions of gold rods*, Thesis, University of Utrecht, 1998

[115] Z. Cai, J. Lei, W. Liang, V. Menon, C. R. Martin Chem. Mater. **3**, 960 (1991)

[116] C. Schönenberger, B. M. I. van der Zande, L. G. J. Fokkink, M. Henny, C. Schmid, M. Krüger, A. Bachtold, R. Huber, H. Birk, U. Staufer J. Phys. Chem. B **101**, 5497 (1997)

[117] I. Chlebny, B. Doudin, J.-Ph. Ansermet Nano-Structured Materials **2**, 637 (1993)

[118] S. K. J. Lenczowski, C. Schönenberger, M. A. M. Gijs, W. J. M. de Jonge J. Magn. Magn. Mater. **148**, 455 (1995)

[119] B. E. Fischer, R. Spohr Rev. Mod. Phys. **55**, 907 (1983) (*and references therein*)

[120] E. Ferain, R. Legras Nucl. Instr. and Meth. in Phys. Res. B **84**, 331 (1994)

[121] R. Spohr, P. Ambruster, K. Schaupert Radiation Effects and Defects in Solids **110**, 27 (1989)

[122] S. Bouffard, J. Cousty, Y. Pennec, F. Thibaudau Radiation effects and Defects in Solids **126**, 225 (1993)

[123] C. R. Musil, D. Jeggle, H. W. Lehmann, L. Scandella, J. Gobrecht, M. Döbeli J. Vac. Sci. Technol. B **13**, 2781 (1995)

[124] For a brief review, see: M. Hatzakis, IBM J. Res. Dev. **32**, 441 (1988)

[125] S. Demoustier-Champagne, J. Duchet, R. Legras Synthetic Metals **101**, 20 (1999)

[126] S. Demoustier-Champagne, P. Y. Stavaux Chem. Mater. **11**, 829 (1999)

[127] J. Duchet, R. Legras, S. Demoustier-Champagne Synthetic Metals **98**, 113 (1998)

[128] J. W. Diggle, T. C. Downie, C. W. Goulding Chem. Rev. **69**, 365 (1969)

[129] F. Keller, M. S. Hunter, D. L. Robinson J. Electrochem. Soc. **100**, 411 (1953)

[130] K. V. Heber Electrochim. Acta **23**, 127 (1978)

[131] K. V. Heber Electrochim. Acta **23**, 135 (1978)

[132] A. Despic, V. P. Parkhutik, *Modern aspects of electrochemistry*, part 2, chapter 6, ed.: J.O. M. Bockris, R. E. White, B. E. Conway, Plenum Press, New York and London 1989

[133] G. Patermarakis, P. Lenas, Ch. Karavassilis, G. Papayiannis Electrochimica Acta **36**, 109 (1991)

[134] N. Tsuya, T. Tokushima, M. Shiraki, Y. Wakui, Y. Saito, H. Nakamura, Y. Harada IEEE Trans. Magn. **24**, 2661 (1988)

[135] N. Tsuya, T. Tokushima, M. Shiraki, Y. Wakui, Y. Saito, H. Nakamura, Y. Katsumata IEEE Trans. Magn. **23**, 53 (1987)

[136] K. I. Arai, H. W. Kang, K. Ishiyama IEEE Trans. Magn. **27**, 4906 (1991)

[137] A. Bachtold, C. Terrier, M. Krüger, M. Henny, T. Hoss, C. Strunk, R. Huber, H. Birk, U. Staufer, C. Schönenberger Microelectronic Engineering **41/42**, 571 (1998)

[138] M. S. Dresselhaus, G. Dresselhaus, P. C. Eklund *Science of Fullerenes and Carbon nanotubes* Academic Press Inc., San Diego 1996

[139] T. W. Ebbesen Physics Today **49**, nr.6, 26 (1996)

[140] C. Dekker Physics Today **52**, nr.5, 22 (1999)

[141] C. Schönenberger Physics World **13**, 37-41 (2000)

[142] M. S. Dresselhaus, G. Dresselhaus, K. Sugihara, L. Spain, H. A. Gold-berg *Graphite Fibers and Filaments* "Springer Series in Materials Science" Vol.5 Springer Verlag 1998

[143] H. W. Kroto, J. R. Heath, S. C. O' Brien, R. F. Curl, R. E. Smalley Nature **318,** 162 (1985)

[144] W. Krätschmer, L. D. Lamb, K. Foristopoulos, D. R. Huffman Nature **347**, 354 (1990)

[145] O. Gunnarson Rev. Mod. Phys. **69**, 575 (1997)

[146] S. Iijima Nature **354**, 56 (1991)

[147] D. Ugarte Nature **359**, 707 (1992)

[148] D. S. Bethune et. al. Nature **363**, 605 (1993)

[149] A. Thess et al., Science **273**, 483 (1996)

[150] A. Fonseca, et al. , Applied Physics A **67**, 11 (1998)

[151] J. Kong et al. Applied Physics A **69**, 305 (1999)

[152] J. Kong et al. Nature **395**, 878 (1998)

[153] M. Terrones et al. Nature **388**, 52 (1997)

[154] Langer et al. Phys. Rev. Lett **76**, 479 (1996)

[155] T. W. Ebbesen et al. Nature **328**, 54 (1996)

[156] S. J. Tans et al. Nature **393**, 49 (1998)

[157] M. Bockrath et al. Science **275**, 1922 (1997)

[158] P. Poncharal, Z. L. Wang, D. Ugarte, A. A. de Heer Science **283**, 1513 (1999)

[159] H. Dai, A. G. Rinzler, D. T. Colbert, R. E. Smalley Nature **384**, 147 (1996)

[160] K. Tsukagoshi, B. W. Alphenaar, H. Ago Nature **401**, 572 (1999)

[161] M. M. J. Treacy, T. W. Ebbesen, J. M. Gibson Nature **381**, 678 (1996)

[162] V. Barwich, University of Basel, unpublished

[163] P. Chen, X. Wu, J. Lin, K. L. Tan Science **285**, 91 (1999)

[164] R. Saito, M. Fujita, G. Dresselhaus, M. S. Dresselhaus Phys. Rev. B **46**, 1804 (1992)

[165] R. Saito, M. Fujita, G. Dresselhaus, M. S. Dresselhaus Appl. Phys. Lett. **60**, 2204 (1992)

[166] N. Hamada, S. Swada, A. Oshiyama Phys. Rev. Lett. **68**, 1579 (1992)

[167] J. W. Mintmire, B. I. Dunlap, C. T. White Phys. Rev. Lett. **68**, 631 (1992)

[168] K. Tanaka, K. Okahara, M. Okada, T. Yamabe Chem. Phys. Lett.**191**, 469 (1992)

[169] H. Ajiki, T. Ando J. Phys. Soc. Jpn. **62**, 1255 (1993)

[170] J. W. G. Wildöer, L. C. Venema, A. G. Rinzler, R. E. Smalley, C. Dekker Nature **391**, 59 (1998)

[171] T. W. Odom, J. L. Huang, P. Kim, C. M. Lieber Nature **391**, 62 (1998)

[172] J. Nygard, D. H. Cobden, M. Bockrath, P. L. McEuen, P. E. Lindelof Appl. Phys. A **69**, 297 (1999)

[173] C. Schönenberger, A. Bachtold, C. Strunk, J.-P. Salvetat Appl. Phys. A **69**, 283, (1999)

[174] C. Schönenberger *Electric properties of multiwall carbon nanotubes* to appear

[175] S. Frank, P. Poncharal, Z. L. Wang, W. A. de Heer Science **280**, 1744 (1998)

[176] A. Bachtold, C. Strunk, J.- P. Salvetat, J.-M. Bonard, L. Forro, T. Nussbaumer, C. Schönenberger Nature **397**, 673 (1999)

[177] Y. Imry *Physics of mesoscopic systems* in Directions in Condensed Matter Physics, eds.: G. Grinstein, G. Mazenko World Scientific Press, Singapore, 1986

[178] A. Y. Kasumov et al. Europhys. Lett. **43**, 89 (1998)

[179] S. N. Song, X. K. Wang, R. P. H. Chang, J. B. Ketterson Phys. Rev. Lett. **72**, 697 (1994)

[180] J. Hone et al. Phys. Rev. Lett. **80**, 1042 (1998)

[181] W. Yi, L. Lu, Zhang Dian-lin, Z. W. Pan, S. S. Xie Phys. Rev. B **59**, R9015 (1999)

[182] L. Grigorian et al. Phys. Rev. B **R11309**, (1999)

[183] P. G. Collins, K. Bradley, M. Ishigami, A. Zettl Science **287**, 1801 (2000)

[184] G. U. Sumanasekera et al. Bulletin of the APS March **45**, 414 (2000)

[185] Li Lu, Wie Yi, Z. Pan, S. S. Xie Bulletin of the APS March **45**, 414 (2000)

[186] J. Kong et al. Science **287**, 622 (2000)

[187] P. H. Rieger *Electrochemistry* 2nd edition, Chapman & Hall, New York, London 1994

[188] J. Pichumani J. Britto, Kalathur S. V. Santhanam, Angel Rubio, Julio A. Alonso, Pulickel M. Ajayan Adv. Mater. **11**, 154 (1999)

[189] D. Babic private communication

Appendix A
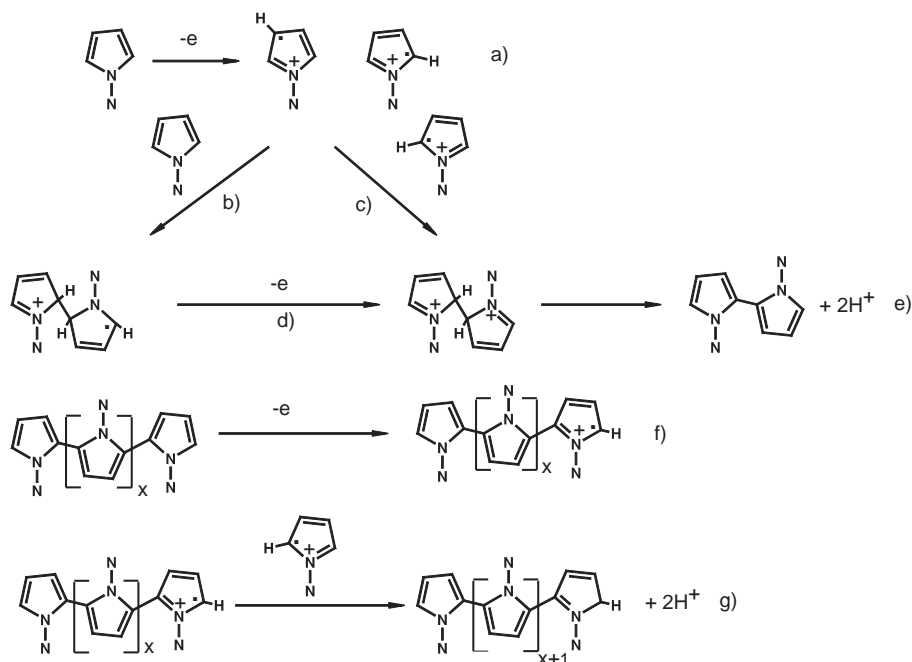
Mechanism of the Electropolymerisation of Polypyrrole

Figure A.1: Diagram of the reaction mechanism for the electropolymerisation of polypyrrole: after a neutral monomer is oxidized to a radical cation (a) near the surface of the electrode, there exist two possible reaction pathways for the following step leading to the double-charged dihydrodimer: b) the radical cation reacts with a neutral monomer to a single charged dihydroderivative and after an additional oxidation step (d) the double-charged dihydrodimer is formed or c) the radical cation reacts with an other radical cation forming directly the charged dihydrodimer. f) the dimeric or oligomeric compounds are oxidized more easily than the monomer to radical cations g) chain growth is accompanied by the addition of new cations of the monomeric pyrrole to the already charged dimers or oligomers. During every chain propagation step two protons are set free.

Appendix B

Optical Lithography and E-Beam Lithography

Substrate:

- $2 \times 2\,\text{cm}^2$ oxidized (400 nm) and highly doped silicon wafer for the nanotube experiments and $2 \times 1.5\,\text{cm}^2$ oxidized (400 nm) and normal doped silicon wafer for the fabrication of the microelectrodes were used for the growth of CPs and the fabrication of lateral nanopores in a polyimide resist.
- The wafer were cleaned in isopropanol and pure water by ultrasonic treatment for 10 minutes, respectively.
- The wafer were dried in an oven for two hours at $200°\text{C}$

Optical lithography:

- maskaligner MJB 3 (Karl Suss, München, Germany)
- negative photoresist: ma-N-420 (micro resist technology, Berlin, Germany)
- developer: ma-D-332 (micro resist technology, Berlin, Germany)
- After cleaning the wafer HMDS (Hexamethyldisilazane) was spin-coated on top of the wafer (2000 rpm, 40 s) to achieve a hydrophobic surface in order to improve the adhesion of the negative photoresist which was spin-coated onto the substrate afterwards (4000 rpm, 40 s, resist thickness of about 2 - 2.2 μm). After baking the resist at 87.5° C for 30 minutes in an oven and cooling down to room temperature optical lithography was applied by using a Hg-lamp (exposure time 1 - 1.5 minutes and developing time 20 - 25 minutes).

E-beam-lithography

- A Jeol JSM-IC 848 scanning microscope was used (35 keV acceleration voltage, 45 pA current and 10^{-6} C/m line dose for small structures).

- proxy-writer (Reith, Germany) was used as software program for pattern generation and e-beam exposure control.

- PMMA 950 K e-beam resist (Allresist, Germany) was used as resist. Dilution of the 9% (w/w) solution with additional chlorbenzene led to an decrease of the resist thickness (400-600 nm).

- the development was done for 40 s in a solution of MIBK (4-Methyl-2-pentanone) : IPA (isopropanol) 1 : 3; to stop the development the sample was rinsed in pure IPA for 30 s.

Metal evaporation

- A Balzers Pfeiffer PLS 500 labor evaporation system was used.

- Ti, Al, Si-oxide, Ni and Au was evaporated by an e-gun. In the case of Au the sample holder was cooled down to $\simeq 0$ ° C.

- The lift off was done by immersing the sample in acetone for one hour.

Appendix C

Arrangement for the Electrochemical Doping of Single MWNTs
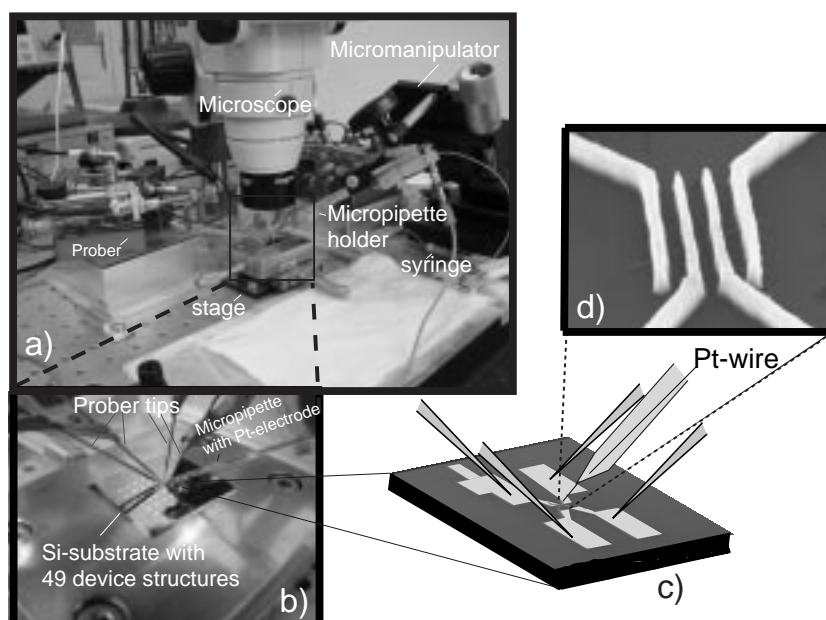
Figure C.1: Arrangement for the electrochemical doping of a single MWNT. a) The multi-device array is put onto a stage under an optical microscope. The micropipette is put onto the contacted nanotube by using a micromanipulator. b) One nanotube is contacted by four-terminal contacts. The micropipette including the Pt counter-electrode is on top of the contacted tube. c)-d) A closer look at the four-terminal contacted device.

List of publications

Publications in journals and proceedings:

- *Synthesis of new bifunctional maleimide compounds for the preparation of chemoimmunoconjugates,*
  U. Beyer, M. Krüger, P. Schumacher, C. Unger, F. Kratz,
  Monatshefte für Chemie (Chemical Monthly) **128**, 91-102 (1997).

- *Synthesis of new maleimide derivatives of daunorubicin and biological activity of acid labile transferrin conjugates,*
  F. Kratz, U. Beyer, P. Schumacher, M. Krüger, H. Zahn, T. Roth, H. H. Fiebig, C. Unger,
  Bioorganic & Medicinical Chemistry Letters **7**, 617-622 (1997).

- *Synthesis and Stability of four maleimide derivatives of the anticancer drug doxorubicin for the preparation of chemoimmunoconjugates,*
  M. Krüger, U. Beyer, P. Schumacher, C. Unger, H. Zahn, F. Kratz,
  Chem. Pharm. Bull. **45**, 399-401(1997).

- *Template-synthesis of nanowires in porous polycarbonate membranes: electrochemistry and morphology,*
  C. Schönenberger, B. M. I. van der Zande, L. G. J. Fokkink, M. Henny, C. Schmid, M. Krüger, A. Bachtold, R. Huber, H. Birk and U. Staufer,
  Journal of Physical Chemistry **B 101**, 5597-5605 (1997).

- *Electron heating effect in diffusive metal wires,*
  M. Henny, H. Birk, R. Huber, C. Strunk, A. Bachtold, M. Krüger, C. Schönenberger,
  Appl. Phys. Lett. **71**, 773 (1997).

- *Contacting single template synthesized nanowires for electric measurements,*
  A. Bachtold, C. Terrier, M. Krüger, M. Henny, T. Hoss, C. Strunk, R. Huber, H. Birk, U. Staufer, C. Schöneneberger,
  Microelectronic Engineering **41/42**, 571-574 (1998)

122

- **In Preparation:** *The electrochemical carbon nanotube field-effect transistor,* M. Krüger et al. (probably in Appl.Phys.Lett.)

Talks:

- *Towards Single Molecule Electronics,* PhD defense, July 7, 2000, University of Basel, Switzerland;
- *Electrochemical Doping of Multiwalled Carbon Nanotubes,* International Conference on Science and Technology of Synthetic Metals (ICSM 2000), Bad Gastein (Austria), July 17, 2000;
- *Towards Single Molecule Electronics,* seminar talk, July 27, 2000, Technion (Israel Institute of Technology), Haifa (Israel)

Poster contributions:

- *Electric Transport in Template-Synthesized Conducting Polymer Wires,* 2nd Hasliberg-Workshop on Nanoscience, October 1996, Hasliberg (Switzerland);
- *Electric Transport in Template-Synthesized Conducting Polymer Wires,* Schloessmann Seminar on Nanostructures in Biology, Chemistry and Physics, 1996, Schloss Elmau, Germany;
- *Template-Synthesized Nanowires for Electric Measurements,* The 1997 Joint International Meeting of The Electrochemical Society and The International Society of Electrochemistry, August 31 - September 5, 1997, Paris (France);
- *Kontaktierung von Nanodräten aus Metallen und leitfähigen Polymeren für Elektrische Transportuntersuchungen,* DPG-Tagung, March 1998, Bayreuth (Germany);
- *Contacting Conducting Polymer Nanowires for Electric Measurements,* International Conference on Science and Technology of Synthetic Metals (ICSM 98), July 1998, Montpellier (France);
- *Towards Electrical Transport Measurements in Single Polymer Nanowires,* 3rd Hasliberg-Workshop on Nanoscience, October 1998, Hasliberg (Switzerland);
- *Electrochemical Doping of Multiwalled Carbon Nanotubes,* XIVth Winterschool on Electronic Properties of Novel Materials, March 4-11, 2000, Kirchberg/Tirol (Austria);
- *Electrochemical Doping of Multiwalled Carbon Nanotubes,* COST P5 workgroup meeting on "Quantum Dots, Nanoparticles and Carbon Nanotubes, April 14-15, 2000, TU Delft (The Netherlands);

Curriculum Vitae

Michael Krüger

05.11.1967	Born in Lörrach (Germany)
1974 - 1987	Visiting school, 1987 Abitur (Hans-Thoma-Gymnasium Lörrach)
1987 - 1988	Military service
1988 - 1996	Study of chemistry at the University of Freiburg (Germany) Diploma work at the Institute of Physical Chemistry in Freiburg (Prof. Gräber) in cooperation with the "Klinik für Tumorbiologie" in Freiburg i. Br. (Cancer research group of Prof. C. Unger, supervisor: Dr. F. Kratz) **Diploma thesis**: "Developement and Synthesis of Chemoimmuno-conjugates of the Clinical Relevant Anticancer Drugs Doxorubicin, Daunorubicin and Methotrexate with Transferrin and Albumine as Protein Components
April 1996	Assistant at the Institute of Physics at the University of Basel (Switzerland) in the group of Prof. Dr. C. Schönenberger **December 1996**: Award from the Max Planck Association at the "Schloessmann Seminar on Nanostructures in Biology, Chemistry and Physics" for an outstanding presentation;
July 2000	**PhD Thesis:** "*Towards Molecule Electronics*"

Folgenden Dozenten verdanke ich meine Ausbildung:

Prof. Ackermann, Prof. Binnewies, Prof. P. Gräber, Dr. F. Kratz, Prof. Kurz, Prof. R. Mühlhaupt, Prof. H. Prinzbach, Dr. Rücker, Prof. Rüchardt, Prof. C. Schönenberger, Prof. Schwesinger, Prof. C. Strunk, Prof. Thiele, Prof. C. Unger, Prof. Vahrenkamp;

Acknowledgements